Liquid-Liquid Interface Ion-Transfer Amperometric Sensors for Tenofovir as a Model Nucleoside/ Nucleotide Anti-Retroviral Drug

By

Sara Hamid Ibrahim Hamid

BSc Honours (Class Two Division Two)

A thesis submitted in fulfillment of the requirements for the degree of

Magister Scientiae in Chemistry

Faculty of Science

University of the Western Cape

Cape Town, South Africa

Supervisor: Prof Emmanuel I. Iwuoha
Co-supervisor: Dr Tesfaye T. Waryo

March 2014

Page left blank

Liquid-Liquid Interface Ion-Transfer Amperometric Sensors for Tenofovir as a Model Nucleoside/Nucleotide Anti-Retroviral Drugs

Sara Hamid Ibrahim Hamid

KEYWORDS

Ion transfer at polarized liquid- liquid interface

Nucleoside anti-retroviral drugs

Nucleotide anti-retroviral drugs

Tenofovir sensor

Dibenzo-18-crown-6

1, 2 Dichloroethane

Cyclic voltammetry

Page left blank

ABSTRACT

Amperometric sensors for Tenofovir, a model nucleotide/ nucleoside reverse transcriptase inhibitor ARV drug, were studied based on the principle of ion-transfer electrochemistry at the membrane-stabilized oil/ water interface (O∥W) in a four-electrode cell set-up. Solutions of the hydrophobic salts tetradodecylammonium tetrakis(4-chlorophenyl) borate (ETH500), ethyl violet tetraphenylborate (EthVTPB), tetrabutylammonium tetraphenylborate (TBATPB), tetraphenylphosphnium tetraphenylborate (TPphTPB) and three ionic liquids (Methyltrioctylammonium bis(trifluoromethyl sulfonyl)imide (IL1), 1-butyl-3-methylimdazolium bis(trifluoromethyl sulfonyl)imide (IL3) and 1-propyl-3-methylimdazolium bis(trifluoromethylsulfonyl)imide (IL4)) in nitrobenzene (NB), 1,2-dichloroethane (DCE), and 2-nitrophenyloctyl ether (NPOE) were each tested as O-phases. The cyclic voltammograms of the resulting O∥W interfaces in aq. Li_2SO_4 or aq. Mg_SO_4 were compared with respect to noise, potential window, and other parameters. The three ILs were also tested as self-sufficient salts without a solvent medium. In the end, the ETH500/ DCE salt/ solvent pair was found to yield the best behaved polarizable O∥W interface in aq. $MgSO_4$. The analytical characteristics of the resulting sensors to tenofovir without (Ag|ETH500/DCE∥) and with the dibenzo-18-crown-6 (Ag|ETH5000/DB18C6/DCE∥ in the O-phase were studied with respect to the two pairs of peaks in the CV, namely the W→O ion transfer peak and the reverse O→W peak. Both sensors exhibited operational stability of 90 min. After consideration of reasonable S/N ratio and sample throughput rates, the scan rate of 25 mV/ s was used in subsequent signal interrogation with CV. The final potential windows were 0.95 V wide for Ag|ETH500 (10 mM)/ DCE∥ in aq. $MgSO_4$ (50 mM) and 0.70 V wide for Ag|ETH500 (10 mM)/ DB18C6 (50 mM)/ DCE∥ in aq. $MgSO_4$ (50 mM). From plots of peak currents versus square of scan rate, tenofovir diffusion coefficients of about 2.48×10^{-11} cm^2/ s were estimated, which indicated diffusion through the supporting membrane as the rate

limiting process. Based on W→O ion transfer peaks, the first one exhibited a detection limit of about 5 μM, a linear range of 15 – 100 μM, and sensitivity of 7.09 nA μM^{-1} towards tenofovir, whereas for the second one these were respectively 3 μM, 6.32 nA μM^{-1}, and 9 – 100 μM. In this way, a four-electrode amperometric detection of ion transfer process at liquid | liquid interface, both under simple and ionophore-facilitated mode, has been demonstrated as promising for analysis of tenofovir as a representative of the nucleotide/ nucleoside reverse transcriptase inhibitor ARV drugs.

DECLARATION

I declare that **Liquid-Liquid Interface Ion-Transfer Amperometric Sensors for Tenofovir as a Model Nucleoside/Nucleotide Anti-Retroviral Drugs** is my own work, that it has not been submitted for any degree or examination in any other university, and that all the sources I have used or quoted have been indicated and acknowledged by complete references.

Sara Hamid Ibrahim Hamid

February   2014

Signed ....

UNIVERSITY *of the*

WESTERN CAPE

Page left blank

# ACKNOWLEDGEMENT

Page left blank

X

PUBLICATIONS

Rachel F. Ajayi1, et al., Sara Hamid, Tesfaye T. Waryo, Emmanuel I. Iwuoha, **Chemically amplified cytochrome P450-2E1 drug metabolism nanobiosensor for rifampicin anti-tuberculosis drug**, *Electrochimica Acta* 2014, Accepted.

Sara Hamid, Tesfaye T. Waryo, Getrude Fomo, Abebaw A. Tsegaye, Rachel F. Ajayi, Priscilla G. Baker, Emmanuel I. Iwuoha, **Ion transfer volatmmetric detection and characteristics of the model nucleoside/nucleotide ARV drug tenofovir at the membrane-stabilized water/dichloroethane interface** (Being submitted to *Nanohybrids*)

Sara Hamid, Tesfaye T. Waryo, Emmanuel I. Iwuoha, **A review of recent progress in the application of the membrane-stabilized interface between two immiscible electrolytes in electrochemical sensors for drugs** (Being submitted to *International Journal of Electrochemical Sciences*)
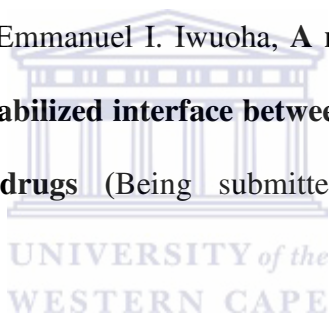
CONFERENCES

Sara Ibrahim, Tesfaye T. Waryo, Immanuel I. Iwuoha, **Amperometric Ion -Transfer Sensors for Nucleoside and Nucleotide Reverse Transcriptase Inhibitor Molecules,** 13th Topical Meeting of the International Society of Electrochemistry, from 7 to 10 April 2013, CSIR ICC, Pretoria, South Africa (Accepted abstract submission) (http://topical13.ise-online.org/general/PRETORIA-program.pdf)

Page left blank

TABLE OF CONTENTS

LIST OF FIGURES

Page left blank

LIST OF TABLES

XXV

Page left blank

LIST OF ABBREVIATION

NB   : Nitrobenzene

DCE   : 1-2Dichlorethane

NPOE   : 2-Nitrophenyl octyl ether

ETH500   : Tetradodecylammonium tetrakis-(4-chlorophenyl) borate

DB18C6   : Dibenzo-18-crown-6

EthvTPB   : Ethyl Violet tetraphenylborate

TPphTPB   : Tetraphenylphosphnium tetraphenylborate

TBATPB   : Tetrabutylammonium tetraphenylborate

IL1   : Methyl-trioctylammonium bis (trifluoro-methyl sulfonyl) imide

IL3   : 1-Butyl-3-methyl imdazolium bis (trifluoro-methyl sulfonyl) imide

IL4   : 1-Propyl-3- methyl imdazolium bis (trifluoro-methyl sulfonyl) imide

CV   : Cyclic Voltammetry

NRTIs   : Nucleoside Reverse Transcriptase Inhibitor Anti-Retroviral Drugs

ITITES   : Interface between two immiscible electrolyte solutions

ARV   : Anti-retroviral

HIV   : Human immunodeficiency virus

HAART   : Highly active antiretroviral therapy

PI   : Protease inhibitor

NNRTIs   : Non-nucleoside reverse transcriptase inhibitor

NtRTIs   : Nucleotide reverse transcriptase inhibitor

INI   : Integrase inhibitor

HPLC   : High-Performance Liquid Chromatography

DI   : Deionized water

FIA   : Flow Injection Analysis

CHAPTER I: INTRODUCTION

Ionic charge transfer reactions at a liquid/ liquid (L/L) interface are one of the most important physicochemical processes. The liquid/liquid interface is actually made up of two immiscible electrolyte solutions. For example, organic phase which is hydrophobic and aqueous phase is hydrophilic [1–5]. These charge-transfer reactions which can occur across such an interface can be classified into two main classes:

Simple Ion-transfer (IT) reactions:

Are the easiest to investigate, when an ion has a relatively low Gibbs energy of transfer and its value is within the potential window of the experimental system, the transfer can occur if the liquid/liquid interface is polarized. The valence state of the ion does not change, so that only the solvation is varied while the transfer is occurring, there have been several reports on this subject, ranging from simple inorganic and organic ions to drugs and biomolecules [2–4,6]. Most IT reactions are fast and can be considered as reversible [2].

Facilitated ion-transfer (FIT) reaction:

It is occurs when an ion has higher (or lower) Gibbs energy of transfer at a liquid/liquid interface, the transfer normally appears outside the potential window or very near the positive or negative end of the potential window, so that it is difficult to study the simple IT reaction directly. In order to solve such a problem, a ligand (ionophore), which can complex with the ion, can be chosen to be put into either phase to lower the Gibbs energy of transfer. Such a process is called a FIT reaction [2,4,5]

Various ionophores, such as crown ethers, antibiotics and calixarenes have been employed to facilitate ion transfer reaction, but in this study among the crown ethers dibenzo-18-crown-6 will play essential role. Fig 1 shows the structure of DB18C6.
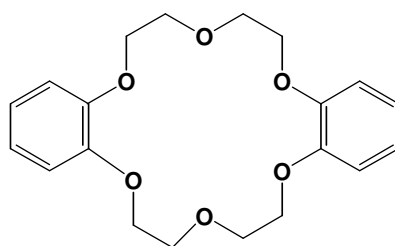
Dibenzo-18- crown -6

Fig 1: structure of dibenzo-18-crown-6 (DB18C6)

Nucleoside reverse transcriptase inhibitors (NRTIs) were the first anti-retroviral (ARV) drugs to be approved for the treatment of human immunodeficiency virus (HIV), with zidovudine (AZT) since 1987; and, these drugs still continue to be the back bone of the current treatment guideline known as highly active antiretroviral therapy (HAART) [7–12]. A HAART prescription usually contains two (or three) ARV drugs in a fixed dose combination, one (or two) of which is an NRTI and the other being an ARV with a different mechanism of action, for instance, a non-nucleoside reverse transcriptase inhibitor (NNRTI), or a protease inhibitor (PI), or an integrase inhibitor (INI) [13,14].
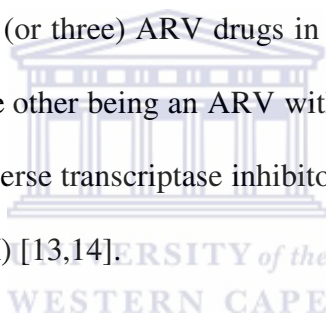
The efficacy of routine treatment of HIV infections with existing HAART drugs and the success of newer clinical trials obviously depend on the availability of specific and accurate standard analytical methods to reliably detect and quantify these substances and their metabolites in-vitro and in-vivo. In this regard, HPLC, GCMS, and UV - visible absorption/ fluorescence/ spectroscopy – based protocols remain to be key tools. However, methods based on electrochemical sensors could be superior when the priorities to address are (a) the increasing demand for quick, economical, portable, and personalized devices; and, (b) futuristic medicine based on implanted devices, real-time monitoring, and controlled drug release.

Of particular interest is the possible application of simple and ionophore-assisted ion-transfer electrochemistry (IT) at an electrified interface between two immiscible electrolyte solutions (ITIES), to develop such sensors for a selection of approved and new NRTIs (zidovudine, didanosine, zalcitabine, stavudine, lamivudine, abacavir and emtricitabine). In contrast with traditional solid-state electrode sensors, at which such analyze could undergo irreversible electrochemistry causing electrode fouling effects, an IT@ITIES-based sensor would generate signals without oxidizing or reducing the analyze. Thus, both the sensor and the sample would be re-usable. It also yields data on drug lipophilicity and partition.

In this MSc thesis work, various membrane-stabilized macro ITIES (water/ nitrobenzene, dichloroethane, hydrophobic room temperature ionic liquids, 2-nitrophenyloctyl ether), and supporting electrolytes were tested and compared with respect to a set of analytical parameters by developing sensors based on simple and DB18C6-facilitated transfer of Tenofovir as a model nucleotide/ nucleoside reverse transcriptase inhibitor ARV drug. The electrochemical technique used was cyclic voltammetry.

The objectives of this thesis include:

(i) Literature review of the electrochemistry of, electrochemical sensors, for nucleoside and nucleotide reverse transcriptase inhibitor (NRTI) ARV drugs.

(ii) Study the analytical performance of simple and facilitated ion transfer based electrochemical sensors for Tenofovir as a model NtRTIs/ NRTIs drug.

Chapter I gives an introduction to liquid/liquid interface technique and (NRTIs / NtRTIs). The rationale and motivation of this project are also given as well as, the objectives that need to be met.

Chapter II gives the literature review which review the classification of NRTIs and NtRTIs

and there structure, and the type of sensors more over the electroanayltical analysis.

Chapter III which retrace the essential theory of electrochemistry at the ITIES and measurements of part ion coefficient also the diffusion coefficient the following topics are covered in the present study.

Chapter IV gives experimental, an account on the specific chemical used in the analysis, before explaining in detail solutions preparation and electrochemical analysis.

Chapter V shows cyclic voltammetry using four electrode cells used to explore the partition and diffusion coefficients of tenofovir.

Chapter VI concludes this thesis by summarizing the main points highlights the novelty of the research and, offers conclusions and recommendations as well as future work.

CHAPTER II: LITERATURE REVIEW

Until now after the human immunodeficiency virus (HIV) was discovered as the tentative a etiological agent of acquired immune deficiency syndrome (AIDS), exactly 25 anti-HIV compounds have been formally approved for clinical use in the treatment of AIDS. These compounds fall into six categories: nucleoside reverse transcriptase inhibitors (NRTIs) nucleotide reverse transcriptase inhibitors (NtRTIs), non-nucleoside reverse transcriptase inhibitors (NNRTIs), protease inhibitors (PIs), fusion inhibitors (FIs), co-receptor inhibitors (CRIs), and integrase inhibitors (INIs) [15]. But the reviews will be in Nucleoside and Nucleotide reverse transcriptase inhibitors a) what they are b) general analysis for (NRTIs and NtRTIs), c) electrochemical analysis

Table 1: Approved Structure of the NRTIs and NtRTIs [15]

Zidovudine   Didanosine   Zalcitabine   Stavudine

Lamivudine   Abacavir   Emtricitabine   Tenofovir
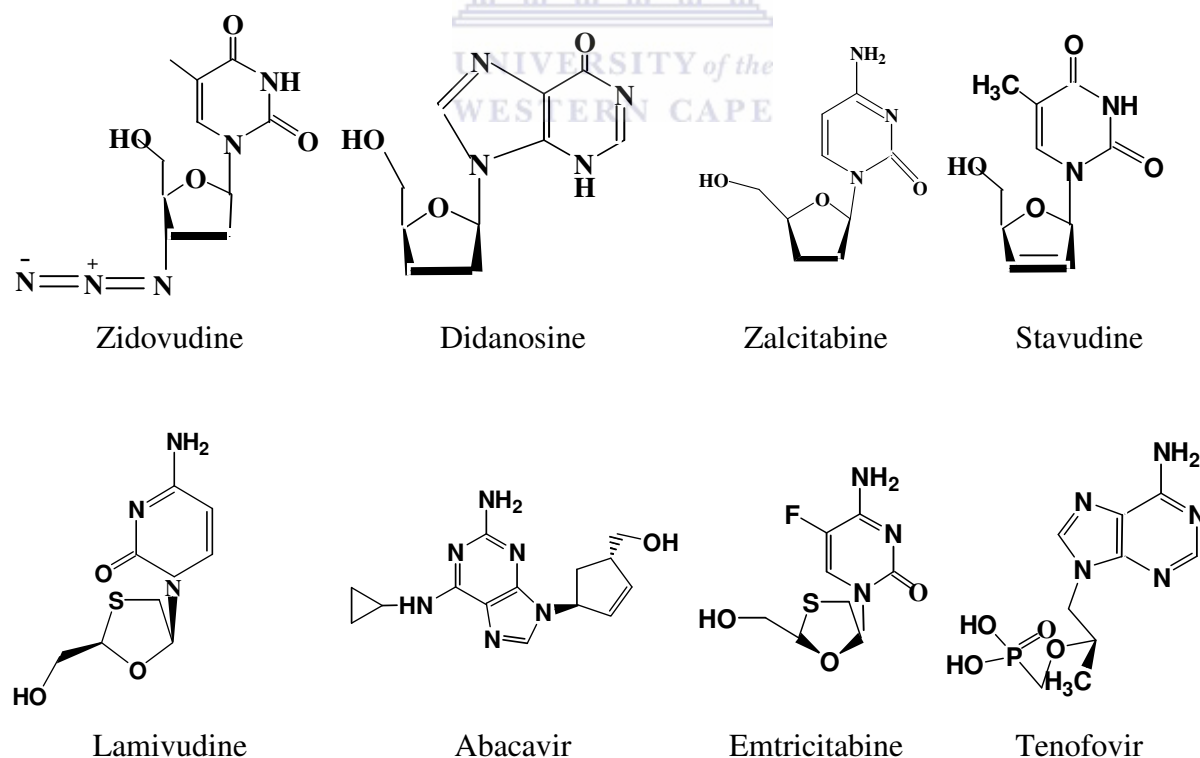
Table 2: Approved anti-HIV (NRTIs and NtRTIs) drugs (adopted from ref. [16])

Categories	Generic Name	Brand name	Manufacturer
NRTIs	Zidovudine	Retroviral	GlaxoSmithKline
	Didanosine	Videx(tablet)	Bristol-Myers Squibb
		Videx EC (capsule)	
	Zalcitabine	Hivid	Hoffmann-La Roche
	Stavudine	Zerit	Bristol-Myers Squibb
	Lamivudine	Epivir	GlaxoSmithKline
	Abacavir	Ziagen	GlaxoSmithKline
	Emtricitabine	Emtriva	Gilead Sciences
NtRTIs	Tenofovir	Viread	Gilead Sciences

2.1 Nucleoside/ Nucleotide reverse transcriptase inhibitors

The reverse transcriptase (RT) enzyme associated with HIV is actually the target of three classes of inhibitors: nucleoside RT inhibitors (NRTIs); nucleotide RT inhibitors (NtRTIs); and non-nucleoside RT inhibitors (NNRTIs). The NRTIs and NtRTIs interact with the catalytic site (that is the substrate-binding site) of the enzyme, whereas the NNRTIs interact with an allosteric site located at a short distance (ca. 15Å) from the catalytic site Fig 2.
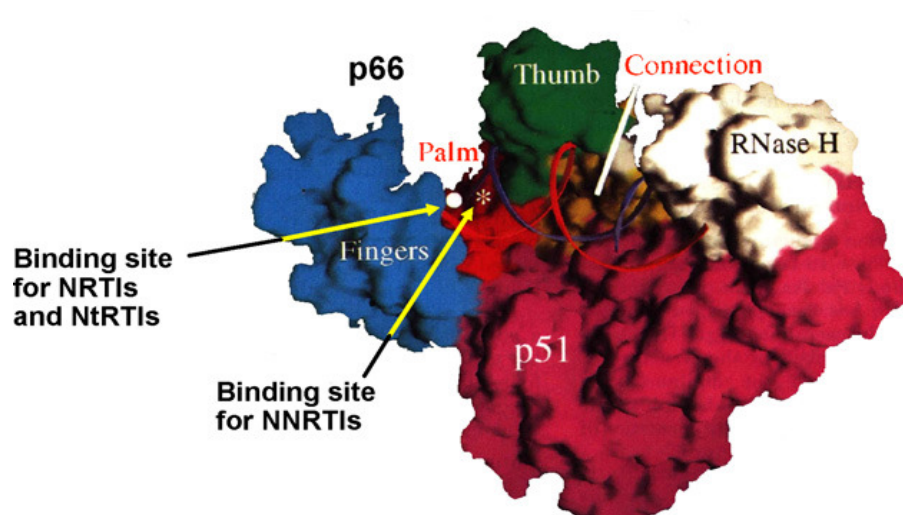
Fig 2: HIV reverse transcriptase with the binding site for the (NRTIs) and (NtRTIs) and the binding site for the (NNRTIs). According to De Clercq [17]; structure of the enzyme according to Tantillo et al. [18]

2.1.1 Nucleoside reverse transcriptase inhibitors (NRTIs)

The reverse transcriptase associated with HIV is actually the target for three classes of inhibitors: NRTIs, NtRTIs, and NNRTIs. The NRTIs and NtRTIs interact with the catalytic site of the enzyme, whereas the NNRTIs interact with an allosteric site located at a short distance from catalytic site. They were seven NRTIs in 2010 that have been formally approved for the treatment of HIV infections, zidovudine (AZT), didanosine (ddI), zalcitabine (ddC), stavudine (d4T), lamivudine (3TC),abacavir (ABC) and emtricitabine (FTC) [15,19] (Table1and 2). All the NRTIs could be considered as 2`,3`- dideoxynucleoside analogues and act in a similar fashion [16]. In Fig 3 shows example for the mechanism of NRTIs.
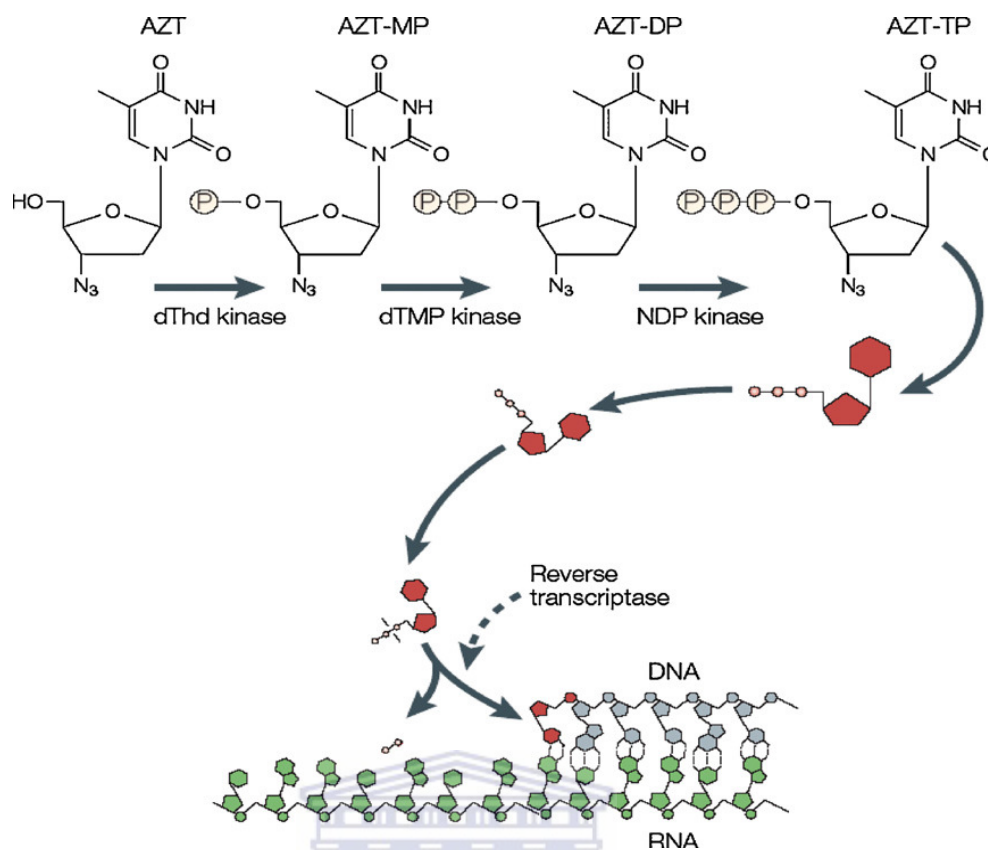
Fig 3: AZT Mechanism of action of Following phosphorylation to its triphosphate form (AZT-TP)

AZT acts as a competitive inhibitor/alternative substrate with respect to dTTP in the reverse transcriptase reaction [20]. But the NRTIs reduced to six, because the Zalcitabine is not any more continue [21].

2.1.2 Nucleotide reverse transcriptase inhibitors (NRTIs)

NtRTIs should be clearly distinguished from the NRTIs as they are nucleotide analogues, which means that they only need two phosphorylation steps to be converted to their active form. Also, they contain a phosphonate group that cannot be cleaved by esterase's, which would make it more difficult to cleaved off these compounds, once incorporated at the 3`-terminal end, compared with their regular nucleotide counterpart. The mode of action of Tenofovir is further illustrated in Fig 4 [16]. After phosphorylation of Tenofovir to its

8

diphosphate, the latter acts as an obligate chain terminator in the reverse transcriptase.

reaction [22].
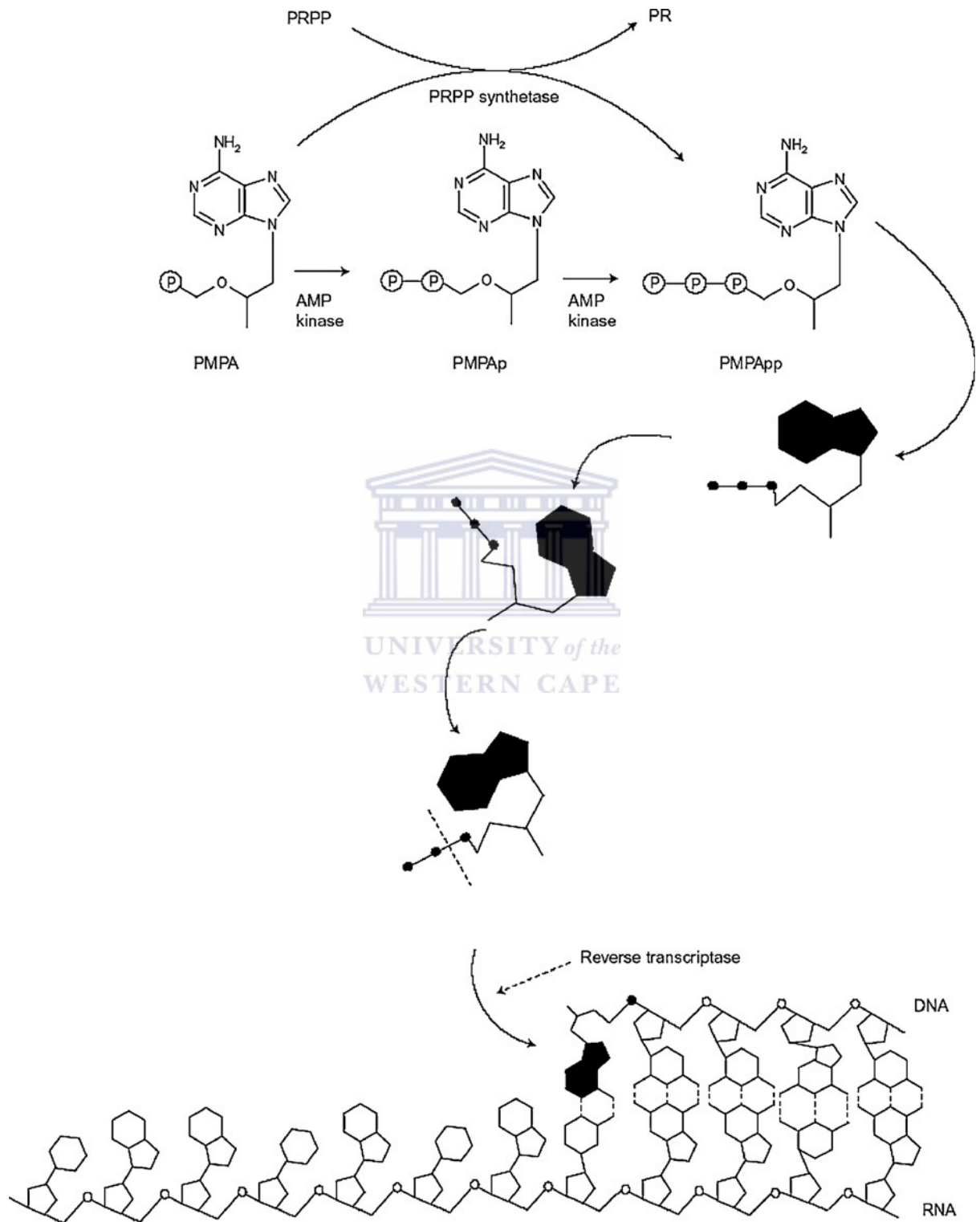
Fig 4: Tenofovir Mechanism of action (from ref. [16])

2.3 General Analytical Methods for Nucleoside and Nucleotide reverse transcriptase inhibitors

High performance chromatography play role in NRTIs detection with the UV-VIS spectroscopy [23].

Dadanosine detected by HPLC-UV assay methods

Table 3: Pharmacokinetic parameters for orally administered didanosine (Adopted from ref. [24])

NRTIs	C_{max} / ng/mL	$T_{max(h)}$	$t_{1/2(h)}$	MRT / h	AUC /ng.h/mL	CL_R /mL/min	UR (%)
Didanosine	1.617± 0.715	0.67±0.19	1.47±0.17	2.12±0.26	2.953±0.851	368±149	17±8

Keys: AUC = The area under the C versus t curve; AUMC = the area under the first moment of the concentration-time curve; C = Concentration; T = Max peak time; $t_{1/2}$ = Elimination half-time; MRT = Mean residence time; UR = Total urinary recovery; CL_R =Renal clearance, were estimated by standard methods [25].

Lamivudine and Zidovudine detected by HPLC-UV methods

Table 4: Analytical performance of HPLC methods for the NRTIs with Uv-Vis detection at 260 nm according to Aymard et al [23]

NRTI	Range of calibration / ng/ mL	Retention time / min	% recovery rate (human plasma)
Lamivudine	20-1000	8.5	80.0±4.2
Zidovudine	10-500	17.4	77.0±4.1

lamivudine concentrations also fix by liquid chromatography-mass spectrometry and intracellular lamivudine-TP concentrations in peripheral blood mononuclear cells by high-performance liquid chromatography/radioimmunoassay methods [26].

Stavudine and Abacavir detected by:

A reversed-phase high-performance liquid chromatography using silica column to detect the stavudine and Abacavir in different wavelength (271 and 230 nm) respectvily, beside that the regression coefficient (r2) of all calibration curve was greater than 0.998. The concentration range was (10 – 10000 ng/mL). The other detections and values in table (4) [27].

Table 5: Analytical performance of a reversed- HPLC methods for the Stavudine and Abacavir (Adopted from ref. [27])

NRTIs	Rerention time (min)	Linearity (mean±SD)	Accuracy	Recovery (%)
Stavudine	15.7	1.396±0.078	94.8 – 104	> 97.4
Abacavir	25.1	1.8719±0.03	101 – 90.5	> 96.8

Tenofovir detection

Tenofovir also known as (phosphorylmethoxy) propyl-adenine [PMPA] is new anti-HIV drug which is a nucleotide reverse transcriptase inhibitor [28,29]. Tenofovir disoproxil fumarate is used for oral management to improve abdominal absorption [30]. The absorption, circulation and intracellular activation of the free Tenofovir occur subsequent to hydrolysis of the pro-drug. Chemically, Tenofovir is a monophosphonate adenosine analogue (as seen in table 1). Tenofovir was determined in human plasma due to a recent increase in use. HPLC has been used to determine Tenofovir in plasma using HPLC coupled with fluorescence and UV detection [31,32]; however, it can not easily detect and quantify tenofovir because of interfering peaks. A rapid and conventional LC-MS method was developed and validated by

estimating the precision and accuracy for inter- and intraday analysis in the concentration range of 0.019-1.567 mg/ml. [33,34].

Pharmacokinetic analysis

Pharmacokinetic parameter for Tenofovir was calculated by noncompartmental methods by use of the WinNonlin software package (version 4.1) and the log/linear trapezoidal rule. On the basis of the individual plasma concentration-time data, the following pharmacokinetic parameters were determined [35].

Eventhough, the study's objective was to investigate if rifampin influences the pharmacokinetics of tenofovir, it gave information regarding the possible plasma concentrations of the drug in question. The period of study was between 10 to 20 days study showed that bioequivalence could be suggested for tenofovir DF combined with rifampin and tenofovir DF given alone and that the combination of tenofovir DF with rifampin was generally well born, under the concentration-time curve from time zero to 24 h (AUC_{0-24}), the maximum concentration of drug in plasma (C_{max}), and the minimum concentration of drug in plasma C_{max}, and C_{min} were 0.84 to 0.92, 0.78 to 0.90, and 0.80 to 0.91 respectively, the data from this study demonstrate that the addition of rifampin to tenofovir DF is well tolerated, and the small decrease in plasma tenofovir levels during combination treatment suggests that these drugs can be co-administered without the need for dose adjust.[35]

Table 6: Pharmacokinetics of tenofovir

Study day and statistics	AUC_{0-24}/ mg · h/ liter	C_{max}/ mg/ liter	C_{min}/ mg/ liter	T_{max}/ h[c]	$t_{1/2}$/ h
Day 10	3.56 ± 0.77	0.36 ± 0.080	0.071 ± 0.016	1.0	13.8 ± 4.5
	(3.48)[b]	(0.36)	(0.069)	(1.0-3.0)	(13.2)
Day 20	3.11 ± 0.57	0.30 ± 0.060	0.060 ± 0.011	1.0	11.6 ± 2.8
	(3.06)	(0.30)	(0.059)	(1.0-2.0)	(11.2)
Geometric mean ratio for day 20/day 10 (90% CI)	0.88	0.84	0.85		
	(0.84-0.92)	(0.78-0.90)	(0.80-0.91)		

[b] Values are arithmetic means ± standard deviations (geometric means), unless indicated otherwise.

[c] Values are medians (ranges).
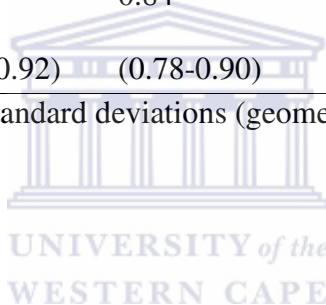
2.3 Electrochemical detection of Nucleoside Reverse Transcriptase Inhibitor

2.3.1 Electrochemical sensors

Electrochemical sensors are chemical sensors in which the chemical information is transduced into an electrical signal [36]

2.3.1.1 Principle of electrochemical sensors

Electrochemistry implies the transfer of charge from an electrode to another phase, which can be a solid or a liquid sample. During this process chemical changes take place at the electrodes and the charge is conducted through the bulk of the sample phase. Both the electrode reactions and/or the charge transport can be modulated chemically and serve as the basis of the sensing process [37]. On the basis of electrical signal which is recorded,

electrochemistry can be divided into amperometric sensors, potentiometric sensors and Conductometric sensors.

2.3.1.2 Potentiometric sensors

In potentiometric sensors, the analytical information is obtained by converting the recognition process into a potential signal, which is proportional (in a logarithmic manner) to the concentration (activity) of species generated or consumed in the recognition event [38]. In such device, use of reference electrode is required to provide a constant half-cell potential.

The change in the potential is related to the concentration of the analyte in a logarithmic manner. Thus, the Nernst equation relates the potential difference at the interface to the activities of species i in sample phases (*s*) and the electrode phase (*β*) and is given by Wang et al [37]:
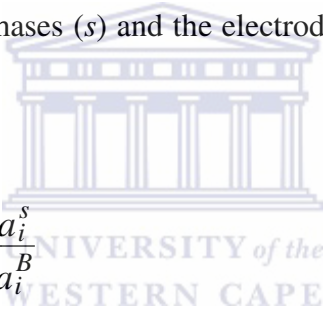
$$E = E_o + \frac{RT}{Z_i} \ln \frac{a_i^s}{a_i^B} \tag{1}$$

where E^o is the standard electrode potential of the sensor electrode; a_i is the activity of the ion, R is the universal gas constant; T is the absolute temperature; F is the Faraday constant and z_i is the valence of the ion. The ion-selective electrode (ISE) for the measurement of electrolytes and for obtaining the potential signal is a common potentiometric sensor [37,38].

2.3.1.3 Amperometric sensors

Amperometry is a method of electrochemical analysis in which the signal of interest is a current that is linearly dependent upon the concentration of the analyte [38]. Amperometric sensors are based on the detection of electro active species involved in the chemical or biological recognition process [37].

The signal transduction process is obtained by applying the potential to the working electrode at a constant value of a reference electrode and monitoring the current as a function of time. That applied potential serves as the driving force for the electron transfer reaction of the electro active species.

The resulting current is flection of the rate of the recognition event, and is proportional to the concentration of the target analyte, because it is a direct measure of the rate of the electron transfer reaction [36].

In redox reactions at the working electrodes, electrons are moving from the analyte to the electrode or to the analyte from the electrode. The direction of flow of electrons can depend upon the properties of the analyte as long as it can be controlled by the electric potential applied to the working electrode [37]. An amperometric cell consists of two or three electrodes, which are working electrode, reference electrode and the counter (or auxiliary).

2.3.1.4 Conductometric sensors

Conductometric sensors are based on the measurement of electrolyte conductivity, which varies when the cell is exposed to different environments. The sensing effect is based on the change in of the number of mobile charge carriers in the electrolyte. If the electrodes are prevented from polarizing, the electrolyte shows ohmic behavior. Conductivity measurements are generally performed with AC supply [36].

Conductivity increases with increasing ion concentration; therefore, it can be used for sensor applications. However, it is nonspecific for a given ion type. On the other hand, both the polarization and the limiting current operation mode must be avoided. Thus, small amplitude alternating bias is used for the measurements with frequencies where the capacitive coupling is not determining the impedance measurement [36].

Table 7: Electroanaylitcal methods for the determination of NRTI are reported between 1990 and 2010 as reviewed by Bonzal et al (2011)[15].

Compound	Electrode/ Platform	Technique	Linear range	LOD	Ref.
Abacavir		DPV	0.80-200 µM	0.220 µM	[39,40]
		SWV	0.80-200 µM	0.118 µM	
		CV	0.10 - 10.0 µM	21.1 nM	
		DPV	0.10 – 10.0 µM	24.1 nM	
		SWV	0.10 – 10.0 µM	26.9 nM	
Didanosine	CoPc-CPE	DPV	2.0 -700.0 µM	0.880 µM	[41]
	FePc-CPE	DPV	1.0-800.0 µM	0.350 µM	
Lamivudine		DPV	4.0 -100.0 µM	62.8 nM	[42,43]
		SWV	4.0-100.0 µM	20.2 nM	
		CAdSV	458.5 – 2.3 µM	0.003 nM	
		DPV	0.09 – 5.73 µM	0.00094 nM	
Zidovudine		SWV		250 nM	[44–47]
		SWV	0.500 nM - 1 µM	1 nM	
	AgHg//Hg	DPV	0.4-1500 µM	0.12 µM	
	AgHg	DPV	0.6-1500 µM	0.20 µM	
	HMDE	DPV	0.03-1900 µM	0.007 µM	
		DPV	0.25-1.25 mg/L	0.0025 mg/L	

DPV = *differential pulse voltammetry;* SWV = *square wave voltammetry;* CV = *cyclic voltammetry*; CAdSV = *Cathodic adsorptive stripping voltammetry;* CoPc-CPE = *Cobalt (II) phthalocyanine carbon paste electrode;* FePc-CPE = *Iron (II) phthalocyanine carbon paste electrode;* HMDE = *Hanging mercury drop electrode;* AgHg/Hg = *Silver amalgam electrode with polished surface;* AgHg = *surface modified by mercury meniscus*.

CHAPTER III: ELECTROCHEMISRY AT THE ITIES: THEORY & APPLICATIONS

A conventional electrochemical set up comprises three electrodes among which we count the working electrode, the counter or auxiliary electrode and the reference electrode. But in the case of electrochemical experiments at the interface between two immiscible electrolyte solutions (ITIES), two counter electrodes and two reference electrodes, one per each phase, are usually required in such a way to measure the potential drop and net ionic charge transfer current across the interface, and in effect the interface acts as the working electrode. ITIES is now regarded as a valuable technique and as such the literature with reference to this type of technique is wider growing.[5,48,49].

3.1 Electrochemistry at the interface between two immiscible electrolyte solutions

In the ITIES experiment, voltage is applied between two reference electrodes positioned on opposite sides of the interfacial boundary, and the current flows between two counter electrodes one in an aqueous phase, the other in an organic phase Fig 5a. The reaction is driven by the voltage applied across the liquid interface, and the measured current arises from ion transfer (IT) or electron transfer (ET) at the ITIES. An ET reaction at the ITIES can be represented as

$$Ox1(aq) + \mathrm{Re}\,d2(org) \Leftrightarrow \mathrm{Re}\,d1(aq) + Ox2(org) \tag{2}$$
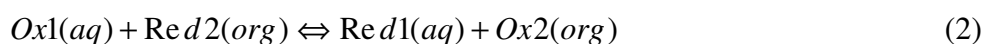
In which Ox1/Red1 and Ox2/Red2 are the aqueous and organic redox couples, respectively. A simple IT reaction involves reversible transfer of a cation or anion between two immiscible liquid phases. If one of the two phases typically, the organic solvent contains a ligand L that can react with ion X to form a complex, such a reaction can assist the transfer of X.

$$X^{+}(aq) + nL(org) \Leftrightarrow X\,L_{n}(org) \tag{3}$$
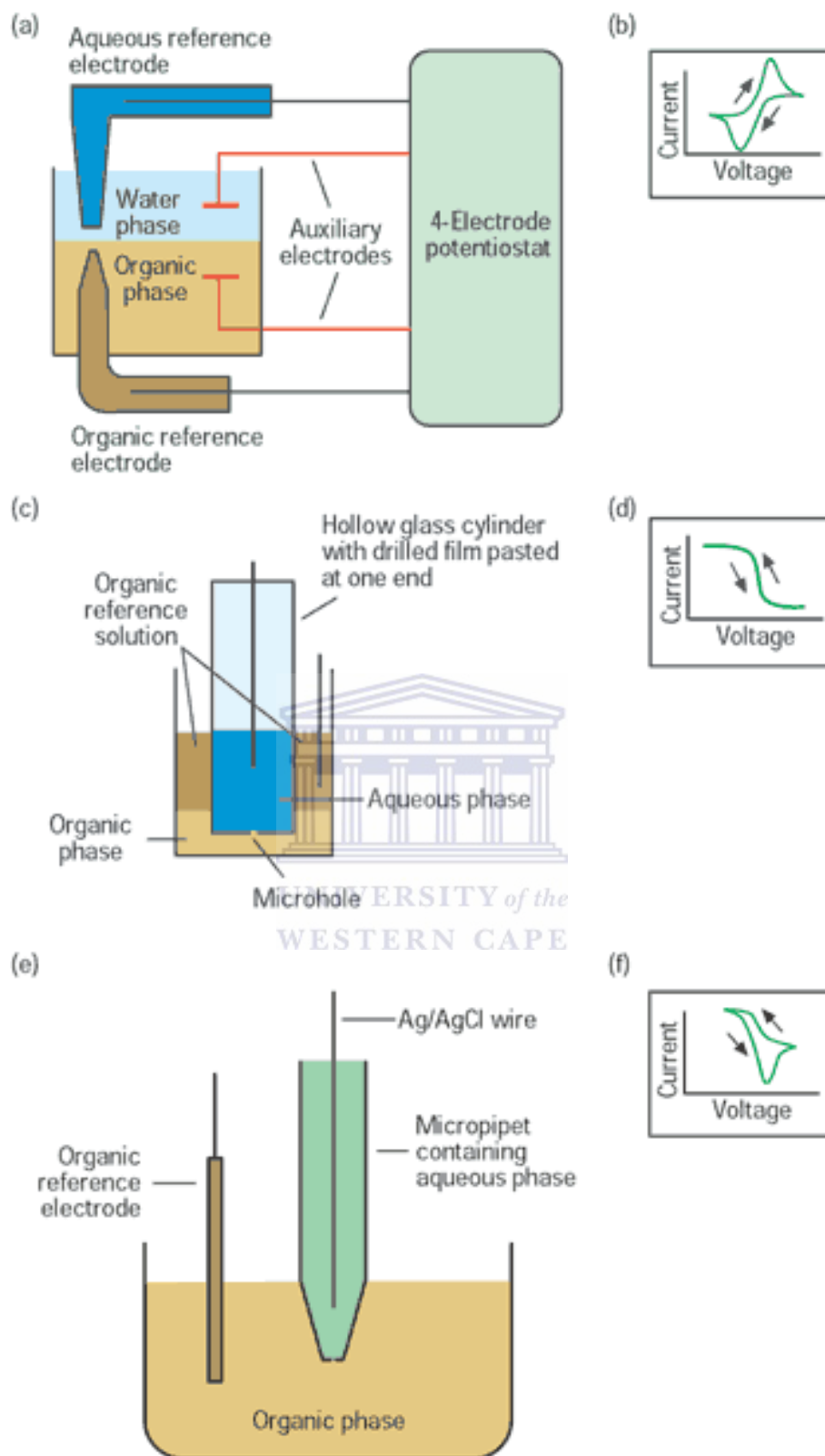
Fig 5: Schematic of voltammetric experiments at (a) a macroscopic and microscopic ITIES supported

at (c) a microhole and at (e) a micropipette. (b, d, and f) The corresponding cyclic

voltammograms. Adapted from Liu & Mirkin [48].

Assisted IT reactions usually require less driving force (i.e., lower external voltage) than the simple transfer of the same ion. When the interfacial area is large, a four-electrode setup (Fig 5a) is necessary to minimize the potential drop in a resistive organic solvent [5,49].

When looking at cyclic voltammograms of IT and ET reactions at the macro-ITIES Fig 5b, they look similar to conventional voltammograms obtained at metal electrodes. As such, the height of a voltammetric peak is still proportional to the concentration of one of the reactants, whose diffusion is rate-limiting, and to the square root of the potential sweep rate. In the case of micrometer-sized interface i.e. micro-ITIES, the resistive effect is less important, and the easier two-electrode set-up represented in Fig 5c and 5e can therefore be used [50].

In such experiment, the current is limited by the spherical diffusion of a reagent to a micrometer-sized orifice of a microhole Fig 5c or a micropipet Fig 5e and sigmoidal steady-state voltammograms can be obtained (Fig 5d and 5f. The diffusion limiting current is proportional to the reagent concentration and independent of the potential sweep rate. In the case where the linear diffusion of ions inside the narrow shaft of a pipet is rate-limiting, peak-shaped voltammograms are obtained with micropipets as in Fig 5f [48].

The presence of the second liquid phase usually augments versatility to electrochemical experiments at the ITIES. A large group of IT reactions occur at the ITIES but not at solid electrodes. Reactions involving substances of different polarities can be conducted, and the permeation of ionic species through bio membranes can be modeled.

3.2 Amperometric sensors and detectors

In the ITIES, the equilibrium potential difference is determined by the activities of the common ion when it is present in both liquid phases just like in potentiometric ion-selective electrodes (ISEs). Moreover, the diffusion-controlled IT current at the ITIES is proportional

to the concentration of the transferred ion. Thus, the ITIES can also be used as an amperometric ISE [51].

Because their selectivity may be tailored by the polarization potential, amperometric systems possess an advantage over a potentiometric ISEs. It is therefore possible to determine two or more ions simultaneously if their half-wave potentials are reasonably well separated. An example is an amperometric ISE using a nitrobenzene/water ITIES for the determination of K^+ and Na^+ in drinking water [48]. Some of these devices already on the market have been used for measuring various analytes in food, pharmaceutical products, toxic water, and industrial samples [52].

Unfortunately, wider development of transducers based on ITIES has been used toxic and high-electrical resistive organic solvents, and by the mechanical instability of liquid/liquid interfaces. To solve the toxicity problem, less toxic solvents, such as 2-nitrophenyloctylether, are replacing traditional media, such as nitrobenzene or 1,2-dichloroethane [48].

Micro-ITIES can be used to minimize the ohmic potential drop problem and analyze small samples. For example, Osborne et al. used a microhole-based ITIES Fig 5c to determine aqueous NH_4^+ at the water/1,2-dichloroethane (DCE) interface [53].

Ammonium's transfer was assisted with DB18C6. Because the ionophore concentration in the organic phase was high, the measured steady-state current was proportional to the concentration of NH_4^+ in the aqueous phase [54].

Ammonium's transfer was assisted with DB18C6, because the ionophore concentration in the organic phase was high, the measured steady-state current was proportional to the concentration of NH_4^+ in the aqueous phase [54].

Ohkouchi, Kakutani, Osakai, & Senda investigated the transfer of acetylcholine (Ach$^+$) by steady-state voltammetry at the tip of a micropipette at a nitrobenzene/water interface [55]. Both the height of the sigmoidal wave for the Ach$^+$ transferred into the pipet and the peak current of the reverse IT reaction were proportional to the bulk concentration of Ach$^+$ in water.

An experimental approach similar to conventional stripping voltammetry improved the sensitivity of ion detection. During the first step (~1 min-long accumulation), a sufficiently negative potential was applied to the nitrobenzene-filled pipet to induce Ach$^+$ to enter from the outer aqueous solution. This was followed by a potential sweep in the positive direction, which expelled Ach$^+$ from the pipet.

With ion concentration in the aqueous phase down to 5 µM Ach$^+$, the peak height was proportional to the square root of the accumulation time. Using a similar technique, Katano & Senda determined nano molar concentrations of polyoxyethylene nonionic surfactants [56]. The stripping voltammetric technique was also successfully used at macro-ITIES for determining Hg (II) and Pb (II) in water, with detection limits as low as 1.6 ppb and 1 ppb, respectively [57].

A lot of work has been done to increase the mechanical stability of liquid/liquid systems by gelling the organic or aqueous phase [52]. Typically, the organic phase has been solidified by adding polyvinylchloride (PVC), and the aqueous phase has been solidified by adding agar.

Different gelling agents, such as 1,3:2,4-dibenzylidene sorbitol, have also been used to prepare organic gels with ionic conductivities similar to electrolyte solutions [58]. Although the diffusion coefficients of ions in gels are significantly reduced, the IT processes could still be used for amperometric detection.

The gelation of the organic phase often increases resistivity, which impedes amperometric determination. Using arrays of liquid/liquid micro interfaces could lessen this problem [54]. Urea and creatinine sensors based on amperometric detection of NH_4^+ were fabricated using this approach.

Recently, Lee, Beattie, Seddon, Osborne, & Girault prepared micro fabricated composite polymer membranes, which combine the advantages of the gelled organic phase and micro-ITIES [59]. The composite membrane consists of a thin, inert, micro perforated polymer layer, which is covered by PVC-2- nitrophenyloctylether (PVC-NPOE) electrolyte gel. The composite membrane electrode can be incorporated into a flow cell.

The IT behavior of the microhole array interface between an analyte solution and a PVC gel electrolyte was similar to that of a conventional micro-ITIES. When the composite polymer membrane was used for the amperometric sensing of choline, the plot of the diffusion-limiting current against the concentration was linear over the range 0.1– 0.9 mM [59]. Sensors for alkali metal ions were produced by adding ionophores (e.g., DB18C6, valinomycin) to the PVC membrane [60].

Another approach to stabilizing the liquid/liquid interface is to insert a thin, porous, hydrophilic Another approach to stabilizing the liquid/liquid interface is to insert a thin, porous, hydrophilic or hydrophobic membrane between the two phases [61]. Such a membrane-stabilized ITIES was used as an amperometric sensor for the flow-injection analysis (FIA) of alkali metal ions, halides, and other anions [61–63]. A successful, simultaneous determination of K^+ and Na^+ in blood serum suggests promising applications of this approach for clinical analysis [62].

The ITIES can be used to detect ionic solutes in FIA and HPLC, In ion-exchange chromatography, a composite polymer membrane showed detection limits similar to those of a conventional conductivity detector [64]. However, an amperometric detector based on a micro-ITIES can offer even higher selectivity by choosing the proper ionophore. For example, introducing an NH_4^+-selective ionophore, such as valinomycin, into the gel membrane substantially increases the selectivity of the detector toward NH_4^+ in the presence of excess Na^+ [64].

A composite polymer membrane detector has been used for the FIA of halides, NO_3^-, and SO_4^{-2} [65]. By using the dual-potential-pulse mode and pure water as an eluent, the detection limit for the anions could be lowered to the parts-per-trillion level. More recently, a microhole-based ITIES amperometric detector for capillary zone electrophoresis determined choline and Ach^+, and aryl sulfate and sulfonate anions in four different determinations [66]. The detection limit in all cases was ~1 μM.

An ITIES supported at a dual-pipet consisting of two closely spaced pipets filled with aqueous solutions and separated by a sub micrometer-wide band of glass [67] was used as a gas sensor [68]. When the outer glass surface is not salinized, the pipet orifices are linked by a thin aqueous film on the outer pipet wall. Such a film can be sufficiently thick and conductive to yield reasonable quality voltammetric responses that are suitable for qualitative and quantitative analytical determinations.

The response of a dual pipet is largely determined by the properties of the aqueous surface layer and is very sensitive to changes in film composition. Such changes occur when the pipet is exposed to a soluble gas.

The IT voltammograms of NH_4^+ and NO_3^- were obtained with a dual pipet in which one barrel was filled with an aqueous solution and the other with an organic phase exposed to vapors of NH3 and HNO3 [68]. The IT current was linear with the concentration of analyte in the vapor generating solution. The surface liquid layer in all the pipets used in this work was aqueous, and only the detection of water-soluble gases was discussed. However, it may also be possible to detect organic compounds in the gas phase using a dual pipet with a no aqueous sensing film.

3.3 Ion partitioning and drug delivery testing

The pharmacological activity of a drug is largely determined by its ability to permeate lipid cell membranes. Permeation depends on the physicochemical properties of the drug, particularly on its lipophilicity, which is conventionally evaluated from the drug partitioning between water and octanol [69].

Because octanol can form hydrogen bonds, the water–octanol partitioning of a polar substance may not always be a good measure of lipophilicity. Hence, a drug's ability to permeate cell membranes or cross the blood–brain barrier does not always correlate well with its water–octanol partition coefficient [51].

The partition coefficient, P, of an ion species, i, in a biphasic system is defined as:

$$p_i = \frac{a_i^o}{a_i^w} \qquad\qquad (4)$$

In which "a" is the activity of the ion in the organic, o, and aqueous, w, phases. At thermodynamic equilibrium, the partition of an ionic species is described by the Nernst equation:

$$\Delta_o^w \phi = \Delta_o^w \phi_i^o + \frac{RT}{z_i F} \ln\left(\frac{a_i^o}{a_i^w}\right) \tag{5}$$

In which $\Delta_o^w \phi$ is the interfacial voltage, $\Delta_o^w \phi_i^o$ is the standard IT potential, and z_i is the charge of the ion. When Equations 3 and 4 are combined and rearranged, lipophilicity can be measured directly by:

$$\ln p_i^o = -\frac{z_i F}{RT} \Delta_o^w \phi_i^o \tag{6}$$

In which $\ln p_i^o$ is the partition coefficient when the interface is not polarized (i.e., $\Delta_o^w \phi = 0$).

For a reversible transfer of a simple ion, $\Delta_o^w \phi_i^o$ is related to the half-wave potential by:

$$\Delta_o^w \phi_i^o = \Delta_o^w \phi_{1/2} - \frac{RT}{2z_i F} \ln\left(\frac{D_i^w}{D_i^o}\right) \tag{7}$$

Thus, the partition coefficient of an ion can be assessed from cyclic voltammograms, and the half-wave transfer potential of an ionizable compound can be used to characterize its lipophilicity. The value of $\Delta_o^w \phi_{1/2}$ can be easily found from an experimental voltammogram because it is equal to the mid peak potential, $(\Delta\phi_{pa} + \Delta\phi_{pc})/2$, in which $\Delta\phi_{pa}$ and $\Delta\phi_{pc}$ are the anodic and cathodic peak potentials, respectively.

Hence, IT voltammetry at the ITIES is a suitable technique for evaluating the lipophilicity of ionic drugs [48]. Extensive voltammetric studies of local anesthetics, such as procaine; antihistamines, for example, doxylamine; and uncouplers, such as 2,4-dinitrophenol, have been reported [49].

Assuming that the transfers of all relevant species across the ITIES are diffusion-controlled, theoretical $\Delta_o^w \phi_{1/2}$ versus pH dependences were obtained and used to evaluate the physicochemical properties of drugs. Reversible Nernstian behavior was demonstrated for different types of drugs.

For example, in cyclic voltammograms of procaine at the interface between nitrobenzene and 10-mM aqueous acetate buffer, the anodic peak height was proportional to the square root of the potential scan rate within the range 5–100 mV/s, and the peak potential separation was close to the 58-mV value, which is characteristic of the reversible univalent IT.

The partition coefficient of procaine, the formal transfer potential of protonated procaine, and the dissociation constants of the first and second protonation–deprotonation reactions were obtained from the half-wave potential versus pH dependence.

The relationship between pharmacological activity and half-wave transfer potential has been established for a number of ionizable drugs [5]. For example, many barbiturate derivatives are weak acids and are transferred across the ITIES as anions. The $\Delta_o^w \phi_{1/2}$ of these ions becomes more positive with an increase in lipophilicity.

Conversely, of $\Delta_o^w \phi_{1/2}$ for some cationic anesthetic drugs becomes more negative with increasing lipophilicity. In either case, the higher lipophilicity corresponds to greater pharmacological activity. A strong correlation between the pharmacological activity and the half-wave potential was found for the families of hypnotic, anesthetic, cholinergic, and adrenergic drugs [5].

Many drugs are weak electrolytes that can undergo protonation–deprotonation reactions. The transfer of such species across the ITIES depends on the interfacial potential drop, the pH of the aqueous phase, and the drug's dissociation constant. Lee et al. constructed ionic partition diagrams Fig 6 that define the domains of predominance for all the species present in the aqueous and organic phases as a function of interfacial voltage and aqueous pH [70].

Partition diagrams offer a simple way to visualize all species at the ITIES, predict the nature of the transferring species, and describe the transfer mechanism of ionizable solutes. Such information can greatly improve our understanding of how drugs cross cellular membranes to reach their biological targets.
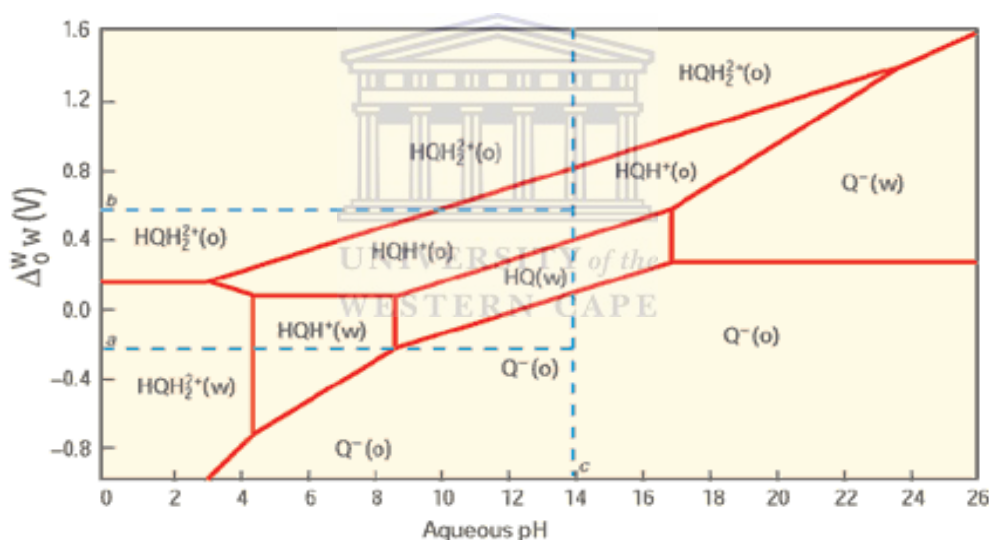
Fig 6: Ionic partition diagram showing transfer mechanisms of various forms of quinidine at the DCE/water interface. Adapted from Frederic Reymond et al. [70]..

HQH_2^{2+}, HQH^+, HQ, and Q^- stand for the doubly protonated, singly protonated, neutral, and deprotonated species, respectively. The solid red lines are the theoretical equiconcentration lines between two adjacent species. The blue lines a and b define the potential limits beyond which Li^+ and TBA^+ transfer preferentially. The domain above pH 14 (blue line c) is beyond experimental reach.

3.4 Cyclic voltammetry (CV)

Cyclic voltammetry (CV) is a very useful electrochemical technique in every parts of chemistry, for example the characterization of electroactive species in modern analytical chemistry, electrochemistry, and biochemistry [71].

Cyclic voltammetry provided information about the electroactive species by measuring the faradic current as a function of applied potential. The current response is measured by applying a potential ramp starting from an initial potential to a first switching potential and at this potential the direction of the potential is reversed and the same potential range is scanned in the opposite direction (hence the term "cyclic"). On the process, the electro active species formed by reduction or oxidation depending on the direction can be oxidized or reduced or on the reverse scan.
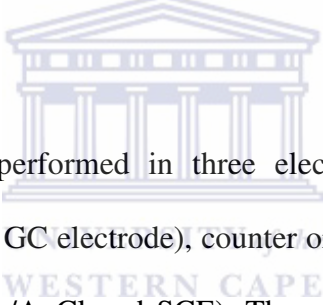
Cyclic voltammetry is usually performed in three electrode arrangement (the working electrode usually being Pt., Au or GC electrode), counter or auxiliary electrode and reference electrode (in aqueous solution Ag/AgCl and SCE). The potential is applied to the working electrode with respect to a reference electrode and the current is measured between the counter and working electrode [71,72]. The current measured between the working electrode and the counter electrode is plotted against the applied potential relative to the reference electrode to give the cyclic voltammogram. Usual cyclic voltammograms of a reversible processes is shown in Fig 7.
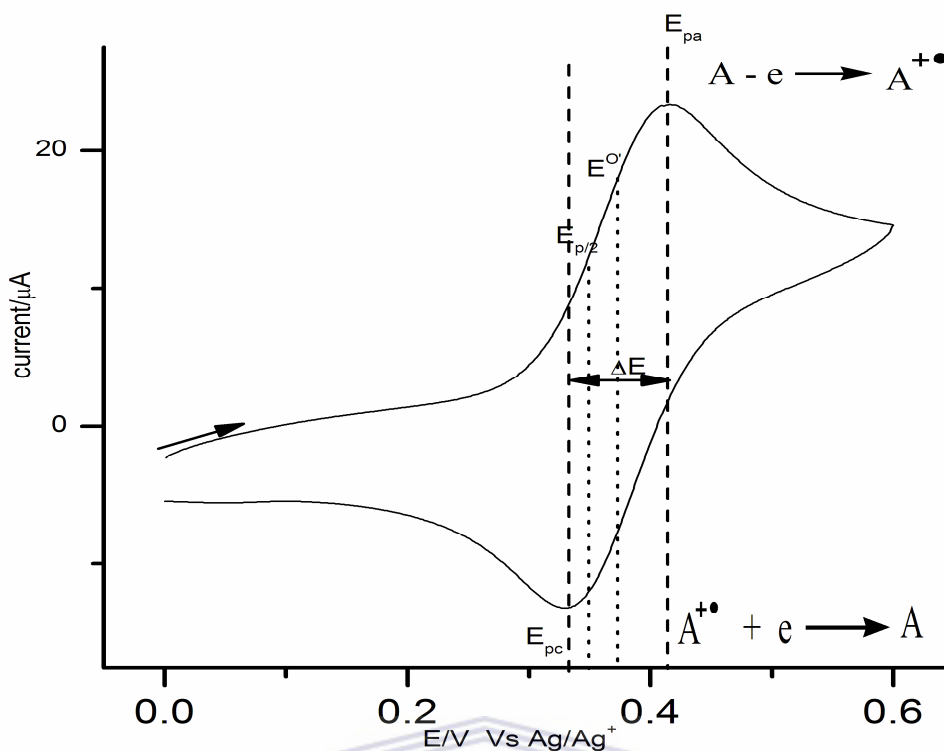
Fig 7: Typical CV of a reversible process.

The following equations can be used for a reversible process to evaluate the electrochemical parameters' from cyclic voltammetry.

Randles –Sevcik equation: $i_p = 0.446 FA \left[\dfrac{F}{RT}\right]^{\frac{1}{2}} n^{\frac{3}{2}} D^{\frac{1}{2}} C \, v^{\frac{1}{2}}$ (8)

$$E^{o'} = \frac{E_{p,c} + E_{p,a}}{2}$$ (9)

$$\Delta E_p = \frac{58}{n} mV \quad \text{at } 25\,^{o}C$$ (10)

$$E_{p/2} = E_{1/2} + 28 mV \quad \text{at } 25\,^{o}C$$ (11)

Where i_p is peak current/A, *F* is Faraday constant (96, 487 C/mol), *D* is diffusion coefficient/cm/s of the electroactive species, *A* is the area of the electrode/cm^2, *v* is the sweep rate/V/s, *R* is the general gas constant (8.413 J/mol K) and T is temperature $25°C$).

CHAPTER IV: EXPERIMENTAL

4.1 Chemicals

- Acetonitrile (Sigma-Aldrich, ≥99.9%, product#34998)

- NH_4Cl (Merck, 99.8%, product# AC001145)

- $(NH_4)_2SO_4$ (Kimix, 99%, product #47k12/0410)

- 1-Butyl-3-methyl-Iimidazolium bis(trifluoromethylsulfonyl)Imide (Merck, product# S5205492031)

- Dibenzo-18-Crown-6 (Fluka, ≥98%, product# 33531)

- 1, 2 Dichloroethane (Sigma-Aldrich, ≥99%, product # 319929)

- Ethyl Violet (Sigma-Aldrich, product#228842)

- Li_2SO_4 (Sigma-Aldrich, ≥98.0%, product# 62613)

- Methyltrioctylammonium bis(trifluoromethylsulfonyl)imide (Fluka, ≥97%, product# 00797)

- $MgSO_4$ (Sigma-Aldrich, ≥99.5%, product# M7506)

- Nitrobenzene (Fluka, ≥99.5%, product # 7298).

- 2-Nitrophenyl octyl ether (Fluka, ≥99%, product#73732)

- KCl (Sigma-Aldrich, ≥99.9%, product#P-3911).

- K_2SO_4 (Kimix, 99%, product# k1710311)

- 1-Propyl-3-methyl-limidazoliumbis(trifluoro-methylsulfonyl)imide(Merck, product#EQ413728850)

- Sodium tetraphenylborate (Sigma-Aldrich, ≥99.5%, product# T25402)

- Tenofovir disoproxil fumarate as brand name Viread, (tablets) was obtained from M-KEM Medicine City, Bellville.

- Tetrabutylammonium tetraphenylborate (Sigma-Aldrich, 99%, product# 281034)

- Tetradodecylammonium tetrakis(4-chlorophenyl)borate (Fluka, product# 87255)

- Tetraphenylphosphnium tetraphenylborate (Fluka, product # 88065)

4.2 Materials

A cellulose tube dialysis sack (Product # 250-7U, SIGMA Diagnostics, Inc, St. Louis, USA) was adapted as membrane in the liquid-liquid interface based sensor used in this study. The specified cut-off size for retention of proteins was 12000. It was always stored dry at 18-26 C° in a vacuum desiccator. A measured (2.5 cm x 2.5 cm) piece of the flattened dry membrane was cut off, sliced into halve, and moisten with water immediately before use.

The Teflon rods used for constructing sensor body (or organic phase holder) were obtained from MAIZEY, Bellville (Stikland), South Africa

Silver and platinum wires were obtained from Sigma Aldrich
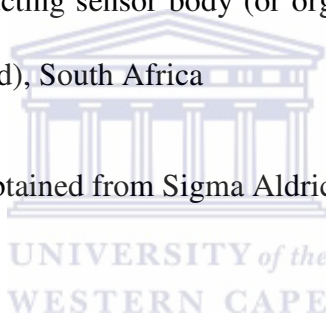
4.3 preparations of solutions

An ultrapure de-ionized (DI) water (18 MΩ cm) produced by a reverse osmosis/ ion-exchange combined water purification system (Rios ^{TM} 3/ Synergy, Millipore) was used for the preparation of all reagent solutions and experimental steps where necessary.

Aqueous lithium sulphate (100 mM)

100 mM of lithium sulphate solution was prepared by dissolving 1.0902 g of lithium sulphate salt in 100 mL volumetric flask with of deionised (DI) water).

Aqueous Ammonium chloride (1000 mM)

The mass of 1.0993 g ammonium chloride salt was dissolved in 10 mL volumetric flask with DI water to prepare 1000 mM of ammonium chloride solution.

Aqueous Potassium chloride (100 mM)

Potassium chloride solution, 100 mM was prepared by dissolving 0.7450 g of potassium chloride salt into 100 mL volumetric flask with DI water.

Aqueous Magnesium sulphate (100 mM)

100 mM of magnesium sulphate solution was prepared by dissolving 1.2038 g of magnesium sulphate salt in a volumetric flask (100 mL) with DI water.

Aqueous Ammonium sulphate (50 mM)

0.06607 g of ammonium sulphate was dissolved in 10 mL DI water to prepare 50 mM of aqueous ammonium sulphate solution. 4.3.6 Aqueous Potassium sulphate (50 mM)

Aqueous Potassium Sulphate *(50 mM)*

The solution of 50 mM potassium sulphate was prepared by dissolving 0.8713 g of potassium sulphate salt with DI water in 100 mL volumetric flack.
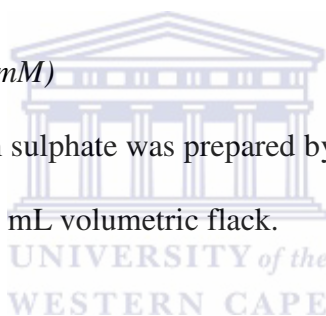
4.4 Preparation of organic electrolyte solutions

In this study nitrobenzene (NB), 1, 2-dichloroethane (DCE) and 2-nitrophenyloctyl ether (NPOE) were used as solvents to prepare the following hydrophobic electrolyte solutions (organic phase) which were always stored in the dark. When indicated these solutions were also equilibrated with DI water.

Preparation of 10 mM *ETH500 in NB*

0.1361 g of ETH500 powder was dissolved with 10 mL of NB measured using micro-pipette into a brown glass bottle

33

Preparation of the mixture of 10 mM ETH500 and 50 mM DB-18-C-6 in NB

0.1361 g of ETH500 and 0.1802 g of DB18C6 were dissolved in 10 mL of NB with or few minutes of gentle shaking to homogenize the solution.

Preparation of 10 mM *TBATPB in NB*

The solution of 10 mM of TBATPB was prepared by dissolving 0.0323 g of TBATPB powder with 5 mL of NB into a brown glass bottle.

Preparation of 10 mM TPphTPB in NB

0.0538 g of TPphTPB was dissolved 5 mL of NB in a brown glass bottle containing.

Preparation of 10 mM IL1 in NB

296 µL of IL1 was pipette out into a brown glass bottle containing 5 mL of NB and shaken gently to homogenize the solution.
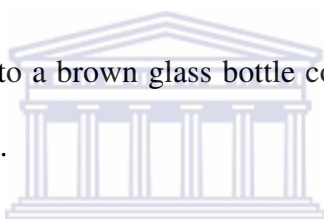
Preparation of 10 mM EthVTPB in NB

EthVTPB was prepared based on a procedure adapted from in the literature [73,74] 0.6954 g of ethyl violet and 1 g of sodium tetraphenylborate were mixed together in DI water in stoichiometric amounts under stirring at 25°C. After three hours, a blue solution was obtained and filtered using suction filtration (Fig. 8) and washed with small quantity of DI water. The resulting filtrate was left at room temperature for drying and the blue powder of EthvTPB with iridescent green surface was. 0.0354 g of this product was weighed out into a brown glass bottle and dissolved in 5 mL NB.
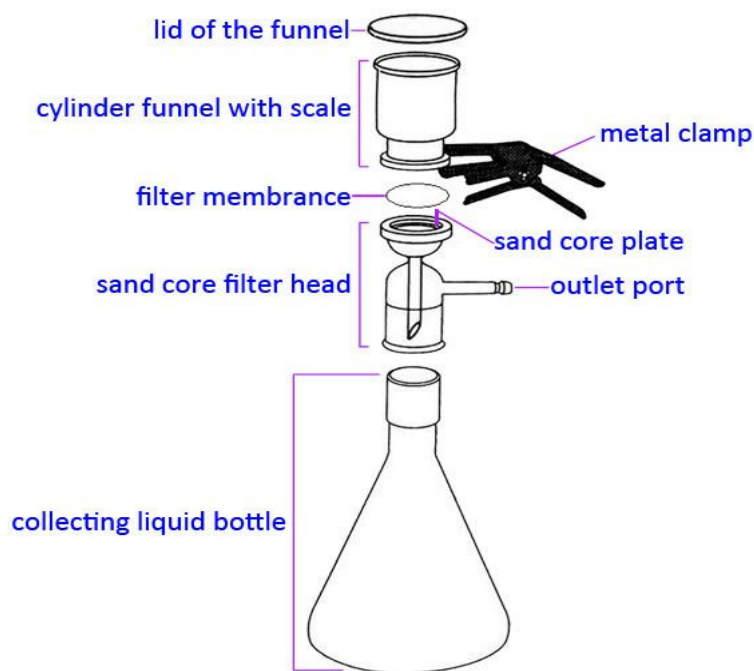
Fig 8: Suction filtration set-up (Adapted from ref [75])

Preparation of 10 mM ETH500 in DCE

0.0572 g of EHT500 was dissolved into brown glass bottle with 5 mL of DCE and 10 mM of ETH500 solution was prepared.

Preparation of 10 mM IL1 in DCE

The volume of 296 µL of IL1 was pipette into a brown glass bottle and 5 mL of DCE was added with micro-pipette also. The mixture was shacked and 10 mM of IL1 solution was obtained.

Preparation of 10 mM ETH500 in NPOE

10 mM of ETH500 solution was prepared by dissolving 0.1140 g of ETH500 powder into a brown glass bottle with 10 mL of NPOE.

Preparation of 10 mM IL1 in NPOE

296 µL of IL1 was pipette out into a brown glass bottle and 5 mL of NPOE was added, the resulting mixture was gently shaken to homogenize it, and always stored in the dark.

Preparation of tenofovir solution10 mM

From the literature, it was found that the tenofovir dissolve in water at 25Cº and methanol [76,77],one tablet was weighed correctly (0.6995 g) and crushed to fine powder using mortar and pestle. An accurately weighed powder equivalent to 0.6485 g of tenofovir was transferred to 50 mL volumetric flask and volume made up to 47 mL with DI water. After that the solution was centrifuged for 20 minutes (speed×1000, 14.5 rpm) adopted from literature [76]. From this stock solution another sample solution of drug was prepared (0.1 mM) by dilutions with DI water. The solution stored in freezer +8Cº.

Fig 9: Centrifuge

4.5 Instrument

Cyclic Voltammetry (CV) experiments were carried out using a MOD-7050 potentiostat (AMEL instrument, Milano Italy) connected to a personal computer through a USB electrochemical interface. All measurements were made at 25°C.

4.6 Liquid-Liquid Interface Ion Transfer Electrochemical Cell Set-up

An in-house made PTFE-based tubular nut (tip *i.d.* = 4 mm), bolt, and O-ring kit was used t constitute a four-electrodes cell shown in **Fig 7** with two reference electrodes, one in the organic (O) phase and the other in aqueous (W) phase (between which applied potentials were measured), and two corresponding counter electrodes to carry and measure the current flow across the O/W interface. The reference electrode in organic phase was merely a Ag wire pseudo reference electrode; the reference electrode in aqueous phase was Ag/AgCl or Ag/Ag$_2$SO$_4$ as indicated. Both counter electrodes were Pt wires. Various hydrophobic electrolytes were employed to serve as the organic phase, but mostly those composed of either of NB, 1, 2-DCE and NPOE and 10 mM of a hydrophobic salt, particularly ETH500 with or without the ionophore DB18C6 (50 mM). The aqueous phase was either aq. Li$_2$SO$_4$ or aq. MgSO$_4$ at 50 mM or 100 mM concentration.
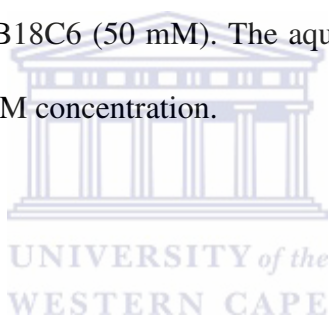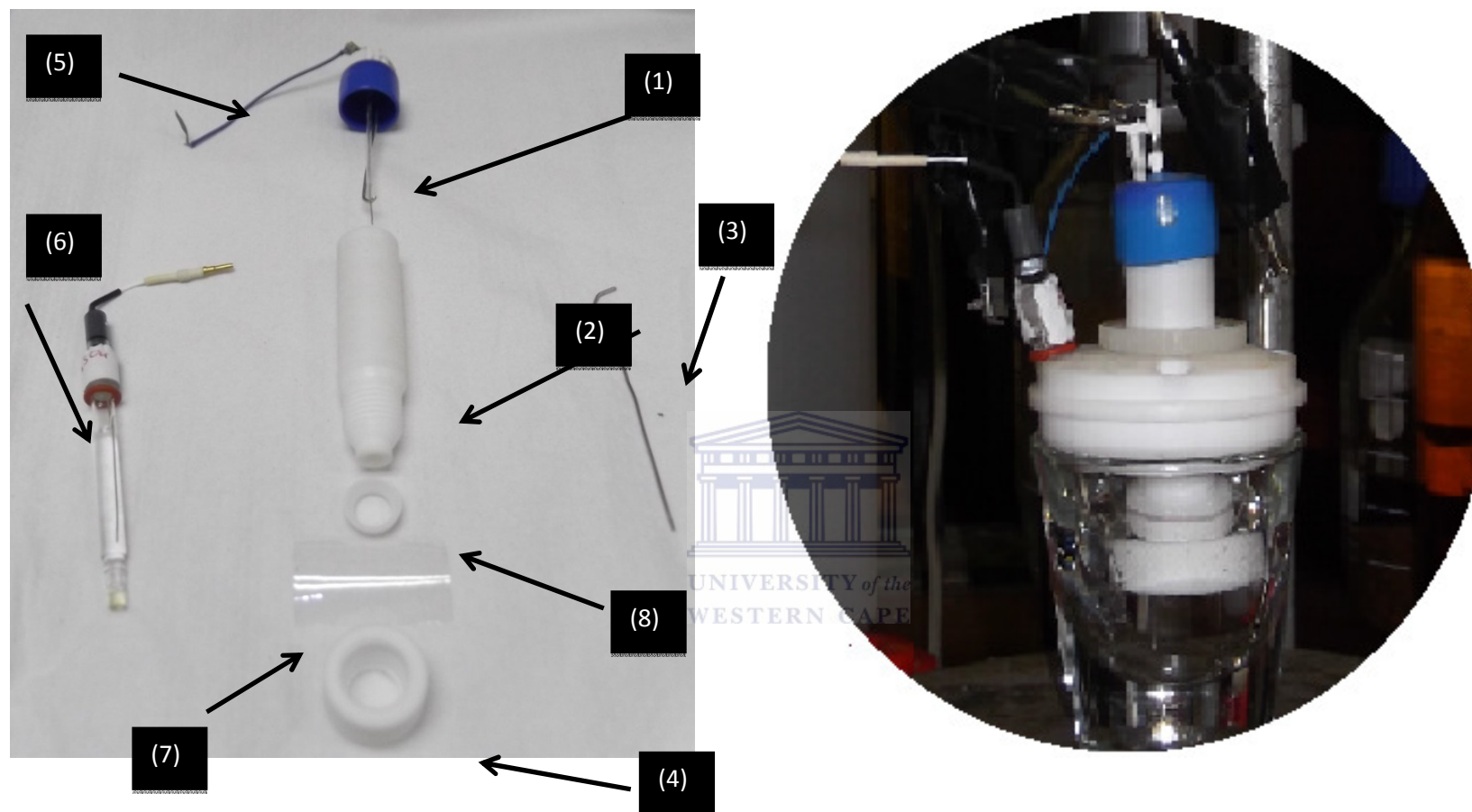
Fig 10: Photograph of parts of the organic phase device (left) and the assembled four-electrode cell (right) for studying membrane stabilized liquid-liquid Interface ion-transfer electrochemical cell: Pt wire counter electrodes (1 and 3), PTFE tubular-bolt (2), PTFE nut (4), Ag-wire pseudo reference electrode (5) for organic phase, Ag/AgCl or Ag/Ag_2SO_4 reference electrode (6) for aq. phase, dialysis membrane (7), and PTFE O-ring (8)
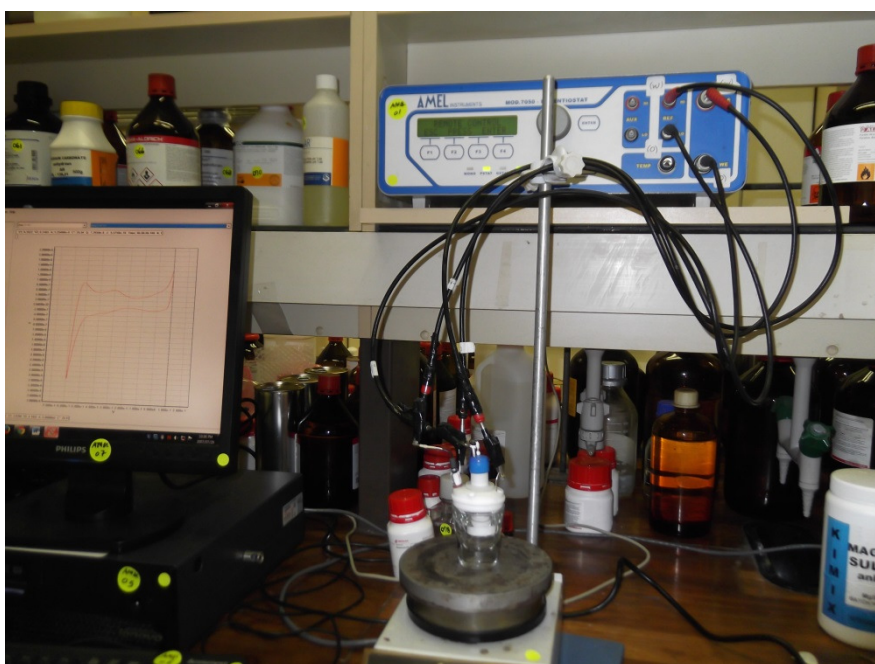
Fig 11: Photograph of cell connected with AMEL instrument and the output shows in the PC.

4.7 Preliminary studies

The project was started with preliminary studies with the objective of screening different traditional solvents (NB, DCE and NPOE), hydrophobic salts (ETH500, TBATPB, TPphTPB, EthVTPB) as well as ionic liquids (IL1, IL3 and IL4) for organic phase applications in the envisaged polarizable liquid-liquid interface-based sensors for tenofovir. CVs of the interfaces of these solutions with aq. Li_2SO_4 were recorded, both in the absence and the presence of K^+ and NH_4^+ ions, and of tenofovir (if indicated) in the aq. phase. Initially only NB was used as the only solvent to compare these salts in NB. Whereas the pure ILs were first tested as self-sufficient organic electrolytes. As IL1 was found to form the most polarizable interface with aq. Li_2SO_4, its solution in NB was then tested against the same aq. phase. Two parameters used to measure the relative friendliness of a liquid-liquid interface to sensor applications were: potential window and capacitance. Two salts were then selected and their solutions in NPOE and DCE were compared similarly. This time, the

ionophore DB18C6 was also incorporated as the third component of the organic phase. Aq. MgSO$_4$ was later on tested as additional hydrophilic salt. It will be shown that, also based on extra-electrochemical consideration, the most suitable organic phase was the solution of ETH500 in DCE against aq. MgSO$_4$.

4.8 Analytical operation and performance of liquid-liquid interface sensor for tenofovir

Cyclic voltammetry is a fast electroanalytical technique used in electrochemical sensor not only to detect and quantify an analyte, but also to estimate its kinetic and thermodynamic properties. Therefore, additional CVs in the presence of tenofovir (0.2 mM) in the aq. phase were recorded at different scan rates without with DB18C6 in the organic phase in order to demonstrate the detection of the analyte and evaluate the rate limiting step in its transfer across the interface. In addition, the stability of sensor was studied by running time-laps CVs for about 3 hours at same scan rate and fixed concentration of tenofovir. From this experiment the suitable time for conditioning the sensor for reproducibility was found. As well as linearity ranges and detection limits, partition coefficients of tenofovir were evaluated from the data of peak heights and peak potentials vs concentrations collected at a selected (optimal) scan rate.

CHAPTER V: RESULTS AND DISCUSSIONS

Ion transfer amperometric studies were carried out with a four-electrode cell and various membrane-stabilized liquid-liquid interfaces between a hydrophobic electrolytes solution (organic (O) phase) and two hydrophilic electrolyte solutions (water (W) phases). The O phases were composed of the hydrophobic salts ETH500, TBATPB, EthvTPB, TPphTPB, as well as three hydrophobic ionic liquids (IL) dissolved in three different polar hydrophobic solvents, namely, nitrobenzene (NB), dichloroethane (DCE), and nitrophenyloctylether (NPOE). The W phases studied were aq. Li_2SO_4 and $MgSO_4$. The three ILs were also tested without the need to incorporate an additional hydrophobic salt.

CV of K^+ and NH_4^+ added to the W phase were also measured for reference potential as well as for performance evaluation purposes. Since the main aim of the research was to develop sensors, the construction of the four electrode cell was simplified by simply using a Ag wire pseudo reference electrode (RE) in the organic phase (Ag(O), while in the aqueous phase a standard Ag/AgCl or homemade Ag/Ag_2SO_4 REs were employed. As a result of this the potentials measured in this manuscript do not solely represent the potential across the O/W interface ($\Delta_W^O\varphi$) unlike those in the literature, where identical reference electrodes are used in both O and W phases may somehow offset each other. Thus, in this work all CV will appear shifted by amount of an error, which indeed won't matter for our purposes. The potentials reported in this manuscript, symbolized as E, were measured from the point of view of the Ag(O) relative to aq. phase RE's (Ag/AgCl or Ag/Ag_2SO_4). Therefore E would represent the total potential given by:

$$E = (E_{Ag|O} + \Delta_w^O\varphi) - E_{Ag|AgCl,cl^-(W)} = \Delta_w^O\varphi + (E_{Ag|O} - E_{Ag|AgCl,cl^-(W)}) = \Delta_w^O\varphi + error \qquad (12)$$

The notation of the studied hydrophobic electrolyte (also O-phase) systems and its two electrodes (Ag RE, Pt CE) and supporting hydrophilic cellulose membrane/ liquid-junction (||) will be simplified as "Ag| salt (x mM)/ O||" or Ag| salt (x mM)/ ionophore (y mM)/ O||", and will be referred to as "sensor 1" and sensor 2, respectively. The existence of the Pt counter electrodes should be simply understood. Both sensor 1 and 2 are dipped in aq. electrolyte phase (also W phase) to form an O/W interface and CVs are recorded by changing the potential difference across this interface ($\Delta_w^O \varphi$) to derive a net ion transfer from one phase to the other, resulting in the observation an electrical current between the two counter electrodes.

5.1. Preliminary investigations

Four hydrophobic salts (ETH500, TBATPB, EthvTPB, and TPphTPB) and ILs were tested as supporting electrolytes (in each case 10 mM) in NB to find out the one which is most suitable with respect to width of the potential window and double layer capacitance noise. Background cyclic voltammograms (CVs) of membrane-stabilized interface between aq. Li_2SO_4 and NB containing the above hydrophobic salts were initially recorded and compared to this end.

5.1.1 Evaluation of traditional hydrophobic salts and ionic liquids

Tetradodecylammonium tetrakis(4-chlorophenyl)borate (ETH500)
Fig 12 shows overlay of triplicate CVs of Ag| ETH500 (10 mM)/ NB|| in aq. Li_2SO_4 (100 mM). This CV indicates the potential window of this interface spans from -0.25 to 0.35 V.
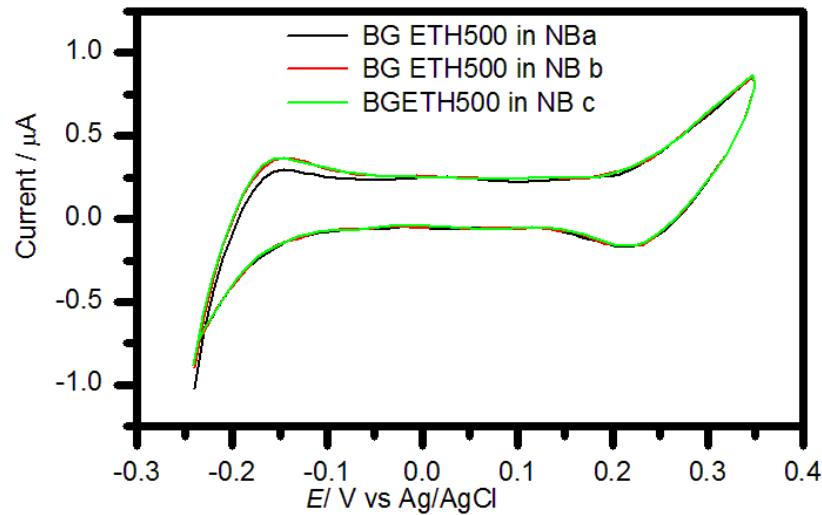
Fig 12: Replicate background CVs of Ag| ETH500 (10 mM)/ NB|| in and aq. Li_2SO_4 (100 mM). $E_{initial}$ = E_{final} = -0.25; E_{high} = 0.35 V; scan rate = 10 mV/ s.

The limits of the potential window arise because of either of the following simple ion-transfer of from water phase to organic phase or the reverse in equation (13 and 14), where A^+ and B^- are ions of the hydrophobic salt in the O phase.

Cathodic limit: $Li^+ (W) \rightarrow Li^+(O)$ (13)

$B^-(O) \rightarrow B^-(W)$

Anodic limit: $SO_4^{2-} (W) \rightarrow SO_4^{2-} (O)$ (14)

$A^+(O) \rightarrow A^+(W)$
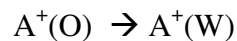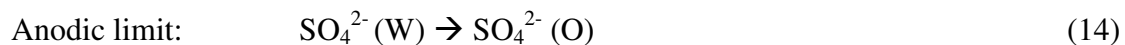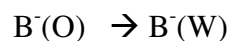
This mechanism will be valid for all except when an ionophore or other complexing agents are incorporated in the organic phase.

There were no new ion-transfer peak after addition of K^+ (4 mM) or NH_4^+ (4 mM) in the aqueous phase (Li_2SO_4) (see Fig 12). This observation is in agreement with literature as the transfer of these ions requires the presence of an appropriate ionophore in the O phase [78].

43
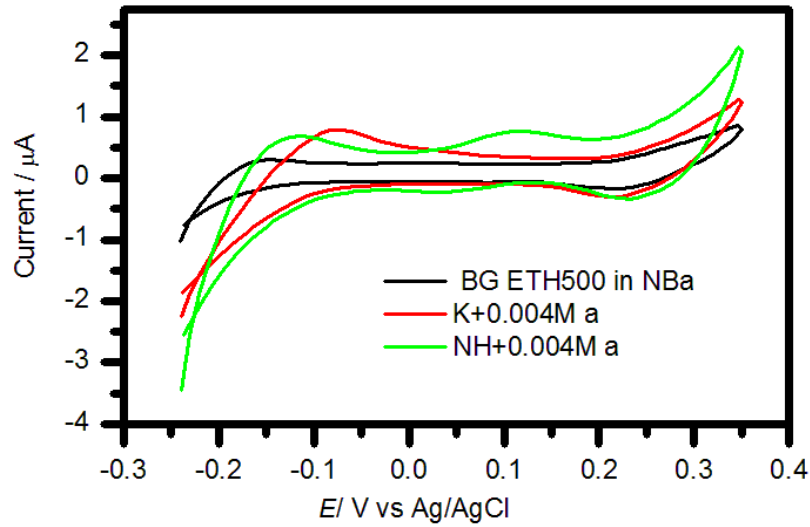
Fig 13: CVs of Ag|ETH500 (10 mM)/ NB|| before (black) and with 4 mM K^+ (red) or NH_4^+ (green) in aq. Li_2SO_4 (100 mM). $E_{initial} = E_{final} = -0.25$; $E_{high} = 0.35$ V; scan rate = 10 mV/ s.

Tetrabutylammonium tetraphenylborate

The second hydrophobic salt tested was TBATPB in NB. The corresponding sensor configuration is: Ag|TBATPB (10 mM)/ NB||. The CV in this case is shown Fig 12. The CVs were repeated to be sure the background was stable before adding the test ions (K^+ and NH_4^+). The potential window of this system was established to range from 0.25 to -0.35 V.
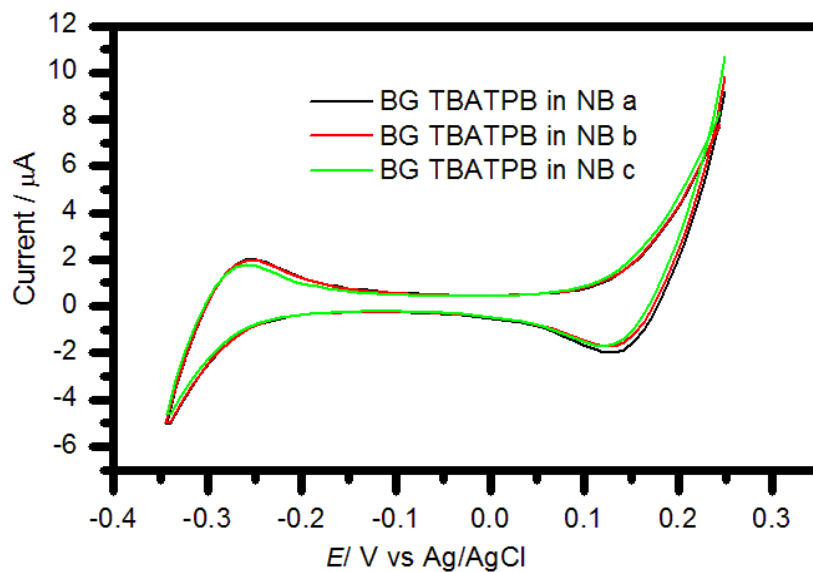
Fig 14: Replicate background CVs of Ag|TBATPB (10 mM)/ NB|| in aq. Li_2SO_4 (100 mM). $E_{initial} = E_{high} = 0.25$ V; $E_{low} = -0.35$ V; scan rate = 10 mV/ s

44

Fig 15 shows an overlay of replicate CVs of this interface in the presence of K^+ or NH_4^+ ions. Except for some sort of distortion or changes in background CV shape, there was no obvious ion transfer peak.
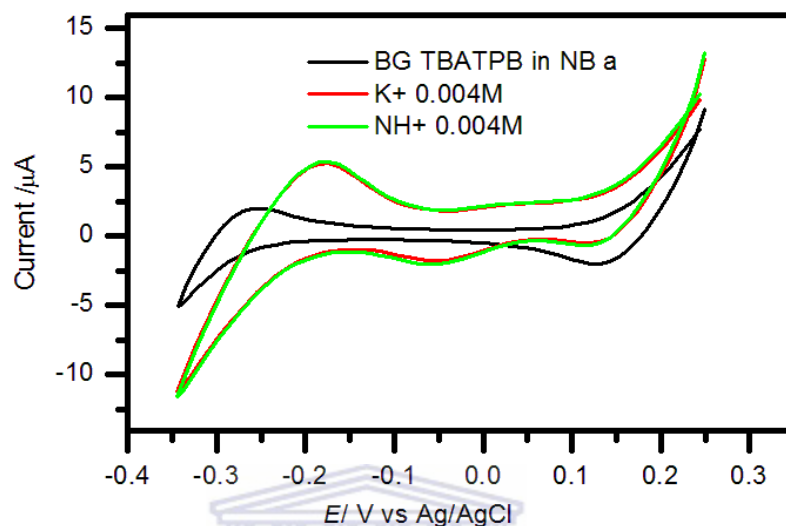
Fig 15: CVs of Ag|TBATPB (10 mM)/ NB|| before (black) and with 4 mM K^+ (red) or NH_4^+ (green) in aq. Li_2SO_4 (100 mM). $E_{initial} = E_{high} = 0.25$ V; $E_{low} = -0.35$ V; scan rate = 10 mV/ s

Ethyl Violet tetraphenylborate

EthvTPB in NB was tested like the previous hydrophobic salts. The corresponding sensor configuration is: Ag| EthvTPB (10 mM)/ NB||. Its background CVs during initial experiments was not stable as shown in Fig 16A. So a potential-step excitation wave form lasting 10 s was imposed immediately before recording the CV and a better CV in Fig 16B was obtained. Fig 16C shows the same CV after cutting out the noise due to the potential-step, Fig 16D shows the system would give a well behaved stable background CV under multicyclic CV experiment. In the end a potentials window of -0.6 to -0.05 V was established for this system. In addition to, when K^+ and NH_4^+, no simple ion transfer was observed as expected (Fig 17).
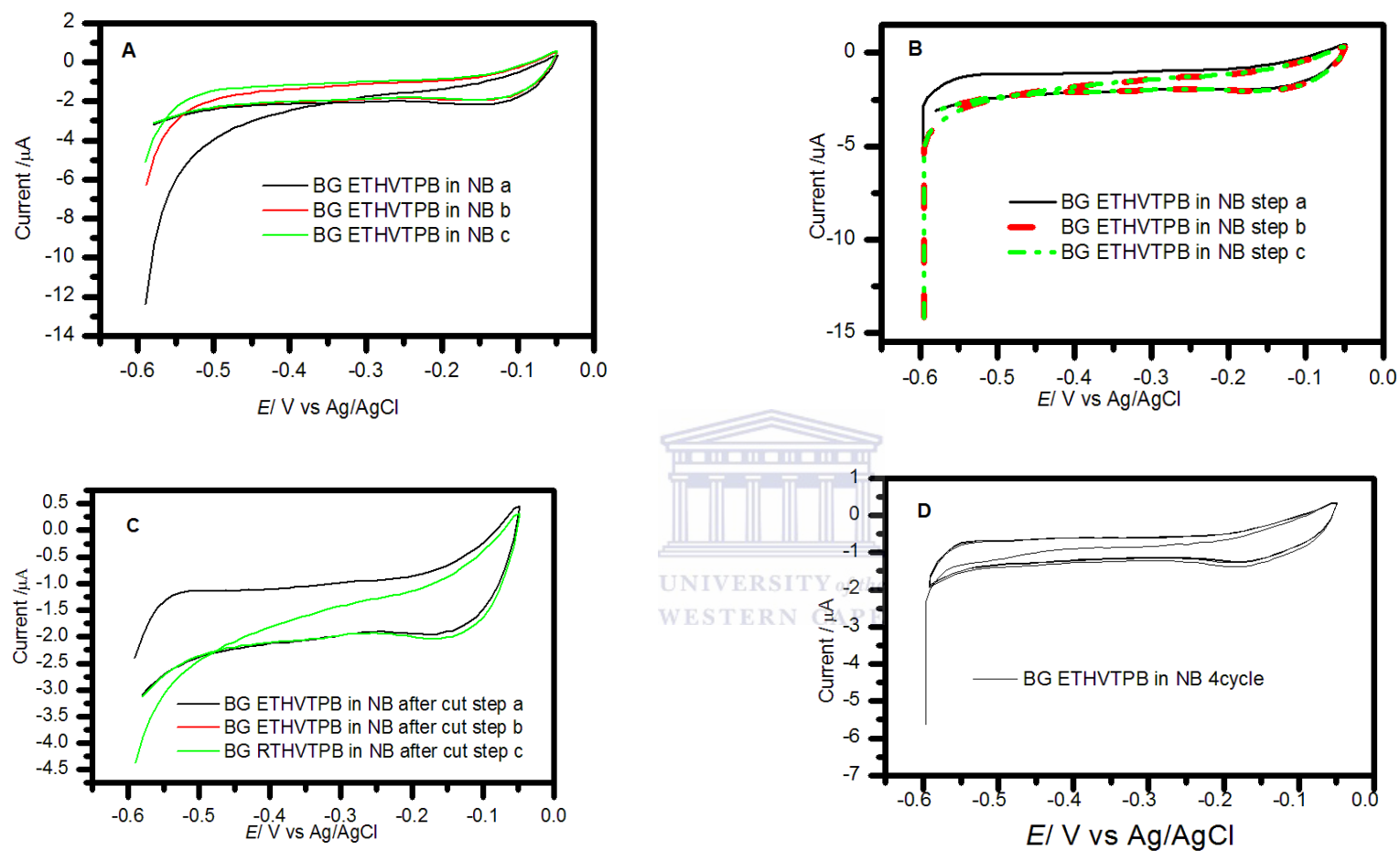
Fig 16: A) Replicate background CVs of Replicate background CVs of Ag| EthVTPB (10 mM)/ NB|| in aq. Li$_2$SO$_4$ (50 mM). E$_{initial}$ = E$_{high}$ = 0.6 V, and E$_{low}$ = -0.05 V, scan rate = 10 mV/ s. B) The same as (A) but preceded by a 10 s potential-step of -0.6 V. C) Same as B, but after removing the noise due to preconditioning potential-step. D) A multicyclic CV preceded by the same potential-step.
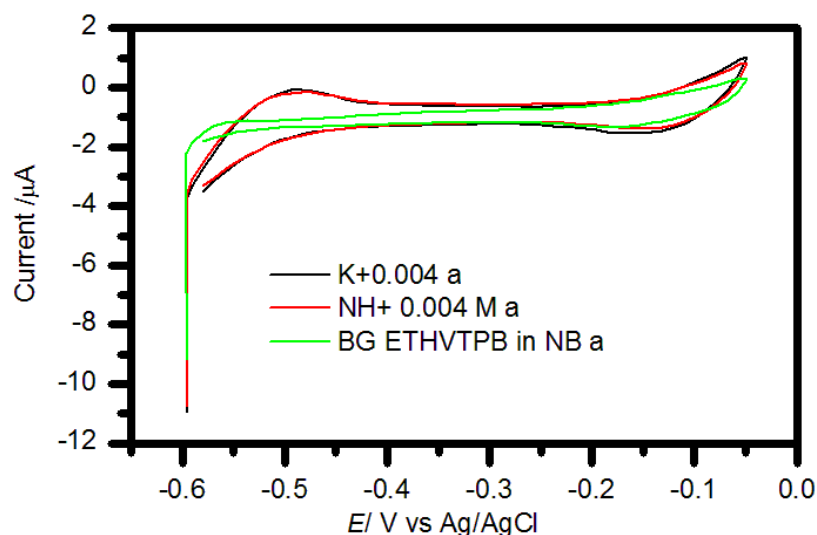
Fig 17: CV of Ag|EthVTPB (10 mM)/ NB|| before (green) and with 4 mM of K^+ (black) or NH_4^+ (red) in aq. Li_2SO_4 (50 mM). $E_{initial} = E_{high} = 0.6$ V, $E_{low} = -0.05$ V; $E_{pre-step} = 0.6$ V for 10 s; Scan rate = 10 mV/ s

Tetraphenylphosphnium tetraphenylborate
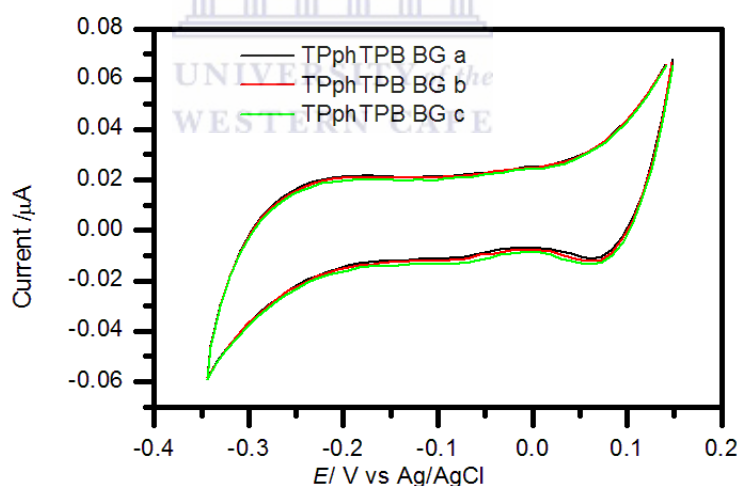
Fig 18: Replicate background CVs of Ag|TPphTPB (10 mM)/ NB|| in aq. Li_2SO_4 (50 mM). $E_{initial} = E_{high} = 0.15$ V; $E_{low} = -0.35$ V; scan rate = 10 mV/ s

The last traditional hydrophobic salt was TPphTPB in NB (10 mM), used the same method of detection. The corresponding sensor configuration is: Ag|TPphTPB (10 mM)/ NB||. Its

potential window was from 0.15 to -0.35 V as can be seen from the background CVs overlaid in Fig 18. No peaks were observed for K^+ and NH_4^+ in the aqueous phase (see Fig 19).
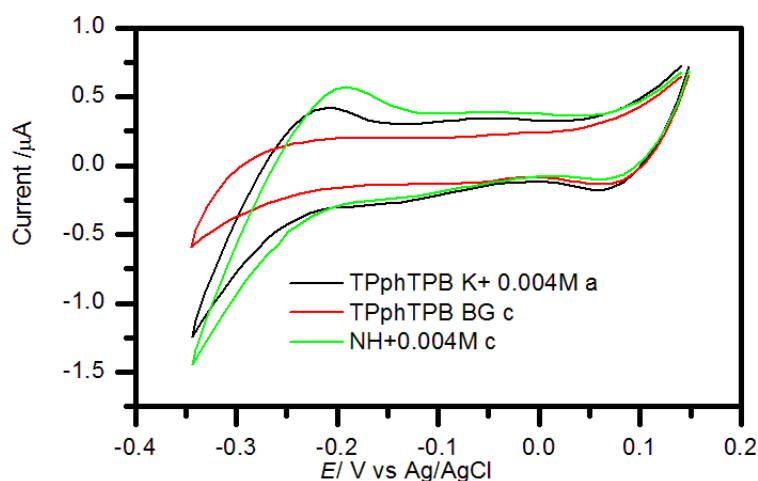
Fig 19: CVs of Ag|TPphTPB (10 mM)/NB|| before (red) and with 4 mM K^+ (black) or NH_4^+ (green) in aq. Li_2SO_4 (50 mM). $E_{initial} = E_{high} = 0.15$ V; $E_{low} = -0.35$ V; scan rate = 10 mV/ s

Ionic liquids

Similar studies were carried out using three hydrophobic room-temperature ionic liquids (ILs):

- Methyltrioctylammonium bis(trifluoromethylsulfonyl)imide (IL1)
- 1-Butyl-3-methylimdazolium bis(trifluoromethylsulfonyl)imide (IL3) and
- 1-Propyl-3- methylimdazolium bis(trifluoromethylsulfonyl)imid (IL4)

The pure forms of three ILs were first tested as self-sufficient hydrophobic electrolytes. The corresponding configurations would be: Ag|IL1||, Ag|IL3||, and Ag|IL4||. However, only one (Ag|IL1||) was found to yield a some-how polarizable interface with the aq. phase as one can see from Figs 20 and 21. The potential window of Ag|IL1|| in aq. Li_2SO_4 (50 mM) was from 0.5 V to 0.1 V. Like the previous hydrophobic electrolyte, no peak was observed when K^+ or NH_4^+ was added to the aq. phase. IL1 was then additionally tested as a hydrophobic salt in

NB. The CVs of Ag|IL3|| and Ag|IL4|| in aq. Li_2SO_4 (50 mM) demonstrated these ILs could only form a poorly polarizable liquid-liquid interfaces (see Figs 22 and 23). Indeed, the CVs exhibited by these two systems were similar with purely resistive elements (see Fig 24).
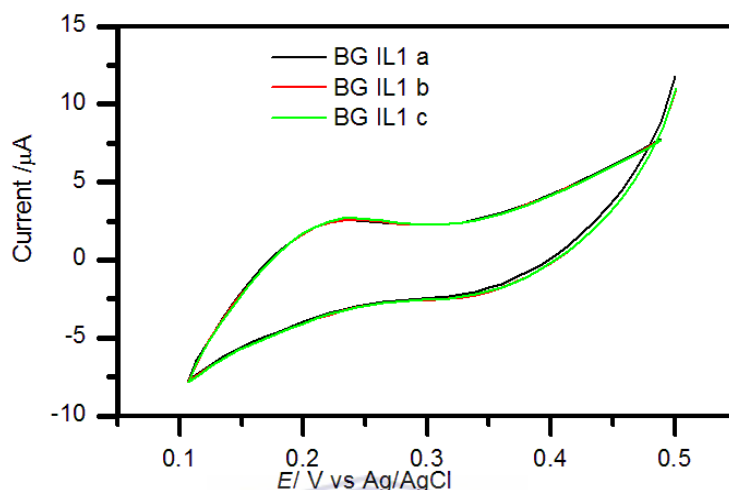
Fig 20: Replicate background CVs of Ag|IL1|| in aq. Li_2SO_4 (50 mM). $E_{initial} = E_{high} = 0.5$ V; $E_{low} = 0.1$ V; scan rate = 10 mV/ s.
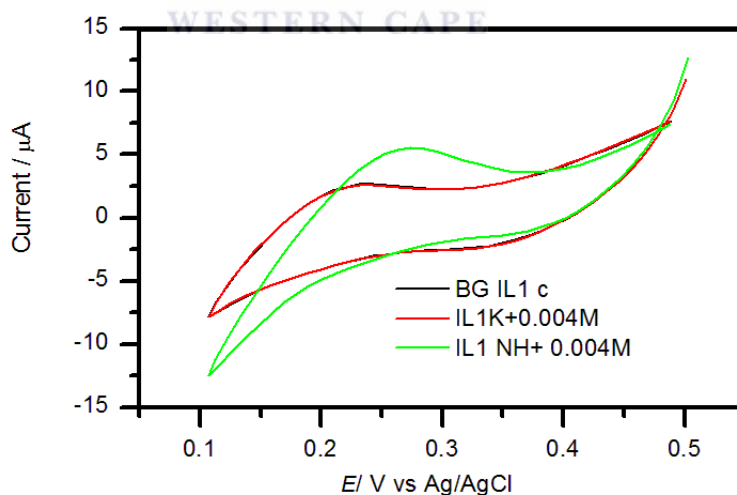
Fig 21: CV of Ag|IL1|| before (black) and with 4 mmM of K^+ (red) or NH_4^+ (green) in aq. Li_2SO_4 (50 mM). $E_{initial} = E_{high} = 0.5$ V; $E_{low} = 0.1$ V; scan rate = 10 mV/ s

According to figures 22 and 23, the interfaces formed with IL3 and IL4 were not suitably polarized and behaved like resistance in liquid- liquid interface as shown in Fig 24.
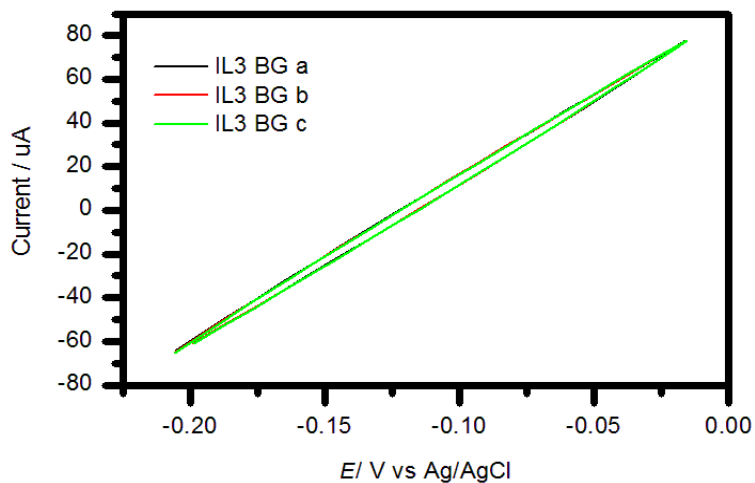
Fig 22: Replicate background CVs of Ag|IL3|| in aq. Li_2SO_4 (50 mM). $E_{initial} = E_{high} = -0.22$ V; $E_{low} = -0.02$ V; scan rate = 10 mV/ s.
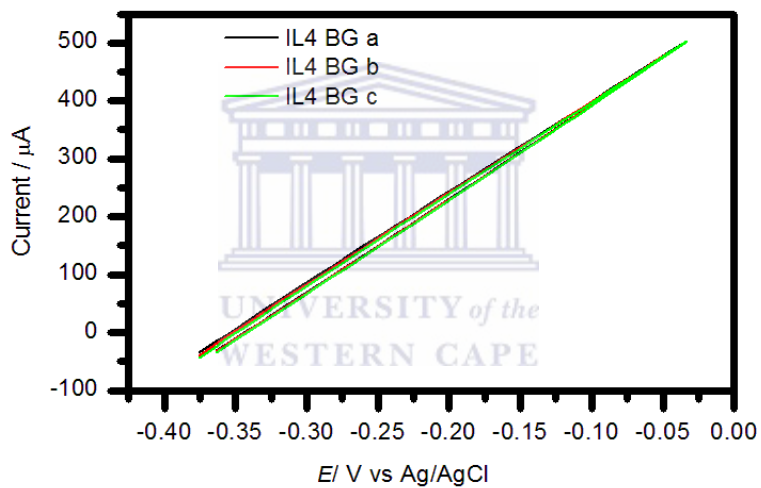
Fig 23: Replicate background CVs of Ag|IL4|| in aq. Li_2SO_4 (50 mM). $E_{initial} = E_{high} = -0.38$ V; $E_{low} = -0.03$ V; scan rate = 10 mV/ s.
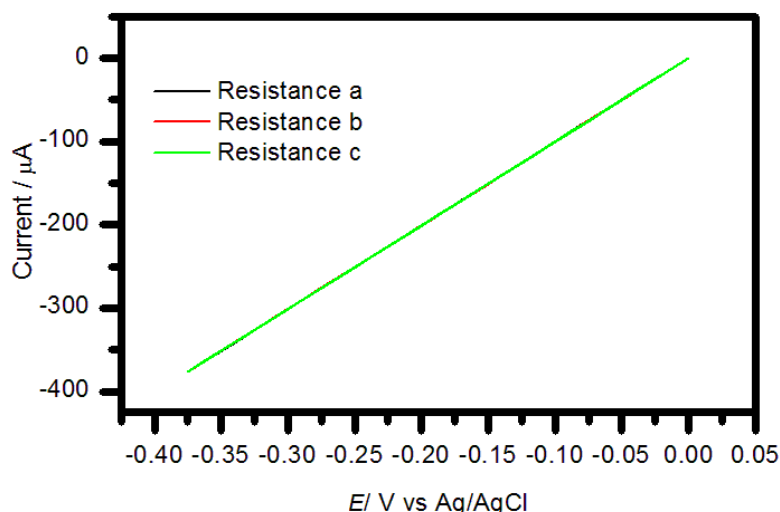
Fig 24: Replicate CVs of a 1 kΩ resistor. $E_{initial} = E_{high} = -0.38$ V; $E_{low} = -0.02$ V; scan rate = 10 mV/s.

Methyltrioctylammonium bis(trifluoromethylsulfonyl)imide (IL1)

The IL1 was also tested like the traditional hydrophobic salt in NB. The corresponding sensor configuration would be Ag|IL1 (10 mM)/ NB‖. The CV of the interface it formed with aq. Li_2SO_4 is shown in Fig 25, and its potential window was found to range from 0.27 V to -0.08 V. No peaks were observed for K^+ and NH_4^+ in the aqueous phase (see Fig 26).
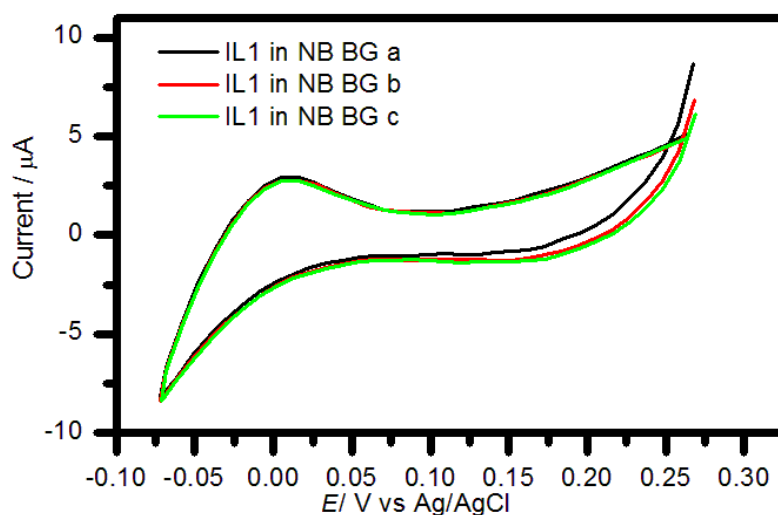
Fig 25: Replicate background CVs of Ag|IL1 (10 mM) /NB‖ in aq. Li_2SO_4 (50 mM). $E_{initial} = E_{high} = 0.27$ V; $E_{low} = -0.08$ V; scan rate = 10 mV/ s
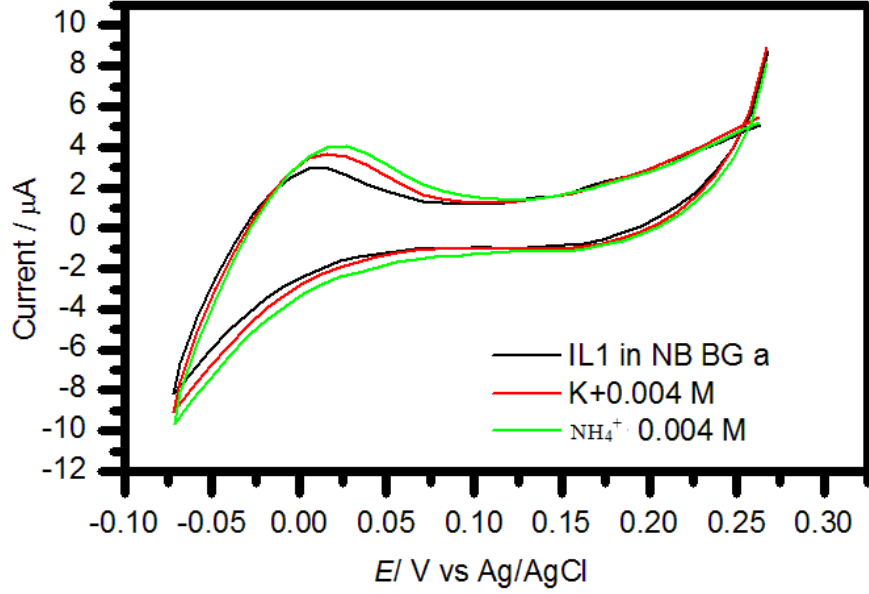
Fig 26: CVs of Ag|IL1 (10 mM)/ NB|| before (black) and with 4 mM K^+ (red) or NH_4^+ (green) in aq. Li_2SO_4 (50 mM). $E_{initial} = E_{high} = 0.27$ V; $E_{low} = -0.08$ V; scan rate = 10 mV/ s

Anodic and cathodic potential limits, thus potential windows, mean background currents ($i_{bg-mean}$), and capacitance (C_{dl}) observed at 10 mV/s scan rate for the above membrane-stabilized interfaces (Figs 12 to 25) between solutions of the hydrophobic salts (10 mM) in NB as well as pure IL1 and aq. Li_2SO_4.(50 or 100 mM) have been compiled in Table 8. $i_{bg-mean}$ was calculated by taking five different data points from background CVs corresponding to each interface. Standard deviations were calculated using equation 15.

$$SD_{i_{bg}} = \sqrt{\frac{\sum (i_{bg-mean} - i_{bg})^2}{N-1}} \tag{15}$$

$$C_{dl} = \frac{i_{bg-mean}}{v} \quad \& \quad SD_{C_{dl}} = C_{dl} \times \sqrt{\left(\frac{SD_{i_{bg-mean}}}{i_{bg-mean}}\right)^2 + \left(\frac{SD_v}{v_{mean}}\right)^2} \tag{16}$$

52

Table 8: Background currents (i_{bg}), double layer capacitance (C_{dl}), and potential limits of Ag|salt (10 mM)/ NB|| and Ag|IL1|| in aq. Li_2SO_4 (50/ **100 mM). Scan rate = 10 mV/s. *vs Ag/AgCl

Organic phase	$i_{bg\text{-mean}}$ / µA	(C_{dl} ±SD)/ µF	*Anodic limit/ V	*Cathodic limit/ V	Window/ V
**TBATPB/ NB	0.44±0.00 [a]	43.9±0.1 [a]	0.25	-0.35	0.60
	-0.24±0.00 [c]	-24.4±0.0 [c]			
TPPHTPB/ NB	0.21±0.00 [a]	21.1±0.2 [a]	0.15	-0.35	0.50
	-0.12±0.00 [c]	-12.2±0.3 [c]			
**ETH500/ NB	0.24±0.00 [a]	24.2±0.0 [a]	0.35	-0.25	0.60
	-0.04±0.00 [c]	-4.4±0.0 [c]			
ETHVTPB/ NB	-0.89±0.03	-89±3 [a]	0.05	-0.60	0.65
	-0.12±0.00 [a]	-12.2±0.1 [c]			
Pure IL1	2.27±0.00 [a]	227.2±0.4 [a]	0.50	0.10	0.40
	-2.56±0.00 [c]	-255.9±0.5 [c]			
IL1/ NB	1.05±0.00 [a]	104.6±0.2 [a]	0.27	-0.08	0.35
	-1.24±0.00 [c]	-124.4±0.2 [c]			

The C_{dl} data in Table 8 have been plotted as bar-graphs in Fig 27 in order to make it much easier to identify the salt with minimal C_{dl}, hence lowest background noise. In Fig 28, both potential window and C_{dl} have been plotted against the corresponding salts. The wider potential window is the best it would be. Based on Fig 16, one can see that EthvTPB resulted in the widest potential window but its background CV was relatively unstable and unsymmetrically off-set, possibly because of excessive impurities. IL1 resulted in highest double layer capacitance and the narrowest potential window, both in its pure and NB-

solution forms, so it would make the least favourable interface with aqueous phase among the electrolytes tested in this work. In contrast, ETH500 resulted in the smallest double layer capacitance and the second widest potential window. Thus, we can conclude that ETH500 would be the best choice for developing the envisaged sensor. However, in anticipation of any possible surprises, both the best (ETH500) and the worst (IL1) were taken to the next stage of the study, in which DCE and NPOE would be tested as solvents in the organic phase.
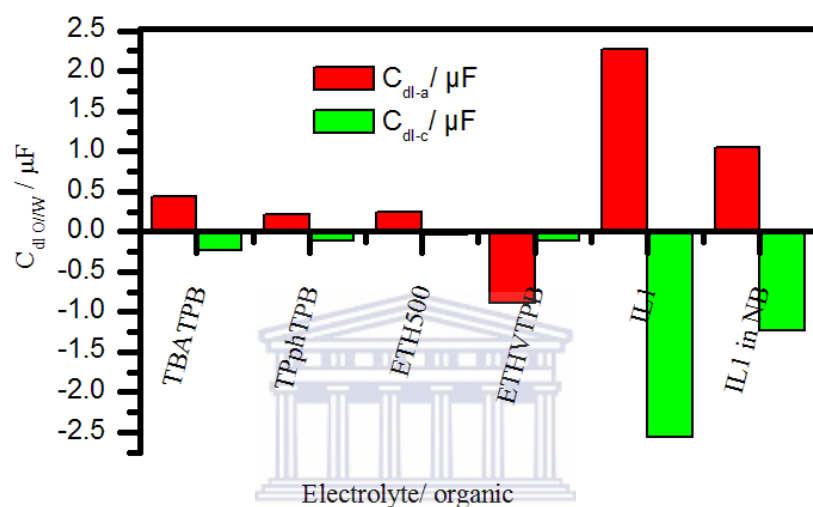
Fig 27: Bar-graphs of bi-double layer capacitances (C_{dl}) at Ag|salt (10 mM)/ NB|| and Ag|IL1|| in aq. Li_2SO_4 (50 or 100 mM) observed with different salts
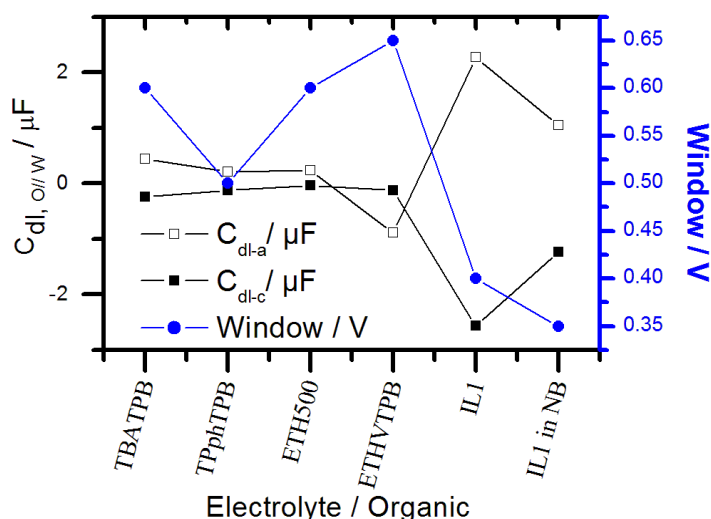
Fig 28: Bi-double layer capacitances (C_{dl}) and potential windows of Ag|salt (10 mM)/ NB|| and Ag|IL1|| in aq. Li_2SO_4 (50 or 100 mM) observed with different salts

5.1.2 Evaluation and selection of hydrophobic solvents: DCE and NPOE against NB

Solutions of ETH500 and IL1 in DCE and NPOE were similarly tested, each at 10 mM, and the results have been discussed below.

ETH500 in DCE

Fig 29 shows the background CV of Ag|ETH500 (10 mM)/ DCE|| in aq. Li_2SO_4 at the scan rate of 10 mV/ s, according to which the potential window was found to range from 0.4 to - 0.45 V (vs Ag/AgCl). The overlaid CVs confirm this configuration resulted in reproducible background CVs and potentially reproducible signals. No peaks were observed for K^+ and NH_4^+ in the aqueous phase (see Fig 30).
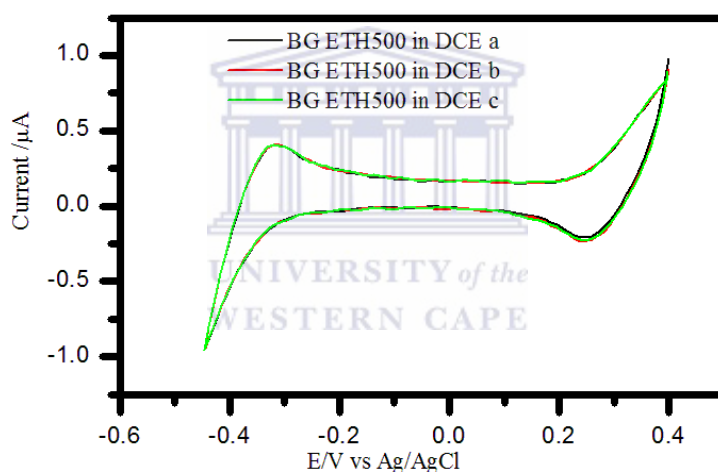
Fig 29: Replicate background of CVs of Ag|ETH500 (10 mM)/ DCE|| in aq. Li_2SO_4 (50 mM). $E_{initial\ =}$ 0.40 V; $E_{final\ =}$ - 0.45 V; E_{final} = 0.40 V; scan rate = 10 mV/ s
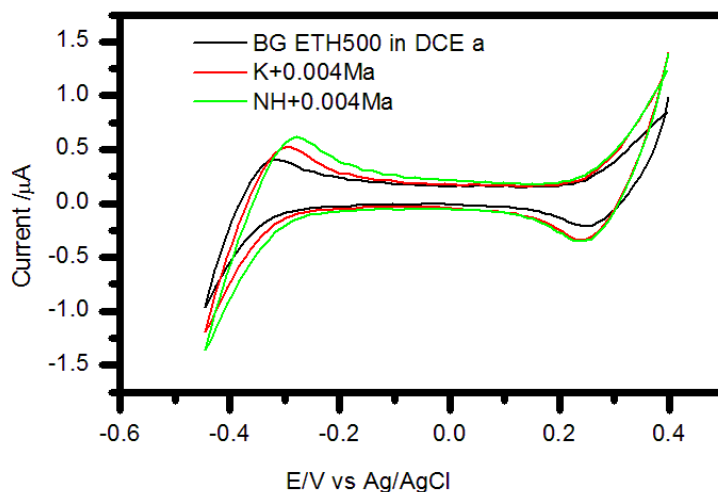
Fig 30: CVs of Ag|ETH500 (10 mM)/ DCE||before (black) and with 4 mM K^+(red) or NH_4^+ (green) in aq. Li_2SO_4 (50 mM).$E_{initial}$ =0.40 E_{final} = -0.45 V; E_{final} = 0.40 V; scan rate =10 mV/ s

IL1 in DCE

Fig 31 shows the background CV of Ag|IL1 (10 mM)/ DCE|| in aq. Li_2SO_4 at the scan rate of 10 mV/ s, according to which the potential window was found to range from 0.4 to -0.06 V (vs Ag/AgCl). This configuration also resulted in a reproducible background CV, but the window is much narrower. No peaks were observed for K^+ and NH_4^+ in the aqueous phase (see Fig 32).
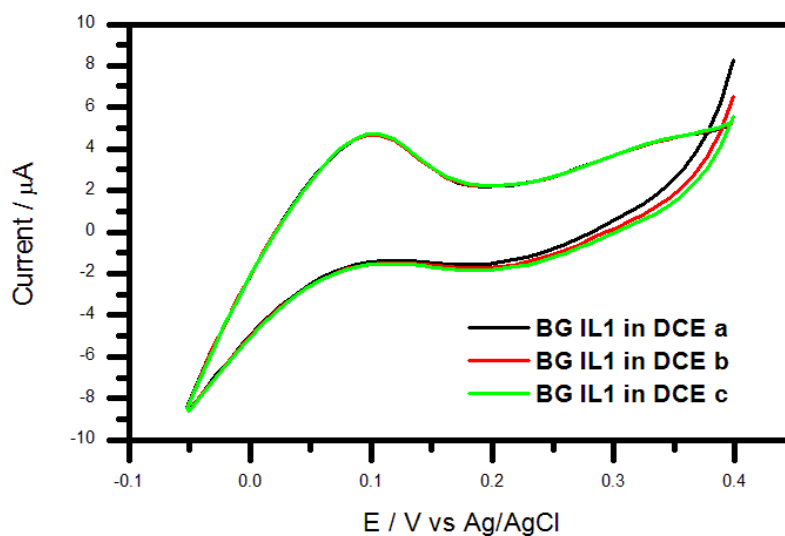
Fig 31: Replicate background CVs of Ag|IL1 (10 mM)/ DCE in aq. Li_2SO_4 (50 mM). $E_{initial}$ = E_{final} = 0.40 V; E_{low} = -0.08 V; scan rate = 10 mV/ s
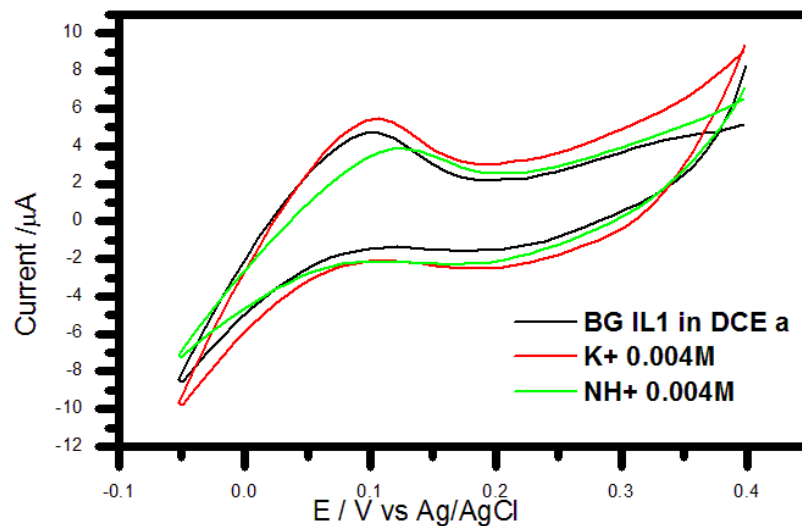
Fig 32: CVs of Ag|IL1 (10 mM)/ DCE‖ before (black) and with 4 mM K^+ (red) or NH_4^+ (green) in aq. Li_2SO_4 (50 mM). $E_{initial} = E_{final} = 0.40$ V; $E_{low} = -0.08$ V; scan rate = 10 mV/ s

ETH500 in NPOE

Fig 33 shows the background CV of Ag|ETH500 (10 mM)/ NPOE‖ in aq. Li_2SO_4. The CVs are reproducible but appear distorted, possible because this electrolyte has a high resistance. Thus, the potential window range would be narrower than it appeared to be (0.45 V to -0.65 V vs Ag/AgCl). No peaks, but a slight distortion was observed on addition of K^+ and NH_4^+ in the aqueous phase (see Fig 34).

57
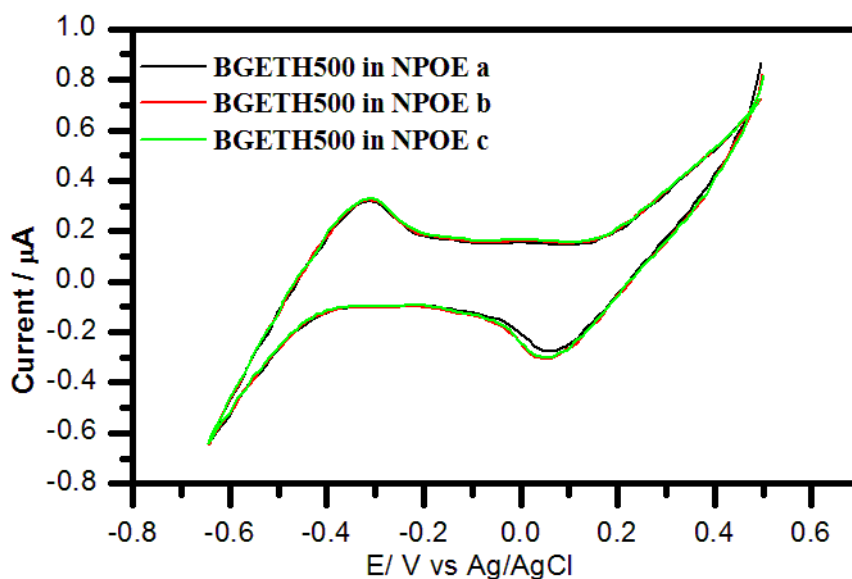
Fig 33: Replicate background CVs of Ag|ETH500 (10 mM)/ NPOE‖ in aq. Li_2SO_4 (50 mM). $E_{initial\ =}$ $E_{final\ =}$ 0.45 V; E_{low} = -0.65 V; scan rate = 10 mV/ s
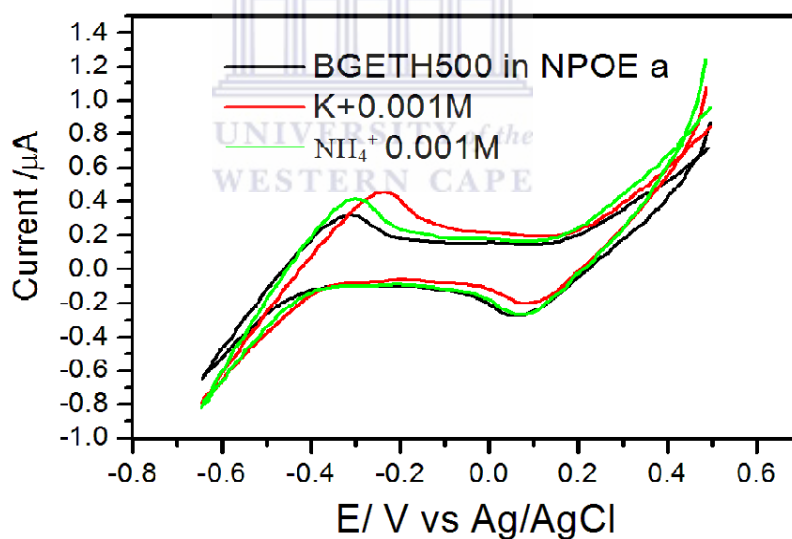
Fig 34: CVs of Ag|ETH500 (10 mM)/ NPOE‖ before (black) and with 1 mM K^+ (red) or NH_4^+ (green) in aq. Li_2SO_4 (50 mM). $E_{initial\ =}$ $E_{final\ =}$ 0.45 V; E_{low} = -0.65 V; scan rate = 10 mV/ s

IL1 in NPOE

Fig 35 shows the background CV of Ag|IL1 (10 mM)/ NPOE‖ in aq. Li_2SO_4. The CVs are less reproducible and appear more severely distorted than that of ETH500/NPOE, indicating an even higher electrolyte resistance. The apparent potential window would be 0.5 V to -0.2

V vs Ag/AgCl. No peaks, but, compared to ETH500/NPOE, a greater degree of distortion was observed in the background CV after addition of K^+ and NH_4^+ in the aqueous phase (see Fig 36).
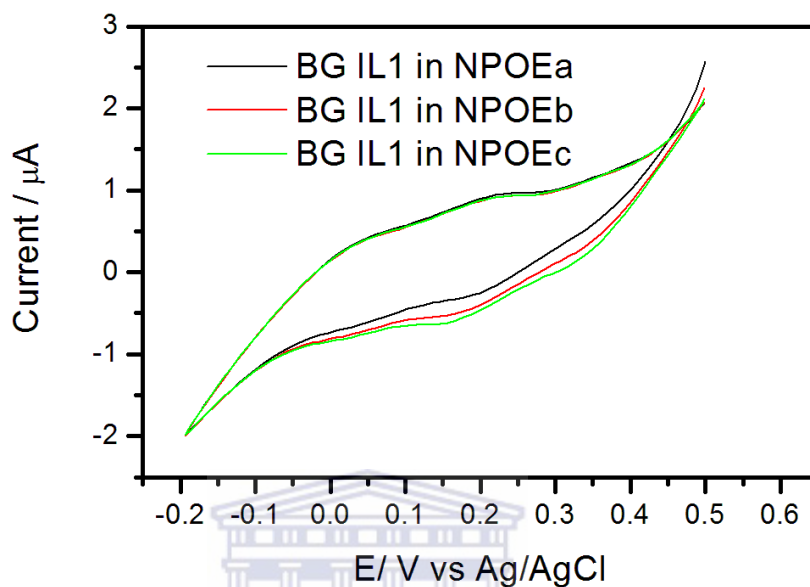
Fig 35: Replicate background CVs of Ag|IL1 (10 mM)/ NPOE|| in aq. Li_2SO_4 (50 mM). $E_{initial} = E_{final} = 0.5$ V; $E_{low} = -0.2$ V; scan rate = 10 mV/ s
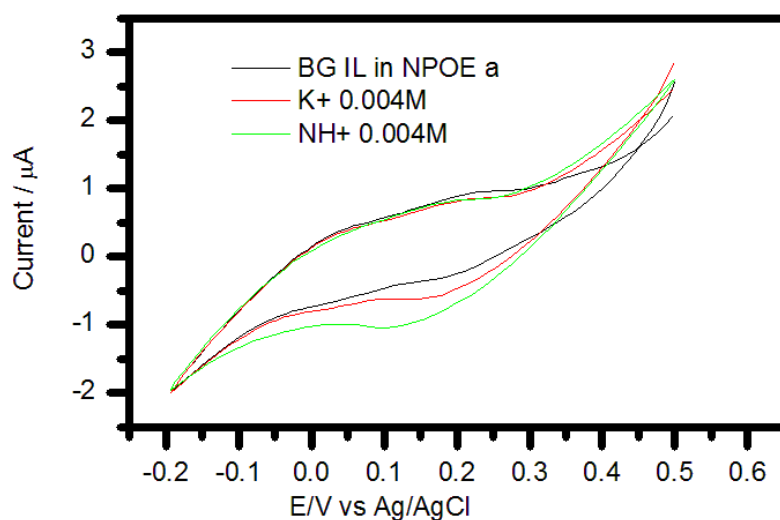

Fig 36: CVs of Ag| IL1 (10 mM)/ NPOE|| before (black) and with 4 mM of K^+ (red) or NH_4^+ (green) in aq. Li_2SO_4 (50 mM). $E_{initial} = E_{final} = 0.5$ V; $E_{low} = -0.2$ V; scan rate = 10 mV/ s

Inter-comparison among NB, DCE, and NPOE

To facilitate the identification of the most favourable hydrophobic solvent among NB, DCE, and NPOE, based on the preceding CVs, the corresponding C_{dl} and potential windows have been plotted in the Fig 37 and Fig 38. Anodic/ cathodic potential limits and potential window ranges (or simply: windows) have been compiled in Table 8. As one can see the ETH500/ NPOE pair resulted in the widest potential window, but the second smallest C_{dl}. The ETH500/DCE pair resulted the smallest C_{dl} but in the second widest potential window. ETH500/ DCE had smaller C_{dl} and wider potential window than ETH500/ NB. IL1/ NB, IL1/ DCE, and IL1/ NPOE had the smallest potential windows and highest C_{dl} values, and, thus, these are least favourable ones.
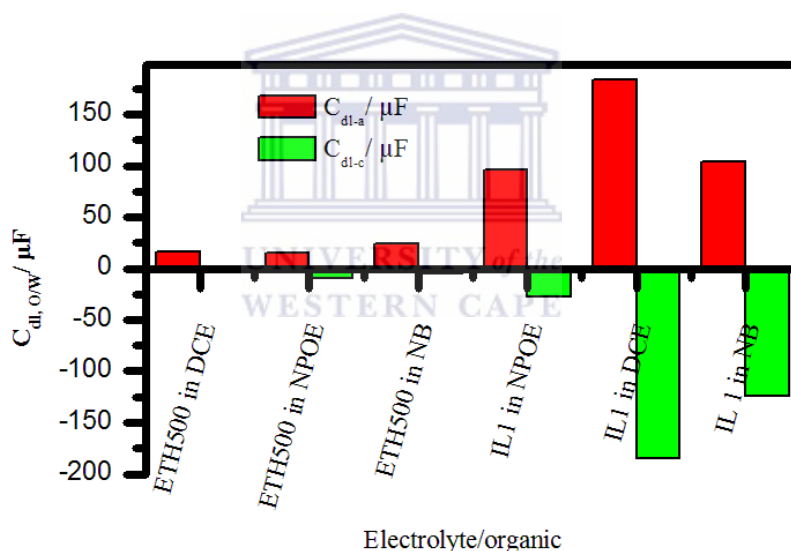
Fig 37: Bar-graphs of bi-double layer capacitances (C_{dl}) observed for Ag|ETH500 or IL1 (10 mM)/ solvent|| in aq. Li_2SO_4 (50 or 100 mM) across solvents (NPOE, DCE, and NB)

If it were only for pure quantitative considerations, one would find the ETH500/ NPOE pair to be the most favourable organic phase. However, the ETH500/ DCE pair could also be more favourable because of the following two reasons (a) the fact that the CV of this phase was very distorted meant it suffered high resistive loss resulting in a positive error in the value of the potential window, and (b) economic reason (according to Sigma Aldrich at the

time of writing this manuscript, the price for 25 mL of NPOE was R 1248.62 while that of 500 mL of DCE was R 283.13). However, both the ETH500/DEC and ETH500/NPOE phases will be employed in the next stage of the study in which aq. Li_2SO_4 will be evaluated against aq. $MgSO_4$.
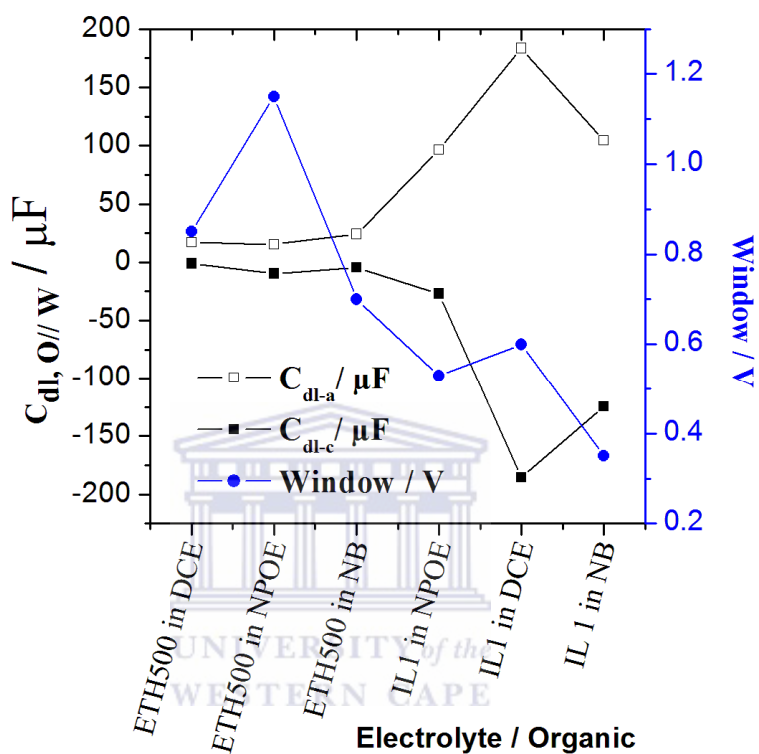
Fig 39: Bar-graphs of C_{dl} and potential windows observed for Ag|ETH500 or IL1 (10 mM)/ solvent|| in aq. Li_2SO_4 (50 mM) across solvents (NPOE, DCE, and NB)

Table 9: Potential limits (vs Ag/AgCl) observed at 10 mV/s scan rate for Ag|ETH500 or IL1 (10 mM)/ solvent|| in aq. Li_2SO_4 (50 mM) across solvents (NPOE, DCE, and NB).

Solvent	Salt	Anodic limit/ V	Cathodic limit/ V	Window/ V	C_{dl-a}/ μF	C_{dl-c}/ μF
DCE	ETH500	0.40	-0.45	0.85	17	-1.03
	IL1	0.40	-0.08	0.53	183.34	-185.37
NPOE	ETH500	0.45	-0.65	1.1	15	-9.78
	IL1	0.50	-0.20	0.70	96.59	-26.98
NB	ETH500	0.35	-0.25	0.60	24.2	-4.4
	IL 1	0.27	-0.08	0.35	104.6	-124.4

5.1.3 Evaluation of two aqueous phases

The CV characteristics of the sensors with ETH500/DCE and ETH500/NPOE organic phases were compared in two aq. phases, namely aq. Li_2SO_4 and aq. $MgSO_4$. Hence forward, unless otherwise indicated, Ag/Ag_2SO_4 was used instead of $Ag/AgCl$ as the aq. phase reference electrode to avoid possible effects of the Cl^- on the anodic limit.
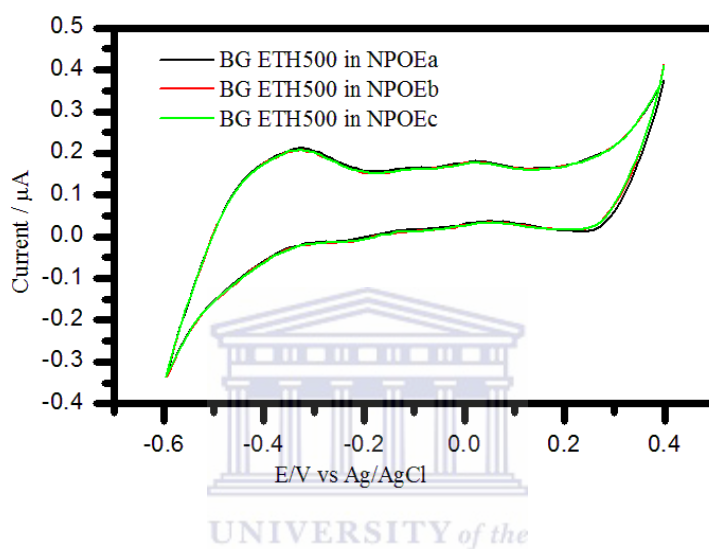
Fig 40: Replicate background of CVs of Ag|ETH500 (10 mM)/ NPOE|| in aq. $MgSO_4$ (50 mM) phases. $E_{initial} = E_{final} = 0.40$ V; $E_{low} = -0.60$V; scan rate = 10 mV/ s
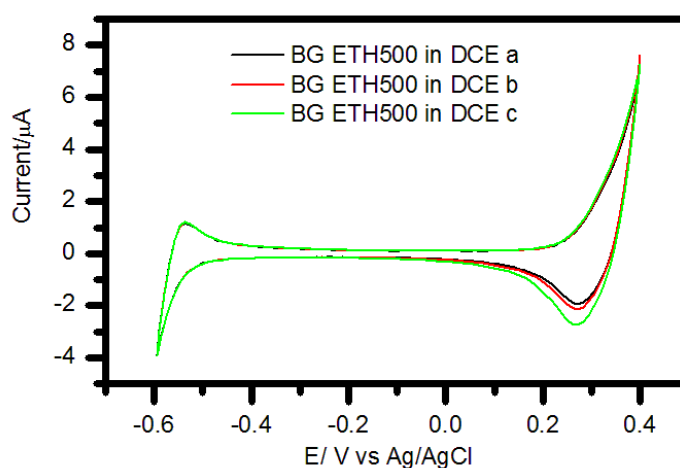
Fig 41: Replicate background of CVs of Ag|ETH500 (10 mM)/ DCE|| in aq. $MgSO_4$ (50 mM) phases. $E_{initial} = E_{final} = 0.40$ V; $E_{low} = -0.60$V; scan rate = 10 mV/ s

The notations of the sensors studied here would be: Ag|ETH500 (10 mM)/ DCE|| and

Ag|ETH500 (10 mM)/ NPOE||. In Table 10, potential limits and windows of these ones in aq.

Li_2SO_4 and aq. $MgSO_4$ have been compiled based on Fig. One can see that wider potential

windows were obtained in aq. $MgSO_4$ in contrast with aq. Li_2SO_4. Besides NPOE still

resulted in apparently wider windows, but this time only wider by about 50 mV and also that

the corresponding CVs in aq. $MgSO_4$ (see Fig 40) are as distorted as the ones observed in aq.

Li_2SO_4. Thus, it was decided to use only the ETH500/DCE phase in subsequent experiments.

Table 10: Potential limits and windows of Ag| ETH500 (10 mM)/ DCE or NPOE|| as

observed in aq. Li_2SO_4 (50 mM) and $MgSO_4$ (50 mM). Potential: against Ag/AgCl and

Ag/Ag_2SO_4

Aq. Phase	Organic phase	Anodic Limit/ V	Cathodic Limit/ V	Window/ V	$C_{dl-a}/$ μF	$C_{dl-c}/$ μF	Fig
Li_2SO_4 (50 mM)	ETH500 (10 mM)/ DCE	0.40	-0.45	0.85	17	-1.03	29
	ETH500 (10 mM)/ NPOE	0.45	-0.65	1.1	15	-9.78	33
$MgSO_4$ (50 mM)	ETH500 (10 mM)/ DCE	0.4	-0.6	1	10.34	-13.96	41
	ETH500 (10 mM)/ NPOE	0.4	-0.6	1	16.54	1.73	42
	*ETH500 (10 mM)/ DCE	0.05	-0.9	0.95	58.97	43.21	43

*In the figure below the Ag| ETH500 (10 mM)/ DCE observed in aq. $MgSO_4$ (50 mM)

Potential: against Ag/Ag_2SO_4
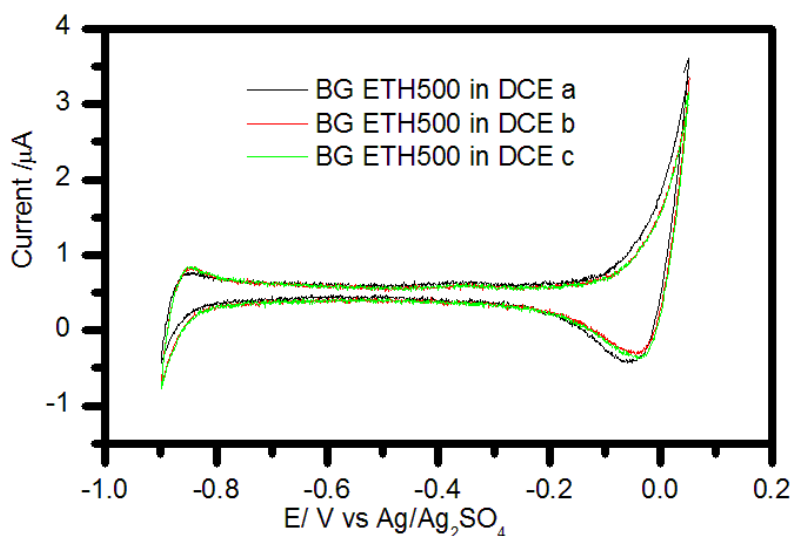
Fig 42: Replicate background of CVs of Ag|ETH500 (10 mM)/ DCE|| in aq. MgSO$_4$ (50 mM) phases. E$_{initial}$ = 0.05 V; E$_{final}$ = 0.05 V; E$_{low}$ = -0.9 V; scan rate = 10 mV/ s

5.2 Preliminary study with the ionophore Dibenzo-18-Crown-6 (DB18C6)

K$^+$ and NH$_4^+$ were used as test ions for the functioning of DB18C6-facilitated ion transfer across the membrane stabilized W| DCE interface assembly with custom made four electrode cell. The notation of the sensor employed hence forth would be:

Ag|ETH500 (10 mM)/ DB18C6 (50 mM)/ DCE||

Fig 43 shows reproducible background CVs of Ag|ETH500 (10 mM)/ DB18C6 (50 mM)/ DCE|| in aq. MgSO$_4$.The corresponding potential window was from 0.05 V to -0.65 V. By comparing this figure with Fig 42, one can see the narrowing of the potential window from 1.0 V to 0.70 V because of DB18C6 in the organic phase. Fig 45 and 46 re-demonstrate the absence of ion-transfer peak for K$^+$ and NH$_4^+$ ions at Ag|ETH500 (10 mM)/ DCE||. Fig 46 and 47 show this is no more the case for Ag|ETH500 (10 mM)/ DB18C6 (50 mM)/ DCE||. For this sensor, peaks which increased with three increasing test concentrations (0, 0.1, 0.2 and 0.4 mM) were observed for both ions. This a demonstration of facilitated ion transfer in

action. Various CV peak characteristics have been compiled in Table 10 and 11 for each ion and each concentration.
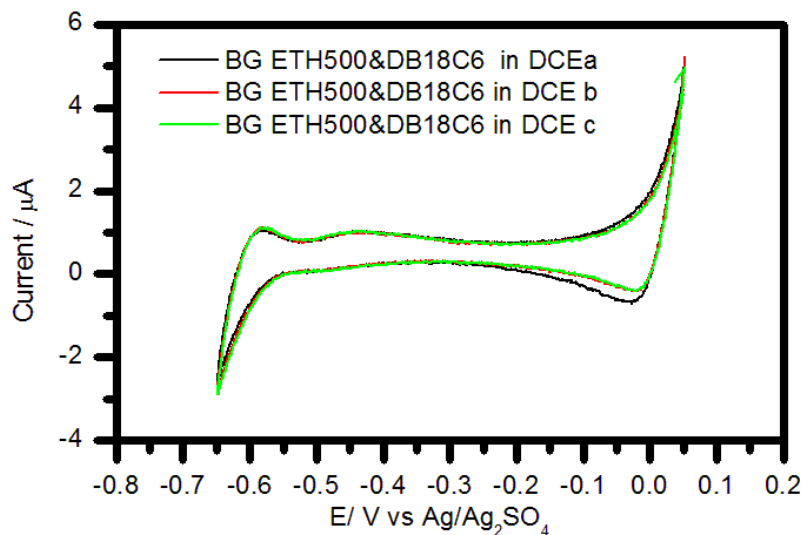
Fig 43: Replicate background CVs of Ag|ETH500 (10 mM)/ DB18C6 (50 mM)/ DCE|| in aq. MgSO$_4$ (50 mM). E$_{initial}$ = E$_{final}$ = 0.05 V; E$_{final}$ = -0.65 V; scan rate = 10 mV/ s
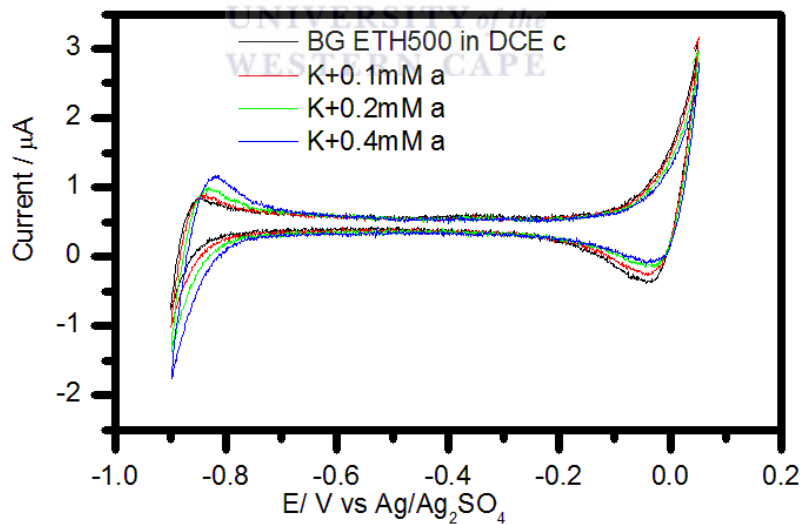
Fig 44: CVs of Ag|ETH500 (10 mM)/ DCE|| before (black) and with K$^+$ (red = 0.1, green = 0.2, and blue = 0.4 mM) in aq. MgSO$_4$ (50 mM). E$_{initial}$ = E$_{final}$ = 0.05 V; E$_{low}$ =- 0.9 V; scan rate = 10 mV/ s
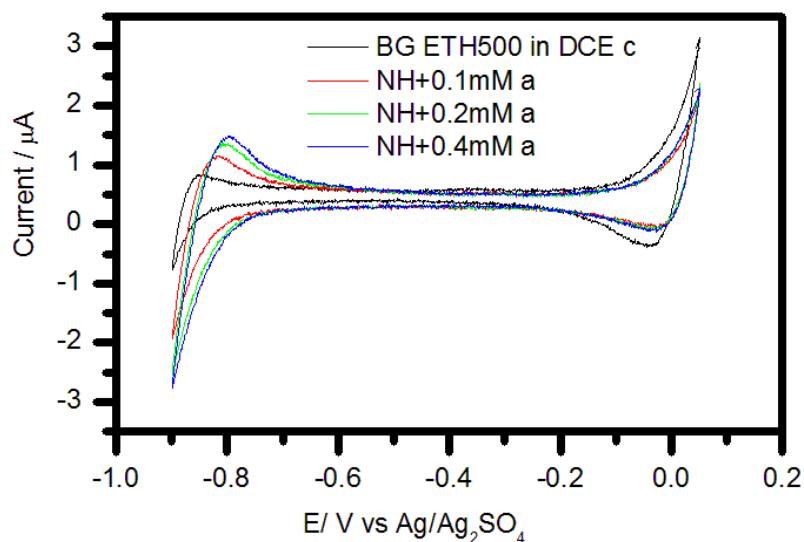
Fig 45: CVs of Ag|ETH500 (10 mM)/ DCE|| before (black) and with NH_4^+ (0, 0.1, 0.2, 0.4 mM) in aq.

$MgSO_4$ (50 mM). $E_{initial} = E_{final} = 0.05$ V; $E_{low} = -0.9$ V; scan rate = 10 mV/ s
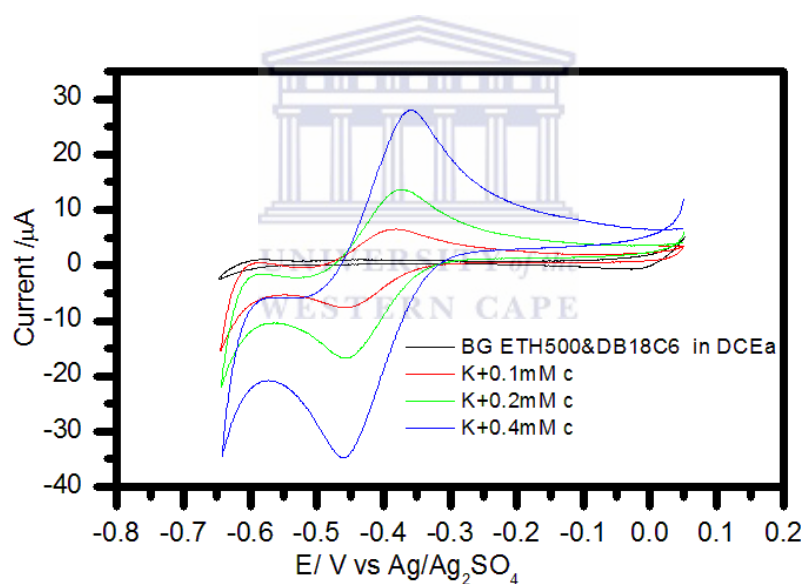
Fig 46: CVs of K^+ (0, 0.1, 0.2, and 0.4 mM) at Ag|ETH500 (10 mM)/ DB18C6 (50 mM)/ DCE|| in aq.

$MgSO_4$ (50 mM). $E_{initial} = E_{final} = 0.05$ V; $E_{final} = 0.65$ V; scan rate = 10 mV/ s
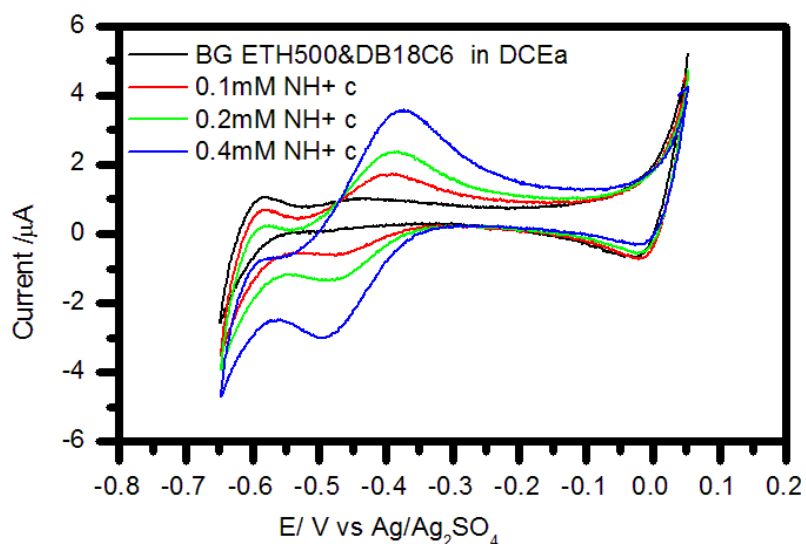
Fig 47: CVs of NH_4^+ (0, 0.1, 0.2, and 0.4 mM) at Ag|ETH500 (10 mM)/ DB18C6 (50 mM)/ DCE|| in

aq. $MgSO_4$ (50 mM). $E_{initial} = E_{final} = 0.05$ V; $E_{final} = 0.65$ V; scan rate = 10 mV/ s

According to Fig 47 and Fig 48, the transfer of K^+ and NH_4^+ ions from the aq. $MgSO_4$ phase

to the ETH500/ DB18C6/ DCE phase is a facilitated ion transfer, and this has already been

explained in the literature by equation (17) [79]:

K^+/ NH_4^+ (aq.) + DB18C6 (DCE) → [K^+ / NH_4^+DB18C6] (DCE)   (17)

In addition, the revers reaction for would be:

[K^+/ NH_4^+DB18C6] (DCE) → K^+ / NH_4^+ (aq.) + DB18C6 (DCE)   (18)

Table 11: Peak characteristics versus concentration for CVs of K^+ at Ag|ETH500 (10 mM)/ DB18C6 (50 mM)/ DCE‖ in $MgSO_4$ (50 mM).

Potentials are according to: $E = E_{Ag|O} - \Delta_w^O \varphi - E_{Ag|Ag_2SO_4, Aq.SO_4^{2-}(1M)}$

Aq. K^+ / mM	$E_{p, W \to O}$ / V	$E_{p, O \to W}$ / V	$i_{p\ W \to O}$ / μA	$i_{p\ O \to W}$ / μA	$i_{bg\ W \to O}$ / μA	$i_{bg\ O \to W}$ / μA	$\Delta i_{p\ W \to O}$ / μA	$\Delta i_{p\ O \to W}$ / μA	ΔE_p	$E^{o'}$/ V
0.1	-0.46	-0.38	-6.00	5.32	0	-0.499	-6.00	5.82	0.08	-0.42
0.2	-0.46	-0.37	-14.4	11.6	0.759	-2.24	-15.2	13.8	0.09	-0.42
0.4	-0.46	-0.37	-16.7	13.7	1.32	-2.20	-18.0	15.9	0.09	-0.42

Table 12: Peak characteristics versus concentration for CVs of NH_4^+ at Ag|ETH500 (10 mM)/ DB18C6 (50 mM)/ DCE‖ in $MgSO_4$ (50 mM).

Potentials are according to: $E = E_{Ag|O} - \Delta_w^O \varphi - E_{Ag|Ag_2SO_4, Aq.SO_4^{2-}(1M)}$

Aq. NH_4^+ / mM	$E_{p, W \to O}$ / V	$E_{p, O \to W}$ / V	$i_{p\ W \to O}$ / μA	$i_{p\ O \to W}$ / μA	$i_{bg\ W \to O}$ / μA	$i_{bg\ O \to W}$ / μA	$\Delta i_{p\ W \to O}$ / μA	$\Delta i_{p\ O \to W}$ / μA	ΔE_p	$E^{o'}$/ V
0.1	-0.48	-0.4	-0.73	1.72	0.28	0.46	-1.01	1.26	0.08	-0.43
0.2	-0.48	-0.38	-0.13	2.33	0.23	0.15	-0.36	2.18	0.1	-0.43
0.4	-0.49	-0.38	-2.74	3.46	0.19	-0.67	-2.93	4.13	0.11	-0.44

From this part of work we can conclude that

a)DB18C6 make good complexation with K^+ and NH_4^+.

b) when we try to detect K^+ and NH_4^+ ions without DB18C6 no peaks were bserved, but after adding DB18C6 in organic phase, the ion transfer from aqueous phase to organic phase and come back again.The disadvantages in presence of DB18C6 the potential window was narrower in Fig 48.
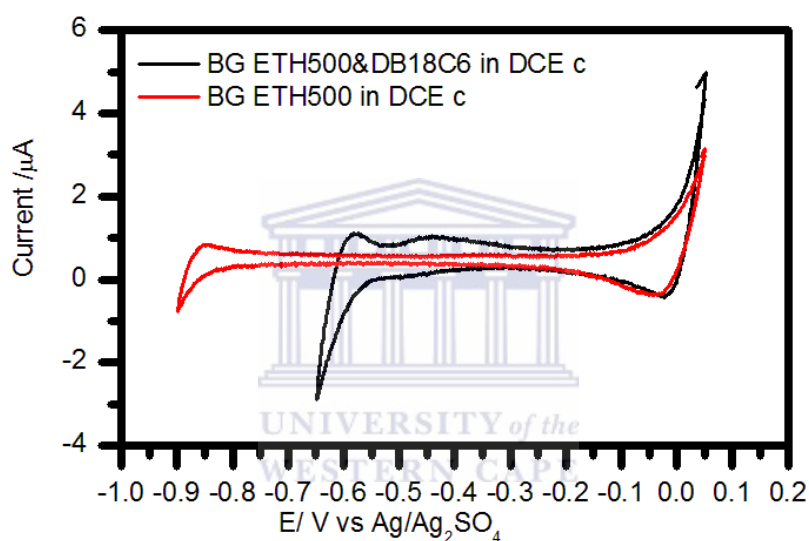
Fig 48: Potential windows of Ag|ETH500 (10 mM)/ DCE|| (red) and Ag|ETH500 (10 mM)/ DB18C6 (50 mM)/ DCE|| (black) in aq. $MgSO_4$ (50 mM). Scan rate = 10 mV/ s.

Fig 49 A and B respectively show the CVs of K^+ and NH_4^+ at the Ag|ETH500(10 mM)/DCE|| and Ag|ETH500(10 mM)/ DB18C6(50 mM)/DCE|| sensors. Furthur more in Table (11) and (12) demonstrate the reproducibility of the CVs characteristics at three different concentrationd based on Figs 46 and 47.
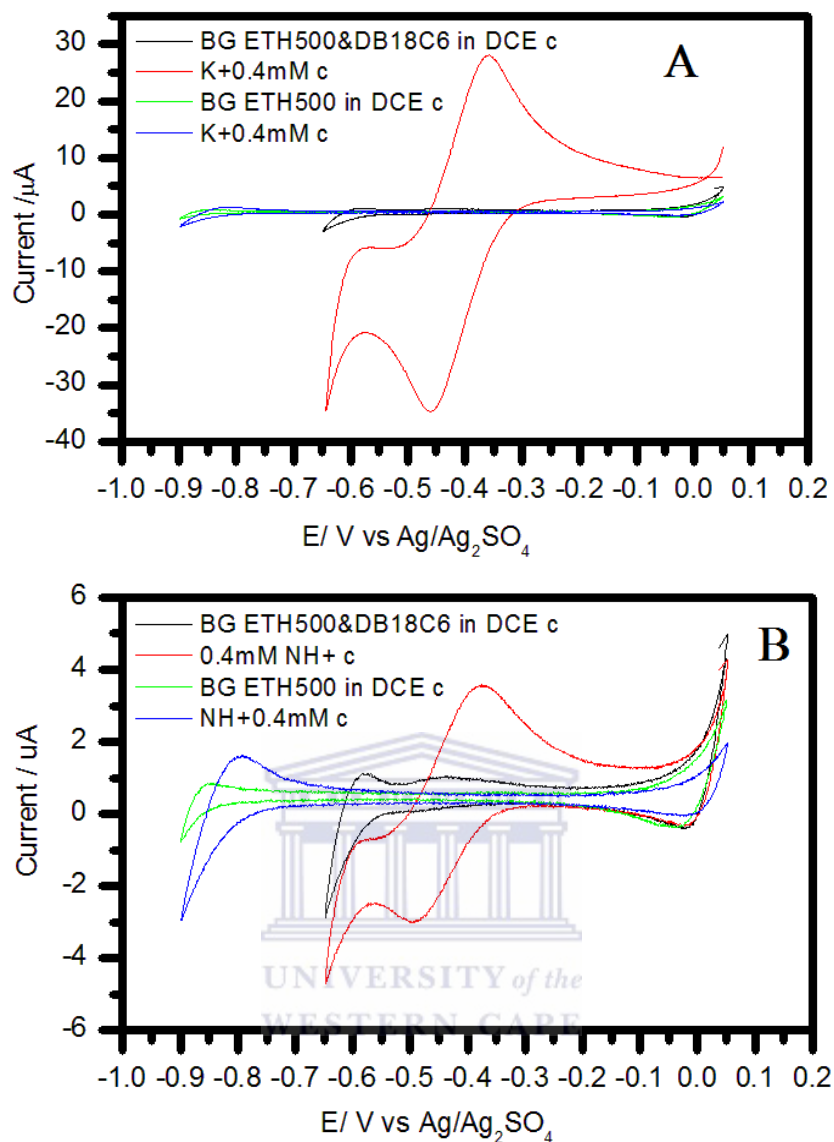
Fig 49: (A) CVs of K^+ (0.4 mM) at Ag|ETH500 (10 mM)/ DCE|| (red) and Ag|ETH500 (10 mM)/ DB18C6 (50 mM)/ DCE|| (black) in aq. $MgSO_4$ (50 mM). (B) As in A but for NH_4^+.

5.3 Sensor operation optimization using Tenofovir

After selecting the most suitable pair of hydrophobic and aqueous phases, in this section the response of the resulting sensors to tenofovir the in aq. phase (Aq. $MgSO_4$) at different concentrations was tested preliminarily as shown in Fig 50. The tenofovir cations transfer from the aq. $MgSO_4$ phase to the ETH500/DCE phase was exhibited differently from that of

the K^+ and NH_4^+ ions (Fig 51). Its CV characteristics at three concentrations are summarized in Table 13.
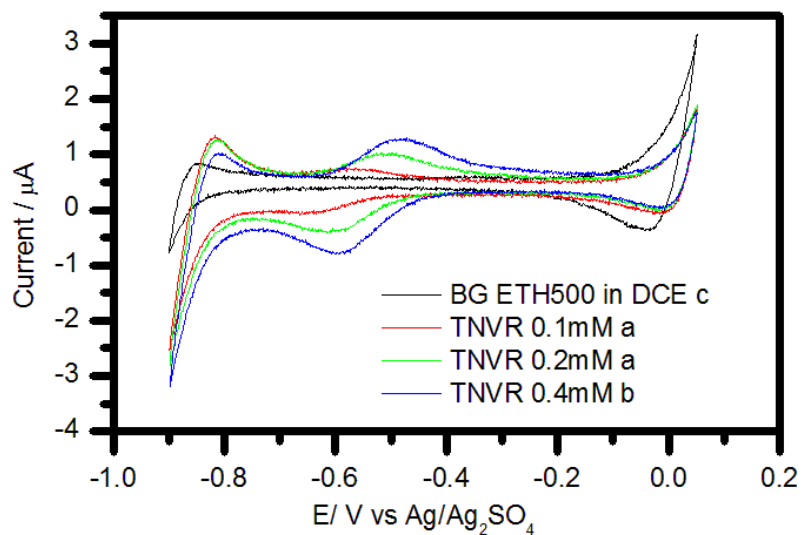
Fig 50: CVs of tenofovir (0, 0.1, 0.2, and 0.4 mM) at Ag|ETH500 (10 mM)/ DCE|| in aq. MgSO$_4$ (100 mM). E$_{initial}$ = E$_{final}$ = 0.05 V; E$_{final}$ = -0.9 V; scan rate = 10 mV/ s
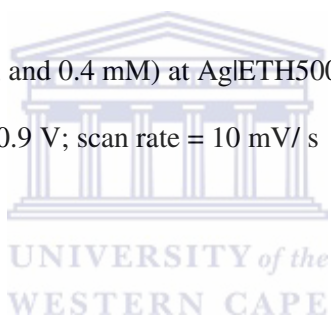
Table 13: Peak characteristics versus concentration for CVs of tenofovir at Ag|ETH500 (10 mM)/ DB18C6 (50 mM)/ DCE‖ in $MgSO_4$ (50 mM). Potentials are according to: $E = E_{Ag|O} - \Delta_w^O \varphi - E_{Ag|Ag_2SO_4,\,Aq.\,SO_4^{2-}\,(1M)}$

Tenofovir/	$E_{p,\,W \to O}$	$E_{p,\,O \to W}$	$i_{p\,W \to O}$	$i_{p\,O \to W}$	$i_{bg\,W \to O}$	$i_{bg\,O \to W}$	$\Delta i_{p\,W \to O}$	$\Delta i_{p\,O \to W}$	ΔE_p	$E^{o\prime}$/ V
mM	/ V	/ V	/ μA	/ μA	/ μA	/ μA	/ μA	/ μA		
0.1	-0.64	-0.57	-0.05	0.74	0.28	0.65	-0.33	0.09	0.07	-0.61
0.2	-0.60	-0.51	-0.38	1.01	0.31	0.64	-0.69	0.37	0.09	-0.56
0.4	-0.60	-0.48	-0.74	1.23	0.31	0.59	-1.05	0.64	0.12	-0.54
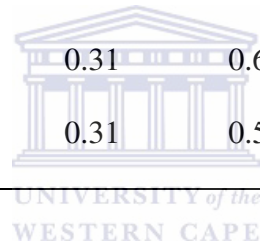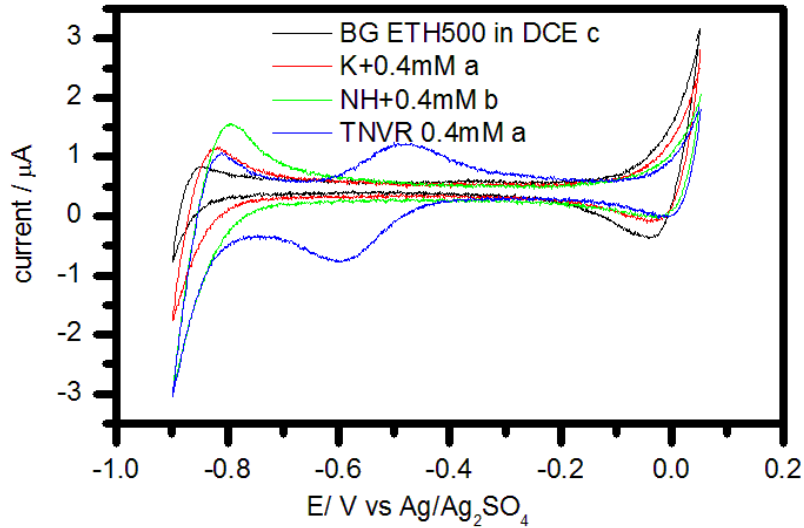
Fig 51: CV responses of Ag|ETH500 (10 mM)/DCE‖ to 0.4 mM K⁺ (red), NH₄⁺ (green), and tenofovir (blue) in aq. MgSO₄ (100 mM). Black curve = 0 mM. $E_{initial} = E_{final} = -0.05$; $E_{low} = -0.9$ V; scan rate = 10 mV/ s.

When the DB18C6 (50 mM) was added to ETH500 in DCE, the resulting sensor's configuration will be as follows: Ag|ETH500 (10 mM)/DB18C6(50 mM)/DCE‖ as shown in fig (52), moreover when the K⁺ and NH₄⁺ ions were added it is observed that the K⁺ ion has higher response than TNVR according to the literature the DB18C6 has strong complexion abilities and has high affinity for alkali metal cations [80] as shown in fig (53)
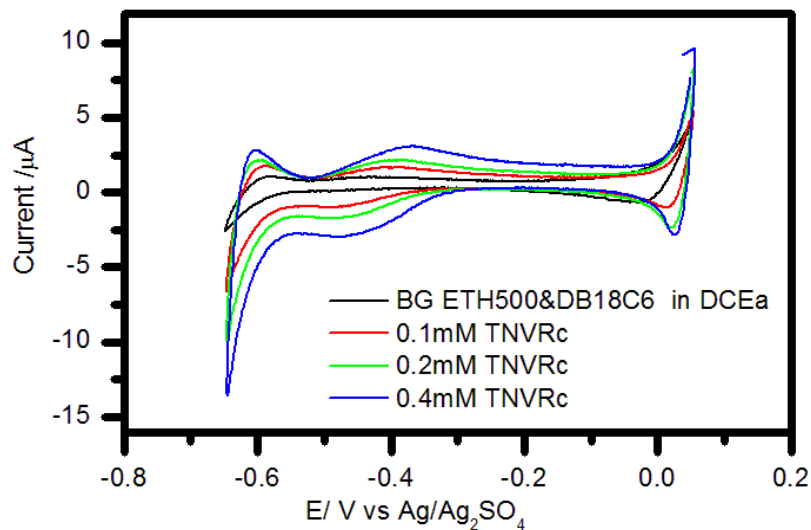
Fig 52: CV responses of Ag|ETH500 (10 mM)/DB18C6 (50 mM)/DCE‖ to 0.4 mM K^+ (red), NH_4^+ (green), and tenofovir (blue) in aq. $MgSO_4$ (100 mM). Black curve = 0 mM. $E_{initial}$ = E_{final} = 0.05 V; E_{low} = -0.65 V; scan rate = 10 mV/ s
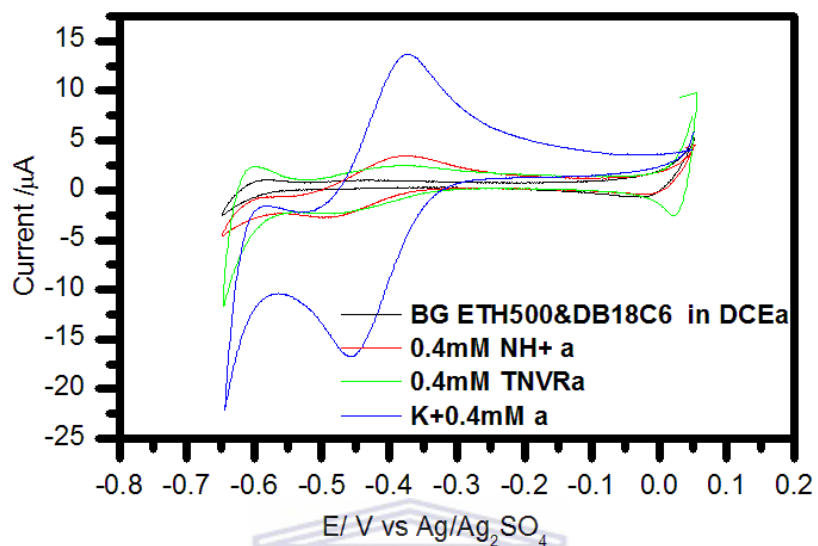
Fig 53: CV responses of Ag|ETH500 (10 mM)/ DB18C6/DCE‖ to 0.4 mM K^+ (blue), NH_4^+ (red), and tenofovir (green) in aq. MgSO4 (100 mM). Black curve = 0 mM $E_{initial}$ = E_{final} = -0.05; E_{low} = -0.65 V; scan rate = 10 mV/ s.

Table 14: Peak characteristics versus concentration for CVs of tenofovir at Ag|ETH500 (10 mM)/ DB18C6 (50 mM)/ DB18C6 (50 mM)/DCE‖

in $MgSO_4$ (50 mM). Potentials are according to: $E = E_{Ag|O} - \Delta_w^O \varphi - E_{Ag|Ag_2SO_4, Aq. SO_4^{2-} (1M)}$

Tenofovir/ mM	$E_{p, W\to O}$/ V	$E_{p, O\to W}$/ V	$i_{p\ W\to O}$/ μA	$i_{p\ O\to W}$/ μA	$i_{bg\ W\to O}$/ μA	$i_{bg\ O\to W}$/ μA	$\Delta i_{p\ W\to O}$/ μA	$\Delta i_{p\ O\to W}$/ μA	ΔE_p/ V	$E^{o\prime}$/ V
0.1	-0.49	-0.41	-0.90	1.60	0.202	0.93	-1.10	0.67	0.08	-0.45
0.2	-0.47	-0.39	-1.57	2.05	0.196	1.09	-1.77	0.96	0.08	-0.43
0.4	-0.47	-0.38	-2.28	2.52	0.234	1.06	-2.51	1.46	0.09	-0.43
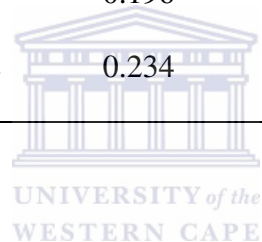
5.3.1 Cyclic voltammetry at different scan rate

The purpose of this section is to choose the best scan rate by using one concentration of tenofovir (0.2 mM) for the two sensors as shown in Fig 54 and Fig 55 respectively.
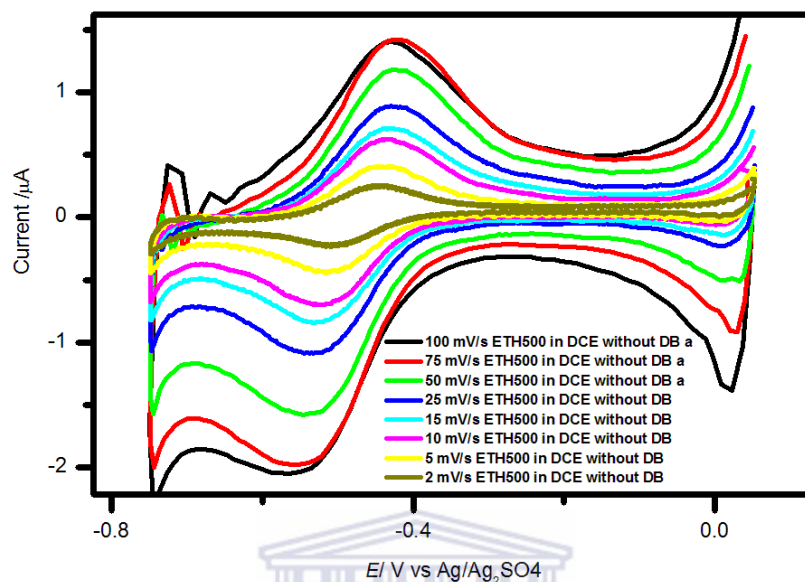
Fig 54: CV of tenofovir (0.4 mM) at various scan rates at the Ag|ETH500 (10 mM)/DCE‖ sensor in aq. Li_2SO_4 (100 mM). Scan rates: 2 to 100 mV/ s.
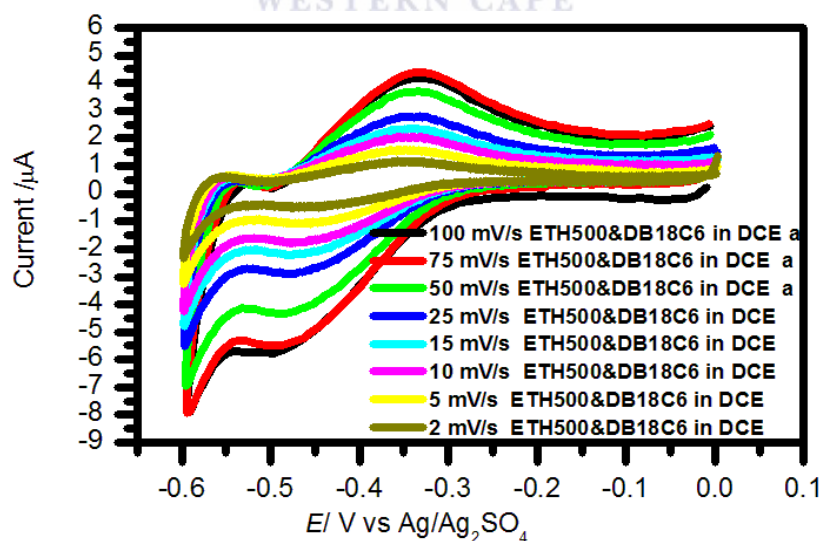
Fig 55 : CV of tenofovir (0.4 mM) at various scan rates at the Ag|ETH500 (10 mM)/ DB18C6 (50 mM)/ DCE‖ sensor in aq. $MgSO_4$ (100 mM). Scan rates: 2 to 100 mV/ s.

In order to select an appropriate scan rate with the best signal-to-noise ratio (S/N) for use in further studies, peak height to background current ratios were plotted against scan rate for both sensors between 2 and 100 mV/s (see Figure 56). The $W \rightarrow O$ ion transfer peak signal of the sensor without DB18C6 exhibited an S/N ratio that increased significantly with decreasing scan rate up to a maximum of S/N = 16 at 5 mV/s. The equivalent of this was not observed for the reverse $O \rightarrow W$ peak, the S/N ratio which remained practically independent of scan rate but with an indication of a slightly broad maxima at about 25 mV/s. The $W \rightarrow O$

and $O \rightarrow W$ peaks of the sensor with DB18C6 also behaved similarly as the respective corresponding peaks of the first sensor. However, this time, the $W \rightarrow O$ peaks S/N ratio dependence on scan rate was only slight and increased only up to S/N of 2 at 2 mV/s. Based on consideration of a reasonable S/N ratio but faster sample through put rate of the current CV operation mode, the scan rate of 25 mV/s was chosen for both sensors and used in further experiments.
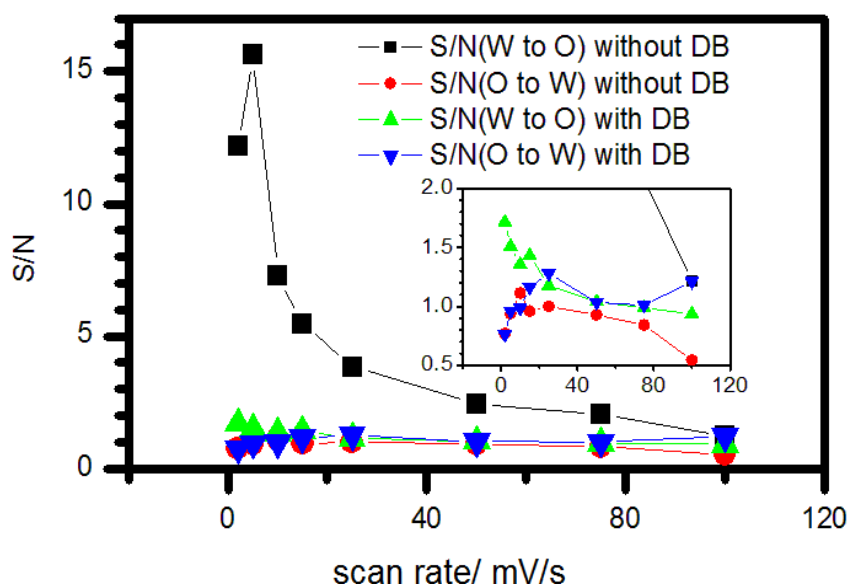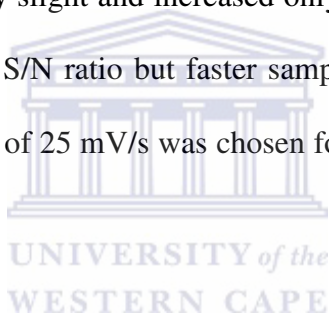
Fig 56: Peak current to background current (S/N) ratio versus scan rate for Ag|ETH500 (10 mM)/DCE|| (▲ and ▼) and Ag|ETH500 (10 mM)/ DB18C6 (50 mM)/ DCE|| (■ and ●) at 0.4 mM 2tenofovir in aq. $MgSO_4$ (100 mM).

It is very important to know whether the reaction is reversible, irreversible or quasi-reversible. If ΔE_p *is* greater than 200/n mV, it is reversible; if ΔE_p is approximately 60/n mV, it is irreversible, but if ΔE_p is between 60/n mV and 200/n mV it is quasi-reversible. But in this case it was reversible.

The observation from Fig 59 combined with Table (16) and (17), the E^o is constant – i.e. independent from the scan rate or log of scan rate.
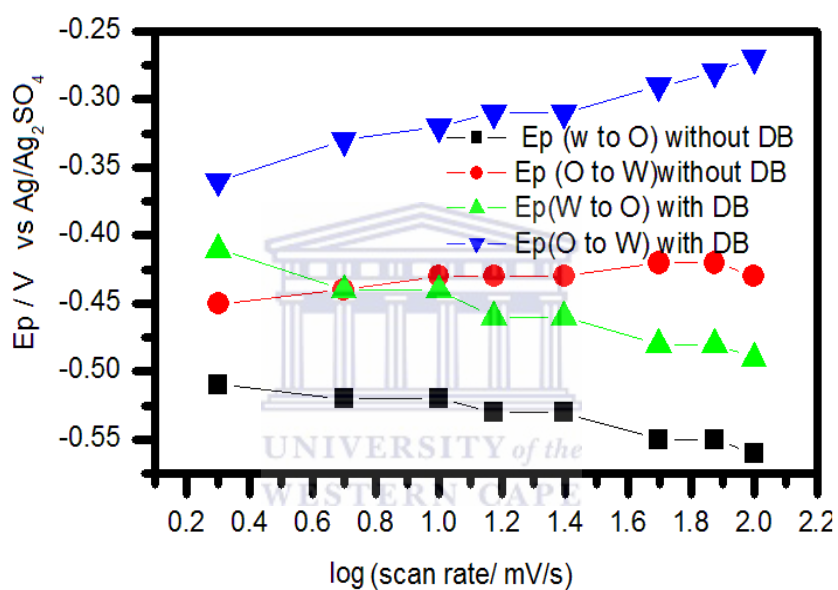
Fig 57: Peak potentials (E_p) versus log scan rate for tenofovir (0.4 mM) at Ag|ETH500 (10 mM)/DCE|| (▲ & ▼) and Ag|ETH500 (10 mM)/ DB18C6 (50 mM)/ DCE|| (■ & ●) in aq. MgSO₄ (100 mM)
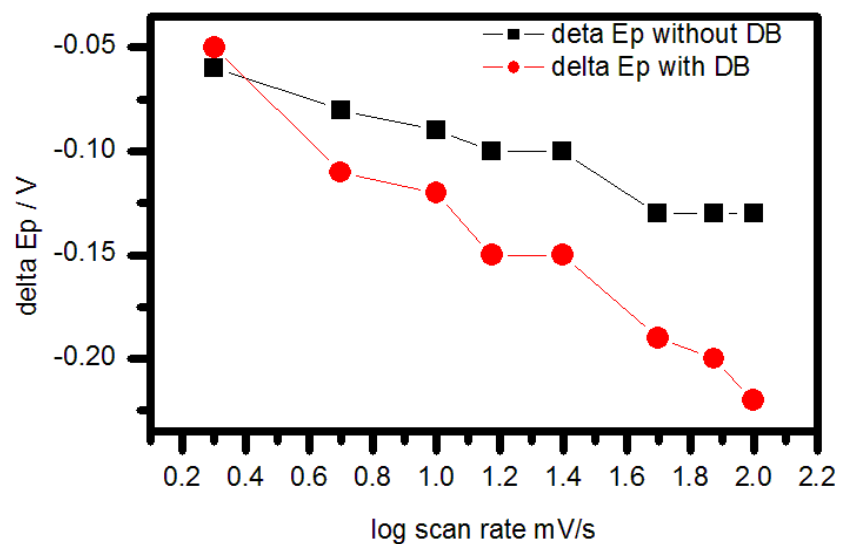
Fig 58: Peak separation (ΔE_p) versus log scan rate for 0.4 mM tenofovir at Ag|ETH500 (10

mM)/DCE|| (■) and Ag|ETH500 (10 mM)/ DB18C6 (50 mM)/ DCE|| (●) in aq. MgSO$_4$ (100 mM)

Table 15: Linear fitting parameters obtained from peak potential (E_p) versus scan rate plots, and formal potentials of simple and facilitated-ion transfer for tenofovir (0.4 mM) in aq. Li_2SO_4 (100 mM). Potentials are according to: $E = E_{Ag|O} - \Delta_w^O \varphi - E_{Ag|Ag_2SO_4,\,Aq.\,SO_4^{2-}\,(1M)}$

Sensor	Configuration	Signal	Scan rate/ mV/s	R	N	$E°\pm SD$ /V	Intercept/ V	Slope / V
Sensor 1	Ag|ETH500 (10 mM)/DCE|	$i_{p,\,W\to O}$	10 – 100	-0.9732	6	-0.48 ± 0.007	-0.482	-0.04 ± 0.004
		$i_{p,\,O\to W}$	2 – 75	0.9691	7	-0.48 ± 0.003	-0.453	0.02 ± 0.002
Sensor 2	Ag|ETH500 (10 mM)/ DB18C6 (50 mM)/ DCE|	$i_{p,\,W\to O}$	2 – 100	-0.9799	8	-0.38 ± 0.003	-0.402	-0.04 ± 0.004
		$i_{p,\,O\to W}$	2 – 100	0.9876	8	-0.38 ± 0.003	-0.370	0.05 ± 0.003

Table 16: Parameters obtained by averaging or from linear plots of the W→ O and O → W ion-transfer peak potentials (E_p) versus log scan rate for tenofovir (0.4 mM) in aq. Li_2SO_4 (100 mM). Potentials: $E = E_{Ag|O} - \Delta_w^O \varphi - E_{Ag|Ag_2SO_4,\,Aq.\,SO_4^{2-}\,(1M)}$

Sensor	Configuration	Scan rate/ mV/s	R ($N = 4$)	$E°\pm SD$/ V	Intercept/ V	Slope / V
Sensor 1	Ag|ETH500 (10 mM)/DCE|	2 – 15	0.9964	-0.48 ± 0.003	0.047	0.04 ± 0.003
Sensor 2	Ag|ETH500 (10 mM)/ DB18C6 (50 mM)/ DCE|	*25 – 100*	0.9902	-0.38 ± 0.003	0.005	0.11 ± 0.01

81
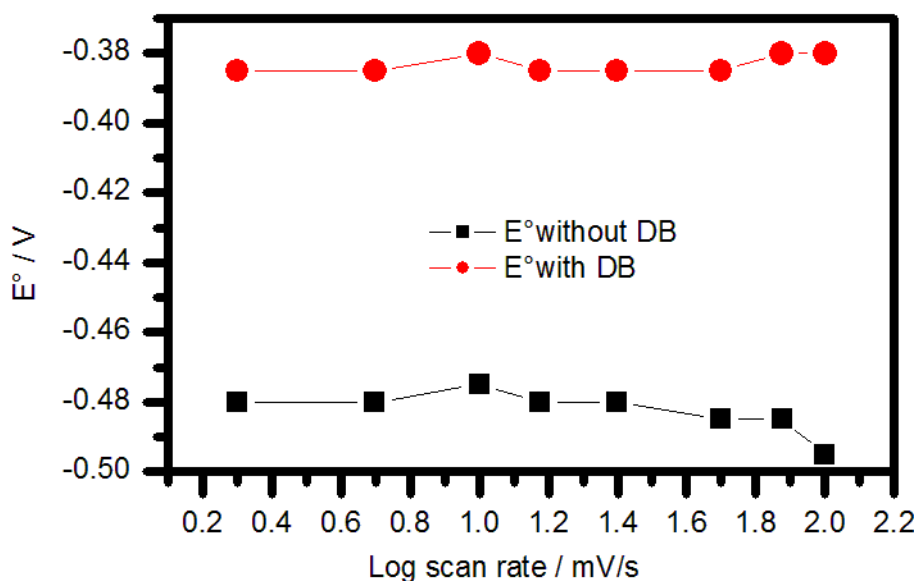
Fig 59: Formal potentials (E°′) obtained at different scan rates with Ag|ETH500 (10 mM)/DCE‖ (■) and Ag|ETH500 (10 mM)/DB18C6 (50 mM)/DCE‖ (●) for tenofovir (0.4 mM) in aq. $MgSO_4$ (100 mM)

In order to estimate the value of diffusion coefficient, Δi_p was plotted versus square root of scan rate and scan rate in Fig (61) and Fig (62). According to equation (18), the value of diffusion coefficient was evaluated from the slope values in Table (15) and (16) as shown in two table below the values of $W \rightarrow O$ not $O \rightarrow W$ because the R values were better than $O \rightarrow W$ in both sensor.

$$\Delta i_p = 0.4463 nFA[nF/RT]^{1/2} C^{bulk} D^{1/2} v^{1/2} \tag{19}$$

Where i_p is peak current; F is Faraday constant (96485 C/ mol); D is diffusion coefficient (cm^2/ s) of the electroactive species; A is the area of the electrode/cm^2; v is the sweep rate (V/ s); R is the universal gas constant (8.413 J/mol K) and T is temperature (298 K) and C^{bulk} concentration (mol cm^{-3}) of the analyte solution. The value found for D (see Table 17 and 18) were very smal, indicating that diffusion through the membrane was rate limiting process.
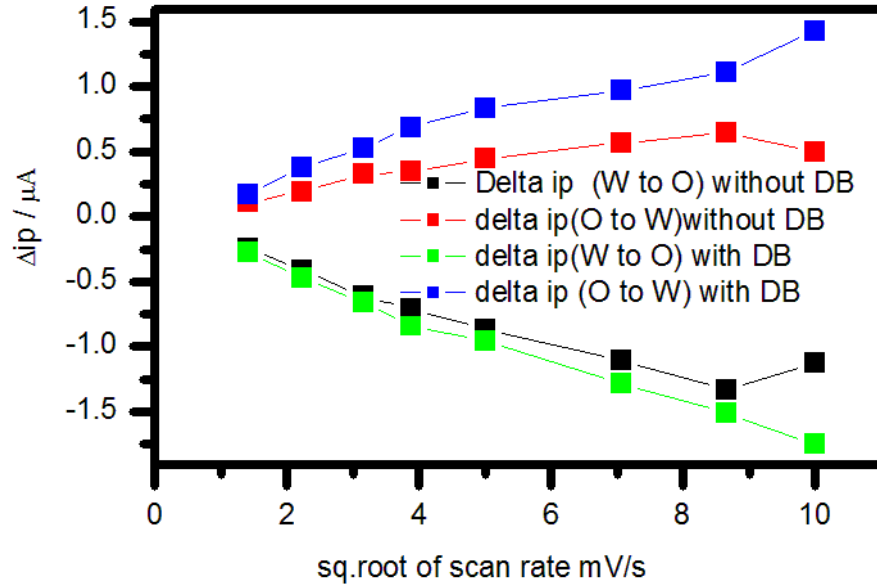
Fig 60: Peak current (Δi_p) versus square root of scan rate plots for tenofovir (0.4 mM) transfer at AglETH500 (10 mM)/DCEll (■ & ■) and AglETH500 (10 mM)/ DB18C6 (50 mM)/ DCEll (■ & ■) in aq. MgSO$_4$ (100 mM)
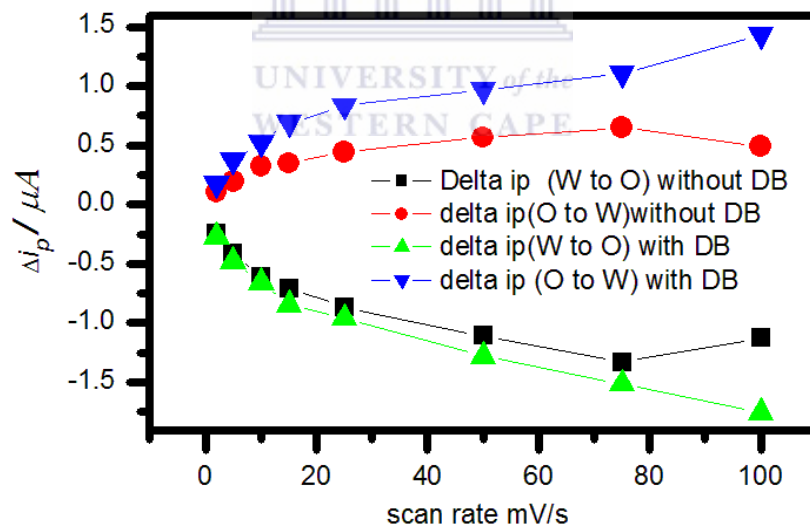
Fig 61: Peak current (Δi_p) versus scan rate plots for tenofovir (0.4 mM) at AglETH500 (10 mM)/DCEll (■ & ■) and AglETH500 (10 mM)/ DB18C6 (50 mM)/ DCEll (■ & ■) in aq. MgSO$_4$ (100 mM)

Table 17: Data obtained by linear-regression of plot of W$\rightarrow$O and O $\rightarrow$ W ion-transfer peak currents (Δi_p) versus scan rate for in tenofovir (0.4 mM)/ aq. Li_2SO_4 (100 mM) with indicated sensors

Sensor	Configuration	Scan rate/ mV/s	Signal	$R(N=5)$	Intercept/ μA	Slope/ nA/mVs^{-1}	D/ cm^{2}s^{-1}
Sensor 1	Ag|ETH500 (10 mM)/DCE||	$10-75$	$i_{p,\,W\rightarrow O}$	-0.9922	-0.548	-10.73 ± 0.7	2.48×10^{-11}
Sensor 2	Ag|ETH500 (10 mM)/ DB18C6 (50 mM)/ DCE||	$15-100$	$i_{p,\,W\rightarrow O}$	-0.9974	-0.699	-107.3 ± 0.4	9.936×10^{-9}

Table 18: Data obtained by linear-regression of plot of W$\rightarrow$O and O $\rightarrow$ W ion-transfer peak currents (Δi_p) versus square root of scan rate for in tenofovir (0.4 mM)/ aq. Li_2SO_4 (100 mM) with indicated sensors

Sensor	Configuration	Scan rate/ mV/s	Signal	R (N=5)	Intercept/ μA	Slope / nA/mVs^{-1}	D/ cm^{2}s^{-1}
Sensor 1	Ag|ETH500 (10 mM)/DCE||	$10-75$	$i_{p,\,W\rightarrow O}$	-0.9995	-0.209	-128.7±2.3	3.573×10^{-9}
Sensor 2	Ag|ETH500 (10 mM)/ DB18C6 (50 mM)/ DCE||	$15-100$	$i_{p,\,W\rightarrow O}$	-0.9979	-0.235	-149.2 ± 5.5	4.803×10^{-9}

Table 19: CV parameters obtained at various scan rates for tenofovir (0.4 mM) with the Ag|ETH500 (10 mM)/DCE‖ sensor in aq. Li_2SO_4 (100 mM). i_p = the total peak current before background substraction; i_{bg} = backckground current at the peak potential; $\Delta i_p = i_p - i_{bg}$; Potentials:

$$E = E_{Ag|O} - \Delta_w^O \varphi - E_{Ag|Ag_2SO_4, Aq.SO_4^{2-}(1M)}$$

ν / mV s⁻¹	log (ν / mV s⁻¹)	$\nu^{\frac{1}{2}}$ / (mV s⁻¹)^½	$E_{p, W\to O}$ / V	$E_{p, O\to W}$ / V	$i_{p\ W\to O}$ / μA	$i_{p\ O\to W}$ / μA	$i_{bg\ W\to O}$ / μA	$i_{bg\ O\to W}$ / μA	$\Delta i_{p\ W\to O}$ / μA	$\Delta i_{p\ O\to W}$ / μA	S/N W→O	S/N O→W	$i_{p\ W\to O}/i_{p\ O\to W}$	$E°$ /V	ΔE_p /V
100	2	10	-0.56	-0.43	-2.05	1.40	-0.923	0.907	-1.13	0.493	1.22	0.54	-1.46	-0.50	0.13
75	1.875	8.660	-0.55	-0.42	-1.97	1.42	-0.642	0.771	-1.33	0.649	2.07	0.84	-1.39	-0.49	0.13
50	1.699	7.071	-0.55	-0.42	-1.56	1.18	-0.453	0.612	-1.11	0.568	2.44	0.93	-1.32	-0.49	0.13
25	1.398	5	-0.53	-0.43	-1.09	0.891	-0.225	0.446	-0.865	0.445	3.84	1.00	-1.22	-0.48	0.1
15	1.176	3.873	-0.53	-0.43	-0.835	0.713	-0.129	0.364	-0.706	0.349	5.47	0.96	-1.17	-0.48	0.1
10	1	3.162	-0.52	-0.43	-0.696	0.621	-0.084	0.294	-0.612	0.327	7.31	1.11	-1.12	-0.48	0.09
5	0.699	2.236	-0.52	-0.44	-0.438	0.405	-0.026	0.209	-0.412	0.196	15.65	0.94	-1.08	-0.48	0.08
2	0.301	1.414	-0.51	-0.45	-0.226	0.253	0.020	0.143	-0.246	0.110	12.19	0.77	-0.89	-0.48	0.06

Table 20: CV parameters obtained at various scan rates for tenofovir (0.4 mM) with the Ag|ETH500 (10 mM)/ DB18C6 (50 mM)/DCE|| sensor in aq. Li_2SO_4 (100 mM). i_p = the total peak current before background substraction; i_{bg} = backckground current at the peak potential; $\Delta i_p = i_p - i_{bg}$; Potentials:: $E = E_{Ag|O} - \Delta_w^O\varphi - E_{Ag|Ag_2SO_4,\,Aq.\,SO_4^{2-}\,(1M)}$

ν	$\log(\nu$	$\nu^{1/2}$	$E_{p,\,W\to O}$	$E_{p,\,O\to W}$	$i_{p\,W\to O}$	$i_{p\,O\to W}$	$i_{bg\,W\to O}$	$i_{bg\,O\to W}$	$\Delta i_{p\,W\to O}$	$\Delta i_{p\,O\to W}$	S/N	S/N	ΔE_p	$i_{p\,W\to O}$	$E°$
/ mV s^{-1}	/ mV s^{-1})	/ (mV s^{-1})$^{\frac{1}{2}}$	/V	/V	/ µA	/ µA	/ µA	/ µA	/ µA	/ µA	$W\to O$	$O\to W$	/ V	/$i_{p\,O\to W}$	/V
100	2	10	-0.49	-0.27	-3.62	2.61	-1.87	1.18	-1.75	1.43	0.936	1.212	0.22	1.39	-0.38
75	1.875	8.660	-0.48	-0.28	-3.04	2.21	-1.53	1.10	-1.51	1.11	0.987	1.009	0.2	1.38	-0.38
50	1.699	7.071	-0.48	-0.29	-2.52	1.91	-1.24	0.939	-1.28	0.971	1.040	1.034	0.19	1.32	-0.39
25	1.398	5	-0.46	-0.31	-1.77	1.49	-0.813	0.654	-0.957	0.836	1.177	1.278	0.15	1.30	-0.39
15	1.176	3.872	-0.46	-0.31	-1.43	1.28	-0.589	0.592	-0.841	0.688	1.428	1.162	0.15	1.18	-0.39
10	1	3.162	-0.44	-0.32	-1.14	1.06	-0.484	0.534	-0.656	0.526	1.355	0.985	0.12	1.47	-0.38
5	0.699	2.236	-0.44	-0.33	-0.788	0.768	-0.314	0.392	-0.474	0.376	1.510	0.959	0.11	1.07	-0.39
2	0.301	1.414	-0.41	-0.36	-0.429	0.407	-0.158	0.231	-0.271	0.176	1.715	0.762	0.05	1.03	-0.39

5.3.2 Sensor Stability

Furthermore, the stability of the sensor was checked by recording CVs at intervals for three hours before and after saturation (washing) of the organic phase with water. Figures 62 and 63 are overlays of typical results for that of the water-washed (saturated) organic phase. Fig 64 and Fig 65 shows how long the sensor will be stable, where peak heights are plotted against time for both sensors (without and with DB18C6).

In order to evaluate the stability of the sensor, the time against peak current were ploted for both sensors between (zero-180 min) fig(64) and fig (65) shows how the sensor was stable without DB18C6 for 90 second (from 30-120 min) $W \rightarrow O$
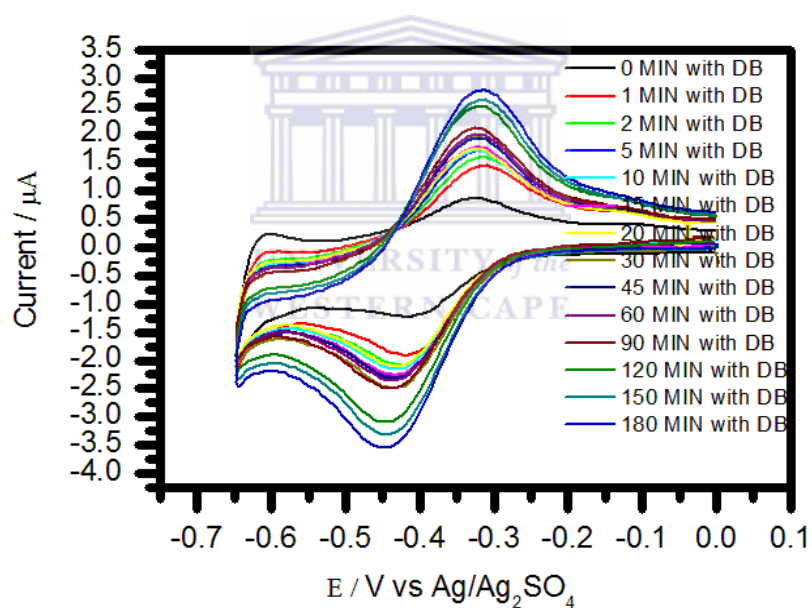
Fig 62: Time-lapse simple-ion transfer CV of tenofovir (0.2 mM) at the Ag|ETH500 (10 mM)/ DB18C6 (50 mM)//DCE|| sensor in aq. MgSO$_4$ (100 mM). Scan rate: 25 mV/ s
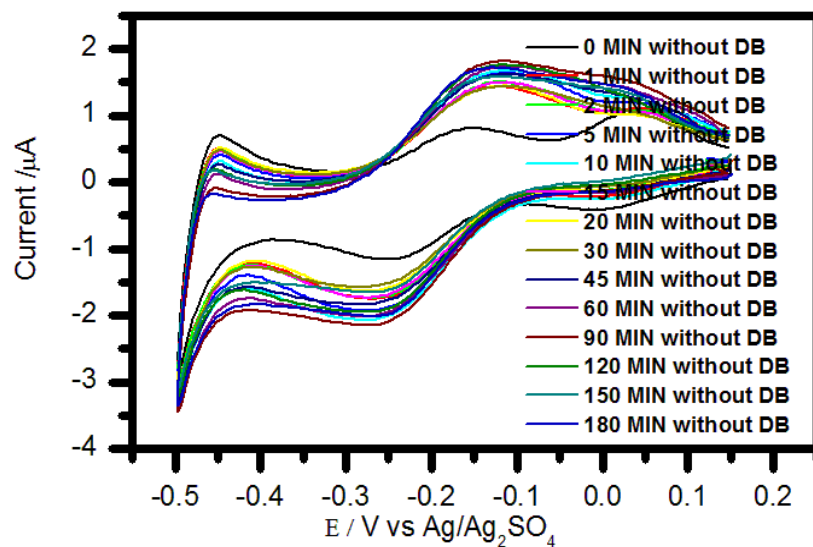
Fig 63: Time-lapse simple-ion transfer CV of tenofovir (0.2 mM) at the Ag|ETH500 (10 mM)/ DCE‖ sensor in aq. MgSO$_4$ (100 mM). Scan rate: 25 mV/ s
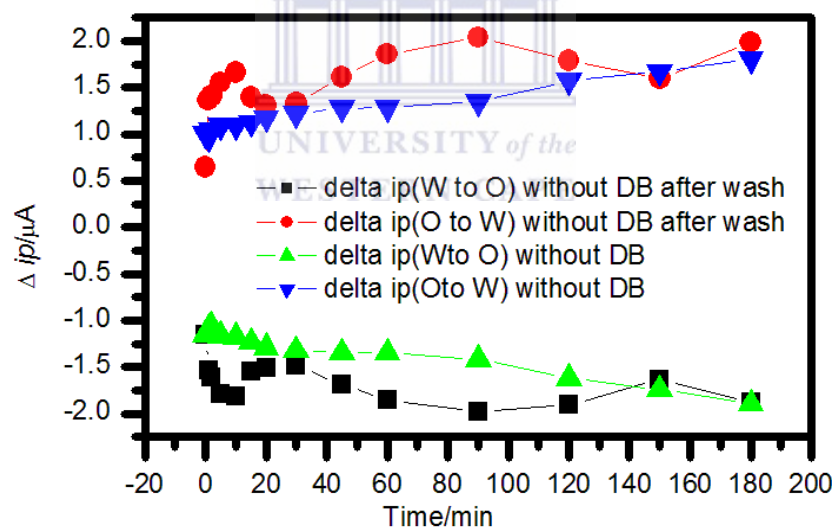
Fig 64: Peak current (Δi_p) versus time for tenofovir (0.2 mM) at the Ag|ETH500 (10 mM)/ DCE‖ in aq. MgSO$_4$ (100 mM). Curves: before (▲ & ▼) and after (■ & ●) overnight equilibration with DI water. Scan rate: 25 mV/ s
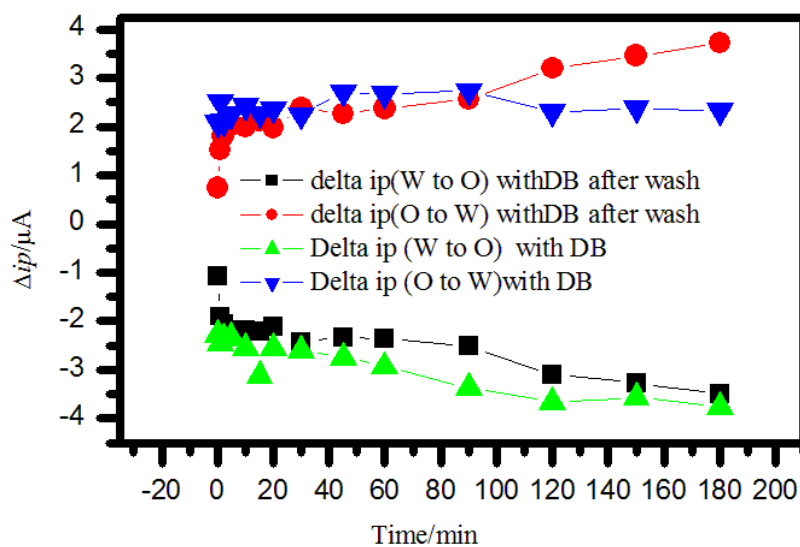
Fig 65: Peak current (Δi_p) versus time for tenofovir (0.2 mM) at the Ag|ETH500 (10 mM)/ DCE|| in

aq. MgSO$_4$ (100 mM). Curves: before (▲ & ▼) and after (■ & ●) overnight equilibration with DI

water. Scan rate: 25 mV/ s

Table 21: Operational stability statistics on peak currents (Δi_p) of tenofovir (0.2 mM) at the Ag|ETH500 (10 mM)/ DCE|| and Ag|ETH500 (10 mM)/ DB18C6 (50 mM)/DCE|| sensors in aq. MgSO$_4$ (100 mM). Scan rate: 25 mV/ s

Sensor	Configuration	CV signal	Before/ After DI water wash	0 – 180 min Mean ± *SD* / µA (N=14)	%SD	10 – 180 min Mean ±*SD*/ µA (N= 6 or *4)	%SD	10 – 100 min Mean ±*SD*/ µA (N = 7)	%SD
Sensor 2	Ag|ETH500(10 mM)/ DB18C6(50 mM)/DCE||	$\Delta i_{p,\ W \to O}$	Before washing	-2.80± 0.5	-18.44	-2.85±0.5	-17.75	-2.62±0.20	-6.78
			After washing	-2.38±0.6	-25.48	2.96±0.6	20.67	-2.31±0.14	-6.17
		$\Delta i_{p\ O \to W}$	Before washing	2.39±0.2	10.38	-2.93±0.5	-18.43	2.48±0.21	8.55
			After washing	2.18±0.7	31.40	2.53±0.2	11.52	2.17±0.45	15.92
Sensor 1	Ag|ETH500 (10 mM)/ DCE||	$\Delta i_{p,\ W \to O}$	Before washing	-1.34±0.2	-18.40	-1.74±0.2	-12.09	-1.30±0.08	-6.13
			After washing	1.26±0.3	20.35	1.71±0.3	17.90	-1.70±0.19	-11.27
		$\Delta i_{p,\ O \to W}$	Before washing	-1.67±0.2	-13.21	-1.56±0.2*	-14.62	1.22±0.090	7.75
			After washing	1.54±0.3	22.72	1.35±0.2	17.94	1.60±0.3	17.28

The started time for sensor 2 before and after wash was same (45 min), but the ending was ranging between (180 – 120) min.

Fig 66 shows plots of i_p (peak current) versus concentration for the two sensors under study at different concentrations of tenofovir from 0.1 µM to 200 µM. The various analytical parameters extracted from these curves have been compiled in Table (22). The detection limit varied from sensor to other as seen in table. The minus signs just show the signals are cathodic, while there is no much difference in sensitivity and the intercept was calculated to determine the background noise. In addition to the R value, detection limit and linearity rang were determined. The working potentials shown are average peak potentials for the sensors with water-saturated organic phase. Indeed, it would be the sensor Ag|ETH500/DCE‖ that will provide more selective tenofovir detection instead of the sensor Ag|ETH500 (10 mM)/DB18C6(50 mM)/DCE‖ because the latter would also respond to K^+, NH_4^+, and similar ions resulting in positive errors.
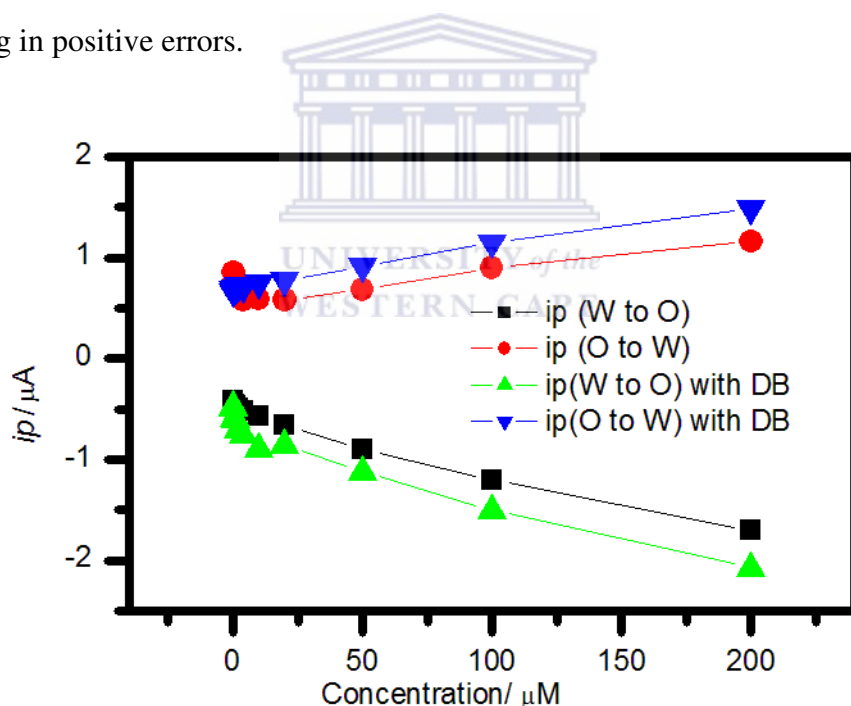
Fig 66: peak current (Δi_p) versus concentration of tenofovir at Ag|ETH500 (10 mM)/ DCE‖ (■ & ●) and Ag|ETH500 (10 mM)/ DB18C6 (50 mM)/DCE‖ (▲ & ▼) sensors in aq. $MgSO_4$ (100 mM). Scan rate: 25 mV/ s.

Table 22: Analytical figures of merit of Ag|ETH500 (10 mM)/ DCE|| (■ & ●) and Ag|ETH500 (10 mM)/ DB18C6 (50 mM)/DCE|| sensors for the the amperometric detection of tenofovir in aq. $MgSO_4$ (100 mM). Scan rate: 25 mV/ s. Potentials:

$$E = E_{Ag|O} + \Delta_w^O \varphi - E_{Ag|Ag_2SO_4, Aq.SO_4^{2-}(1M)} = \Delta_w^O \varphi + error$$

Sensors		Working potential/ V	Signal	R, $N = 5$	Intercept/ µA	Sensitivity / nA µM^{-1}	DOL /µM	Linearity Range/ µM
Sensor (1)	Ag|ETH500 (10 mM)/ DCE||	-0.52 ± 0.05	$i_{p, W \rightarrow O}$	-0.9965	-0.509	-7.09 ± 0.3	5	15 – 100
		-0.33 ± 0.02	$i_{p, O \rightarrow W}$	0.9922	0.548	3.05 ± 0.2	18	60 – 200
Sensor (2)	Ag|ETH500 (10 mM)/ DB18C6 (50 mM)/DCE||	-0.47 ± 0.02	$i_{p, W \rightarrow O}$	-0.9984	-0.823	-6.32 ± 0.2	2.9	9 – 200
		-0.31 ± 0.01	$i_{p, O \rightarrow W}$	0.9986	0.694	4.52 ± 0.1	3	9 – 100

CHAPTER VI: SUMMARY AND FUTURE WORKS

6.1 Summary

This thesis has found that both simple and facilitated ion transfer is possible for tenofovir at the membrane stabilized Water/ dichloroethane interface. The later was demonstrated by using the solution of DB18C6 in dichloroethane. The outcomes could contribute to the goals of this work such as meeting the demand for quick, economical, portable, and personalized devices.

Both the simple ion-transfer sensor (Ag|ETH500 (10 mM) /DCE|) and facilitated ion-transfer sensor (Ag|ETH500 (10 mM)/ DB18C6 (50 mM)/DCE||) exhibited operational stability of 90 min. 25 mV/ s was found to be an optimal scan rate for CV interrogation of the sensors after consideration of reasonable S/N ratio and sample throughput rates. Furthermore the diffusion coefficient of the analyte was estimated as 2.48×10^{-11} and 9.936×10^{-9} cm^2/s for sensor (1) and (2) respectively. These estimates may be taken to be the diffusion coefficient of tenofovir in the hydrophilic membrane separating the organic phase from the aqueous phase. For both of the Ag|ETH500 (10 mM)/ DCE|| (1) and Ag|ETH500 (10 mM)/ DB18C6 (50 mM)/DCE|| (2) sensors, the W$\rightarrow$O ion-transfer peaks provided superior signal quality over the corresponding reverse peaks. According to the calibration curve based on the forward peak, a detection limit of about 5 µM, a linear range of 15 – 100 µM, and sensitivity of 7.09 nA µM^{-1} towards tenofovir were found. For the reverse peak, these were respectively 3 µM, 6.32 nA µM^{-1}, and 9 – 100 µM. In this way, a four-electrode-based amperometric detection of tenofovir at a membrane-stabilized liquid | liquid interface, both under simple and ionophore-facilitated mode, has been demonstrated as promising for analysis of this analyte as a representative of the nucleotide/ nucleoside reverse transcriptase inhibitor ARV drugs.

6.2 Future work or recommendations

(i)   Test other sensor pre-conditioning and conditioning techniques as well as signal interrogation techniques to improve the sensors' analytical characteristics

(ii)   Testing if other ionophores would give better sensors

(iii)   Interference studies

(iv)   Synthetic real sample applications can be compared with standard methods in a single blind experiment.

(v)   Exploring ways of improving analytical performance via membrane-impregnated selectivity and sensitivity enhancing agents

(vi)   Testing the sensor for its response to other nucleotide/ nucleoside reverse transcriptase inhibitor ARV drugs

BIBLIOGRAPHY

[1]   Liu B., Mirkin M. V. Charge Transfer Reactions at the Liquid/Liquid Interface. Anal

        Chem. 73 (2001) 670A–677A

[2]   Fermı D, Lee HJ, Girault HH, Reymond F, Fermın D. Electrochemistry at liquid /

        liquid interfaces: methodology and potential applications. Electrochim Acta. 45 (2000)

        2647–62.

[3]   Girault H. Modern aspects of electrochemistry. Bockris J, Conway B, White R

        (editors) Plenum, New York; 1993.

[4]   Volkov A. (editor) Liquid interfaces in chemical, biological, and pharmaceutical

        applications. New York: Marcel Dekker; 2001.

[5]   Volkov AG, Deamer DW. Liquid-liquid interfaces: theory and methods. CRC Press

        1996.

[6]   Girault H, Schiffrin D. Electroanalytical chemistry. Bard A. (editor) New York:

        Marcell Dekker; 1989.

[7]   Teixeira C, Gomes JRB, Gomes P, Maurel F. Viral surface glycoproteins, gp120 and

        gp41, as potential drug targets against HIV-1: brief overview one quarter of a century

        past the approval of zidovudine, the first anti-retroviral drug. Eur J Med Chem.

        Elsevier 46 (2011) 979–92.

[8]   Whitcomb JM, Parkin NT, Chappey C, Hellmann NS, Petropoulos CJ. Broad

        nucleoside reverse-transcriptase inhibitor cross-resistance in human immunodeficiency

        virus type 1 clinical isolates. J Infect Dis. 188 (2003) 992–1000.

[9]   Sida des Sourds du Québec. Types of Antiretroviral Drugs. 2012. Available at: http://www.cssq.org/medications/antiretroviral-drugs-en.html

[10]   HIV and AIDS Charity AVERT. Antiretroviral Drugs: Approved antiretroviral drugs. 2012. Available at: http://www.avert.org/antiretroviral-drugs.htm

[11]   J. S, Swierzewski, Types of Antiretroviral Drugs. 2000. Available at: http://www.healthcommunities.com/hiv-aids/arvt-drug-types.shtml

[12]   Desai M, Iyer G, Dikshit RK. Antiretroviral drugs: critical issues and recent advances. Indian J Pharmacol. 44 (2012) 288–98.

[13]   De Clercq E. Anti-HIV drugs: 25 compounds approved within 25 years after the discovery of HIV. Int J Antimicrob Agents. 33 (2009) 307–20.

[14]   Courtney V Fletcher P. Pharmacology of nucleoside reverse transcriptase inhibitors. 2012. Available from: http://www.uptodate.com/contents/pharmacology-of-nucleoside-reverse-transcriptase-inhibitors

[15]   Bozal B, Uslu B, Özkan S a., Ozkan SA. A Review of Electroanalytical Techniques for Determination of Anti-HIV Drugs. Int J Electrochem. 2011 (2011) 1–17.

[16]   De Clercq E. Anti-HIV drugs: 25 compounds approved within 25 years after the discovery of HIV. Int J Antimicrob Agents. 33 (2009) 307–20.

[17]   De Clercq E. Anti-HIV drugs. Verh Acad voor Geneeskd van Belgie 69 (2007) 81.

[18]   Tantillo C, Ding J, Jacobo-Molina A, Nanni RG, Boyer PL, Hughes SH, et al. Locations of anti-AIDS drug binding sites and resistance mutations in the three-

dimensional structure of HIV-1 reverse transcriptase: implications for mechanisms of drug inhibition and resistance. J Mol Biol. 243 (1994) 369–87.

[19]   Gallant JE. Initial therapy of HIV infection. J Clin Virol.25 (2002) 317–33.

[20]   De Clercq E. Strategies in the design of antiviral drugs. Nat Rev Drug Discov. 1 (2002) 13–25.

[21]   Oqbru O. Zalcitabine, Hivid - discontinued. 2013. Available at: http://www.medicinenet.com/zalcitabine/article.htm (Editor: Jay W. Marks)

[22]   De Clercq E. Potential of acyclic nucleoside phosphonates in the treatment of DNA virus and retrovirus infections. Expert Rev Anti Infect Ther. 1 (2003) 21–43.

[23]   Aymard G, Legrand M, Trichereau N, Diquet B. Determination of twelve antiretroviral agents in human plasma sample using reversed-phase high-performance liquid chromatography. J Chromatogr B.744 (2000) 227–40.

[24]   Knupp C a, Graziano FM, Dixon RM, Barbhaiya RH. Pharmacokinetic-interaction study of didanosine and ranitidine in patients seropositive for human immunodeficiency virus. Antimicrob Agents Chemother. 36 (1992) 2075–9079.

[25]   Gibaldi M, Perrier D. Noncompartmental analysis based on statistical moment theory. Pharmacokinetics. 2 (1982) 409–17.

[26]   Yuen GJ, Lou Y, Bumgarner NF, Bishop JP, Smith GA, Otto VR, et al. Equivalent Steady-State Pharmacokinetics of Lamivudine in Plasma and Lamivudine Triphosphate within Cells following Administration of Lamivudine at 300 Milligrams

Once Daily and 150 Milligrams Twice Daily. Antimicrob Agents Chemother. 48 (2004) 176–82.

[27] Rezk NL, Tidwell RR, Kashuba ADM. Simultaneous determination of six HIV nucleoside analogue reverse transcriptase inhibitors and nevirapine by liquid chromatography with ultraviolet absorbance detection. J Chromatogr B. 791 (2003) 137–47.

[28] Kearney BP, Flaherty JF, Shah J. Tenofovir disoproxil fumarate. Clin Pharmacokinet. 43 (2004) 595–612.

[29] Tong L, Phan TK, Robinson KL, Babusis D, Strab R, Bhoopathy S, et al. Effects of human immunodeficiency virus protease inhibitors on the intestinal absorption of tenofovir disoproxil fumarate in vitro. Antimicrob Agents Chemother. 51 (2007) 3498–504.

[30] Barditch-Crovo P, Deeks SG, Collier A, Safrin S, Coakley DF, Miller M, et al. Phase I/II trial of the pharmacokinetics, safety, and antiretroviral activity of tenofovir disoproxil fumarate in human immunodeficiency virus-infected adults. Antimicrob Agents Chemother. Am Soc Microbiol 45 (2001) 2733–9.

[31] Sparidans RW, Crommentuyn KML, Schellens JHM, Beijnen JH. Liquid chromatographic assay for the antiviral nucleotide analogue tenofovir in plasma using derivatization with chloroacetaldehyde. J Chromatogr B. 791 (2003) 227–33.

[32] Sentenac S, Fernandez C, Thuillier A, Lechat P, Aymard G. Sensitive determination of tenofovir in human plasma samples using reversed-phase liquid chromatography. J Chromatogr B. 793 (2003) 317–24.

[33]   Takahashi M, Kudaka Y, Okumura N, Hirano A, Banno K, Kaneda T. Determination of plasma tenofovir concentrations using a conventional LC-MS method. Biol Pharm Bull. 30 (2007) 1784–6.

[34]   Delahunty T, Bushman L, Fletcher C V. Sensitive assay for determining plasma tenofovir concentrations by LC/MS/MS. J Chromatogr B Analyt Technol Biomed Life Sci. 830 (2006) 6–12.

[35]   Droste JAH, Wissen CPWGMV, Kearney BP, Buffels R, VanHorssen PJ, Hekster YA, et al. Pharmacokinetic Study of Tenofovir Disoproxil Fumarate Combined with Rifampin in Healthy Volunteers Pharmacokinetic Study of Tenofovir Disoproxil Fumarate Combined with Rifampin in Healthy Volunteers. Antimicrob Agents Chemother. 49 (2005) 680–4.

[36]   Masikini M. The Use of Cyclodextrin Template-Based Metal Oxide Nanomaterials in the Development of Electrochemical Sensors for Phenolic Endocrine Disruptor Compounds. M.Sc. Thesis. University of the Western Cape. South Africa; 2010.

[37]   Wang Y, Xu H, Zhang J, Li G. Electrochemical Sensors for Clinic Analysis. Sensors. 8 (2008) 2043–81.

[38]   Hanrahan G, Patil DG, Wang J. Electrochemical sensors for environmental monitoring: design, development and applications. J Environ Monit. 6 (2004) 657–64.

[39]   Uslu B, Özkan SA. Anodic voltammetry of abacavir and its determination in pharmaceuticals and biological fluids. Electrochim Acta. 49 (2004) 4321–9.

[40]   Dogan B, Uslu B, Ozkan SA, Zuman P. Electrochemical determination of HIV drug abacavir based on its reduction. Anal Chem. 80 (2008) 209–16.

[41]   Ozoemena KI, Stefan-van Staden R-I, Nyokong T. Metallophthalocyanine Based

Carbon Paste Electrodes for the Determination of 2', 3'-Dideoxyinosine.

Electroanalysis. 21 (2009) 1651–4.

[42]   Dogan B, Uslu B, Suzen S, Ozkan SA. Electrochemical evaluation of nucleoside

analogue lamivudine in pharmaceutical dosage forms and human serum.

Electroanalysis. 17 (2005) 1886–94.

[43]   Jain R, Jadon N, Radhapyari K. Cathodic adsorptive stripping voltammetric studies on

lamivudine: An antiretroviral drug. J Colloid Interface Sci. 313 (2007) 254–60.

[44]   Trnková L, Kizek R, Vacek J. Square wave and elimination voltammetric analysis of

azidothymidine in the presence of oligonucleotides and chromosomal DNA.

Bioelectrochemistry. 63 (2004) 31–6.

[45]   Leandro KC, Moreira JC, Farias PAM. Determination of zidovudine in

pharmaceuticals by differential pulse voltammetry. Anal Lett. 43 (2010) 1951–7.

[46]   Vacek J, Andrysík Z, Trnková L, Kizek R. Determination of Azidothymidine--an

Antiproliferative and Virostatic Drug by Square-Wave Voltammetry. Electroanalysis.

16 (2004) 224–30.

[47]   Pecková K, Navrátil T, Yosypchuk B, Moreira JC, Leandro KC, Barek J.

Voltammetric determination of azidothymidine using silver solid amalgam electrodes.

Electroanalysis. 21 (2009) 1750–7.

[48]   Liu B, Mirkin M V. Charge Transfer Reactions at the Liquid / Liquid Interface. Anal

Chem. 73 (2001) 670–7.

[49]   Volkov A. Liquid Interfaces in Chemical, Biological, and Pharmaceutical
        Applications. Dekker Marce, New York; 2009.

[50]   Girault HH. Charge Transfer Across Liquid–Liquid Interfaces. In: Bockris JO,
        Conway BE, White, R. E (editors). Modern Aspects of Electrochemistry. Plenum
        Press: New York; 1993. p. Vol. 25, p 1.

[51]   Vanysek P. Liquid–Liquid Electrochemistry. In: Vanysek P. (editor). Modern
        Electroanalytical Techniques: Chemical Analysis Series, Vol 139. John Wiley: New
        York; 1996. p. 337–64.

[52]   Reymond F, Fermin D, Lee J, Girault H. Potential applications in molecular biology of
        the electrochemistry of liquid/liquid interfaces. Electrochim Acta. 45 (2000) 2647–62.

[53]   Osborne MC, Shao Y, Pereira CM, Girault HH. Micro-hole interface for the
        amperometric determination of ionic species in aqueous solutions. J Electroanal Chem.
        364 (1994) 155–61.

[54]   Osborne MD, Girault HH. The liquid--liquid micro-interface for the amperometric
        detection of urea. Electroanalysis. 7 (1995) 714–21.

[55]   Ohkouchi T, Kakutani T, Osakai T, Senda M. Voltammetry with an ion-selective
        microelectrode based on polarizable oil/water interface. Anal Sci. (Japan Society for
        Analytical Chemistry) 7 (1991) 371–6.

[56]   Katano H, Senda M. Ion-transfer stripping voltammetry of polyoxyethylene alkyl and
        alkylphenyl ether surfactants at the organic-gel| water interface and its application to
        trace analysis. J Electroanal Chem. 496 (2001) 103–9.

[57]   Katano H, Senda M. Stripping voltammetry of mercury (II) and lead (II) ions at liquid/liquid interface. Anal Sci. (Japan) 14 (1998) 63–5.

[58]   Silva F, Sousa MJ, Pereira CM. Electrochemical study of aqueous-organic gel micro-interfaces. Electrochim Acta. 42 (1997) 3095–103.

[59]   Lee HJ, Beattie PD, Seddon BJ, Osborne MD, Girault HH. Amperometric ion sensors based on laser-patterned composite polymer membranes. J Electroanal Chem. 440 (1997) 73–82.

[60]   Lee HJ, Beriet C, Girault HH. Amperometric detection of alkali metal ions on micro-fabricated composite polymer membranes. J Electroanal Chem. 453 (1998) 211–9.

[61]   Hundhammer B, Wilke S. Investigation of ion transfer across the membrane stabilized interface of two immiscible electrolyte solutions: Part II. Analytical application. J Electroanal Chem interfacial Electrochem. 266 (1989)133–41.

[62]   Hundhammer B, Solomon T, Zerihun T, Abegaz M, Bekele A, Graichen M. Investigation of ion transfer across the membrane-stabilized interface of two immiscible electrolyte solutions: Part III. Facilitated ion transfer. J Electroanal Chem. 371 (1994) 1–11.

[63]   Sawada S, Torii H, Osakai T, Kimoto T. Pulse amperometric detection of lithium in artificial serum using a flow injection system with a liquid/liquid-type ion-selective electrode. Anal Chem. 70 (1998) 4286–90.

[64]   Lee HJ, Girault HH. Amperometric ion detector for ion chromatography. Anal Chem. 70 (1998) 4280–5.

[65]   Lee HJ, Pereira CM, Silva AF, Girault HH. Pulse amperometric detection of salt
        concentrations by flow injection analysis using ionodes. Anal Chem. 72 (2000) 5562–
        6.

[66]   Wilke S, Schürz R, Wang H. Amperometric ion detection in capillary zone
        electrophoresis by ion transfer across a liquid-liquid microinterface. Anal Chem. 73
        (2001) 1146–54.

[67]   Shao Y, Liu B, Mirkin M V. Studying ionic reactions by a new generation/collection
        technique. J Am Chem Soc. 120 (1998) 12700–1.

[68]   Liu B, Shao Y, Mirkin M V. Dual-pipet techniques for probing ionic reactions. Anal
        Chem. 72 (2000) 510–9.

[69]   Smith RN, Hansch C, Ames MM. Selection of a reference partitioning system for drug
        design work. J Pharm Sci. 64 (1975) 599–606.

[70]   Reymond F, Steyaert G, Carrupt P-A, Testa B, Girault H. Ionic partition diagrams: a
        potential-pH representation. J Am Chem Soc. 118 (1996) 11951–7.

[71]   Tien HT. Cyclic voltammetry of bilayer lipid membranes. J Phys Chem. 88 (1984)
        3172–4.

[72]   Gosser DK. Cyclic voltammetry: simulation and analysis of reaction mechanisms.
        VCH New York; 1993.

[73]   Spangler BD, Vanysek P, Hernandez IC, Rogers RD. Structure of crystal violet
        tetraphenylborate. J Crystallogr Spectrosc Res. 19 (1989) 589–96.
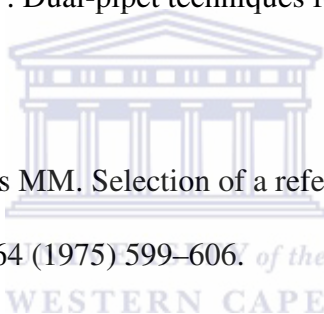
[74] Taddese T. Enzymatic Detetrmination of Urea at a Polarizable memberane- Stabilized
      Liquid- Liquide Interface. M.Sc. Thesis,Addis Ababa University,Addis Ababa,
      Ethiopia, 1996.

[75] Zhengzhou Boke. Vacuum Filtration Apparatus, Available at:
      http://zzbk.en.alibaba.com/product/622708278-0/Vacuum_Filtration_Apparatus.html;.
      2013.

[76] Nevase PA, Nimje HM. Uv Spectrophotometric Method For Estimation Of Tenofovir
      Disoproxil Fumarate Tablet Dosage Form. Int J Pharm Res Dev 3 (2011) 73–5.

[77] Gilead Sciences, Inc. Truvada (Emtricitabine / Tenofovir Disoproxil Fumarate
      Tablets) Antiretroviral Agent. Product Monograph, Submission Control No.: 165812.
      Canada, 2013.

[78] Homolka D, Hung LQ, Hofmanova A, Khalil MW, Koryta J, Marecek V, et al.
      Faradaic ion transfer across the interface of two immiscible electrolyte solutions:
      chronopotentiometry and cyclic voltammetry. Anal Chem. 52 (1980) 1606–10.

[79] Shao Y, Mirkin M V. Probing Ion Transfer at the Liquid / Liquid Interface by
      Scanning Electrochemical Microscopy (SECM). J Phys Chem B. 102 (1998) 9915–
      21.

[80] Choi CM, Heo J, Kim NJ. Binding selectivity of dibenzo-18-crown-6 for alkali metal
      cations in aqueous solution: A density functional theory study using a continuum
      solvation model. Chem Cent J. 6 (2012) 84.

Page left blank

Page left blank